The Effect of Amplitude Control and Randomness on Strongly Coupled Oscillator Arrays

DISSERTATION

Submitted to

The School of Engineering of the

UNIVERSITY OF DAYTON

In Partial Fulfillment of the Requirements for

The Degree

Doctor of Philosophy in Electrical Engineering

by

Hai Jiang

Dayton, Ohio

December, 2009

The Effect of Amplitude Control and Randomness on Strongly Coupled Oscillator Arrays

APPROVED BY:

Robert P. Penno, Ph.D.
Advisory Committee Chairman
Associate Professor
Department of Electrical and Computer Engineering

Guru Subramanyam, Ph.D.
Committee Member
Professor
Department of Electrical and Computer Engineering

Raúl Ordóñez, Ph.D.
Committee Member
Associate Professor
Department of Electrical and Computer Engineering

Muhammad N. Islam, Ph.D.
Committee Member
Professor and Graduate Program Director
Department of Mathematics

Malcolm Daniels, Ph.D.
Associate Dean, School of Engineering

Tony E. Saliba, Ph.D.
Dean, School of Engineering

ABSTRACT

THE EFFECT OF AMPLITUDE CONTROL AND RANDOMNESS ON STRONGLY COUPLED OSCILLATOR ARRAYS

Name: Jiang, Hai
University of Dayton

Advisor: Dr. Robert P. Penno

Phased arrays have many applications such as Radar Communication, Satellite Communication, and Wireless Local Area Networks (WLAN). For the traditional phased array, a phase shifter is used with each antenna element to establish a constant phase progression along the antenna array. A constant phase progression will force the electromagnetic wave to add up so that the energy would radiate at a particular angle with respect to the array. However, it is difficult to integrate the bulky phase-shifters in the monolithic module, especially when the application involves a large number of elements. This dissertation studies an alternative phase beam-scanning technique using arrays of coupled oscillators (COA), which avoids the use of phase shifters. This technique of COA may reduce the complexity of phase control circuits and provide for a phased array of lower volume and weight. Consequently, it simplifies the architecture of the T/R module and reduces the overall cost.

In this work, dynamic equations of the nonlinear COA with arbitrary coupling networks are derived using both time and frequency domain methods. From the dynamic analysis, it is shown that the phase distribution along the array, and hence the beam scanning angle of the array, can be controlled by free running frequencies of the coupled oscillators. The stability and nonlinear behaviors of synchronized coupled oscillators are studied via the nonlinear control theory and applied to radar beam scanning arrays. Analysis indicates that a stable, unique equilibrium point exists when choosing a specific set of free running frequencies, and it is associated with the desired phase shift but within a given range.

By means of previous dynamic analysis, effects of amplitude dynamics are studied for COAs with uniform, triangular and Chebyshev amplitude distributions. The array with different coupling strengths, nonlinear parameters, and synchronization frequencies are considered. Results demonstrate that beam shapes and SLLs can be controlled for the coupled oscillator array using strong coupling. The influence of the random, free-running frequency distribution of the phase error in COAs, which causes the phase shift error and hence the error of main beam scanning angle (EMBSA), is also investigated through a Monte Carlo analysis. It is found that strongly COAs are more robust than weakly COAs under the same level of randomness in free running frequencies. Furthermore, when random deviations become larger, the robustness of strongly COA is especially obvious.

To Xiaoyan, my parents and grandmother.

ACKNOWLEDGMENTS

I am deeply indebted to many people who encouraged, supported and helped me to accomplish this dissertation. My foremost thanks go to my well-beloved father, Jiwen Jiang and mother, Yulan Liu. Just like many Chinese born after the 80s, I am the only child in this family and my parents put lots of heart, time and money on my education to make sure that I would go to the better high school, college and then graduate school in the States. Without their encouragement, support and love, this dissertation would not be possible. Next person I would like to thank is my beloved wife, Xiaoyan Ruan. Her endless love gives me confidence and happiness; it motivates me to achieve a higher level of my career. Beyond personal lives, she also gives me many advices on my study and research. I appreciate the fact that I could have the chance to marry such a sharp beautiful women, and live with her for the rest of my life.

I would like to express my true gratitude to my deceased advisor Dr. Krishna M. Pasala. I met Dr. Pasala 6 years ago at University of Dayton when I just came to the States. His age is like my father, and he also behaves like a father to me. He really is my first mentor for studies and researches in the area of Antennas and Electromagnetics. During the four years working together with Prof. Pasala, I finished my master thesis under his supervision and support; he guided and helped me on writing technical papers and proposals; his serious academic attitude and integral view on research made a deep impression on me and influenced me significantly. Now all these things he left to me become an invaluable asset, and they assist me to keep working on my Ph.D. dissertation and complete it. I am really glad that I got the chance to know Professor Pasala, and all his family in my life. I wish all the best to his family.

I would like to thank my current advisor, Dr. Robert Penno, also a real good friend of mine. When he accepted me as his Ph.D. student, I was only halfway in completing this dissertation. Dr. Penno spent lots of his time and energy on my dissertation and gave me many invaluable suggestion and comments. He also helped to review and advise my previous papers which have not been done before. Without his support, suggestion and help, this dissertation would not be possible either. I would like to give a special thanks to Dr. Guru Subramanyam. When Dr. Pasala left, he expressed to accept me as his Ph.D. student without any doubt or hesitation. Later he also gave me the chance to work and learn in his RF and Wireless Sensor Laboratory on reconfigurable antennas using RF ferroelectric varactors. Dr. Guru also invited me as a guest instructor for the undergraduate course, Applied Electromagnetics to introduce antenna fundamentals. These lectures gave me the opportunity to develop my teaching skills which allowed me to transfer my knowledge of antennas, electromagnetics, and software modeling techniques to students with a large range of qualifications. I really owe Dr. Guru a debt for all his help. I would also like to thank Dr. Raul for his comments and advices on my dissertation and paper. It was my great pleasure to collaborate with him and I learned a lot from him.

I would like to thank the secretary of our department, Marilyn for her assistance on my dissertations, papers and traveling arrangement for the conference. I would like to thank DAGSI for providing me financial support of three years fellowship which made this dissertation possible. I would like to thank Dazhi, Wei Han, Wen Chen, NXX, Star, Axing, Weidong, Jay, Weibin, Jiadong, Henry, Bob, Sree, Andy, Lei Jiang, Hua Jiang, Qian Li, Xiao Me, Hui Wang, Jinlan Dong, Feng Du, Ding Lin, Xiang Nan, Feng Qijun, and all my good friends in Dayton for their help and care. For six years at University of Dayton, I made tons of friends and got to know lots of nice people here, which makes Dayton a second home to me and I do not want to leave. However things are not always as we wished, but I wish I could come back to work in Dayton some time in the future.

TABLE OF CONTENTS

LIST OF FIGURES

LIST OF TABLES

CHAPTER 1

INTRODUCTION

1.1 Statement of Problem

When two or more antennas are arranged in space and driven from a source of power (a transmitter) at the same frequency, the directional radiation pattern will be produced due to the mutual coupling between the signals transmitted from the individual elements. The radiation pattern can be scanned through space by manipulating the phase distribution of the exciting currents along the arrays. Such array is referred to as a phased array which can scan the beam at a desired angle electronically. Phased arrays have many applications including Wireless Local Area Network (WLAN), Global Satellite Communication, Mobile Communication, and Radar Communication.

For traditional phased array, a phase shifter is used with each antenna element to establish a constant phase progression along the antenna array. A constant phase progression will force the electromagnetic wave to add up so that the energy can radiate at a particular angle to the array. Recently, Monolithic Microwave Integrated Circuits (MMICs) have attracted much attention due to the reproducibility and smaller size.

However, it is difficult to integrate the bulky phase-shifters with other RF circuitries, such as distribution networks, DC bias lines, and planar antennas in the monolithic module, especially when the application requires a large phased array.

A new phase beam-scanning technique using arrays of coupled oscillators is proposed. This attractive approach to applications of phased arrays is to use coupled oscillators for achieving the constant phase progression along the array avoiding any use of phase shifters. When the free-running frequencies of the oscillators are within a collective locking range, the oscillators will spontaneously synchronize with a phase relationship that is controlled by the original distribution of free-running frequencies. For a linear phased array, a desired beam angle can be achieved by simply detuning the free-running frequencies of the oscillator on the edges. This technique reduces the complexity of phase control circuits and makes the integration of a phased array more easily. Consequently it simplifies the architecture of the phased array module and reduces the overall cost.

1.2 Review of selected research and significance of proposed research

The design technique of a phased array using coupled oscillator comes from the concept of injection locking of free running oscillators. R. Alder [1] demonstrates that, under the influence of an external injection signal whose free running frequency are within the locking range of the free running oscillator, a constant phase difference can be established between the external source and free running oscillator. Then Kurokawa extends Alder's theory by deriving the general dynamic equations for both amplitude and phase from amplitude dependent Z parameters [2, 3]. In 1986, the theory of injection-locked oscillators is applied to the coupled oscillator array by Stephan and Morgan [4]. Based on these analysis, coupled nonlinear differential equations describing instantaneous amplitude and phase dynamics of the oscillator array are developed by York through modeling the oscillator with RLC resonant circuits and using coupled Van del Pol equations [5]. The dynamic equations of amplitude and phase are

$$\begin{aligned} \frac{dA_i}{dt} &= \frac{\mu\omega_i}{2Q}\left(\alpha_i^2 - A_i^2\right) + \frac{\omega_i}{2Q}\sum_{j=1}^{N} |\kappa|_{ij}\, A_j cos\left(\Phi_{ij} + \theta_i - \theta_j\right) \\ \frac{d\theta_i}{dt} &= \omega_i - \frac{\omega_i}{2Q}\sum_{j=1}^{N} |\kappa|_{ij}\, \frac{A_j}{A_i} sin\left(\Phi_{ij} + \theta_i - \theta_j\right) \qquad (1.1) \\ & i = 1, 2, \cdots, N, \qquad (1.2) \end{aligned}$$

where ω_i, A_i, θ_i, Q, μ, $|\kappa|_{ij}$, and $\Phi_i j$, are the free-running frequency, instantaneous amplitude and phase of antenna, quality factor, nonlinear parameter of oscillator, coupling strength and coupling phase, respectively. With the understanding of system dynamics, the beam scanning technique for a one-dimensional array of loosely coupled oscillators was demonstrated by numerically solving the phase dynamic equations in [6, 7, 8]. Methods in the frequency domain [8, 9] are also used to developed the system dynamics and similar results have been obtained. Although the full dynamic analysis for both amplitude and phase of coupled oscillator array has been developed, the amplitude dynamics were typically ignored. It was assumed that due to the use of weak coupling, the instantaneous amplitudes are assumed to remain at their free running values.

Since then, this technique for designing a one-dimensional array has been developed by many groups theoretical and experimentally. Hwang and Myung [10] designed such an array by controlling the coupling phase between the adjacent elements. Pogorzelski and his coauthors [11] proposed a simplified version of York's theory in which the relative phases of the oscillator signals are represented by a continuous function. T. Heath [12] presented a theoretical analysis of simultaneous beam steering and null generation using coupled oscillator array. Also, using this technique, two-dimensional arrays are developed and tested by several groups [13, 14, 15]. Recently, Shen and Pearson presented Monte Carlo analysis of the randomness of free running frequencies, which causes phase errors and beam-pointing errors in a one-dimensional array [16]. A few attention has been given to the amplitude dynamics as well [17, 9, 18]. In [17, 18], beam shaping in COAs was introduced and side lobe reduction was demonstrated.

In this dissertation, the theoretical modeling of coupled oscillator array will be extended and applied to the array with tapered amplitudes for side lobe reduction. The oscillator array with strong coupling will be studied. The effects of amplitude dynamics will be considered, and compared for loosely and strongly coupled oscillators. A large two-dimensional array with 400 elements will be studied and the performance of it will be demonstrated by computer simulation. In addition, the effects of randomness of free-running frequency on the beam pointing error and side lobe levels will be investigated for arrays with different coupling strengths and operation frequencies.

1.3 Objectives and Organization of the Dissertation

A better understanding of mathematical modeling of the system dynamics is essential in the design of coupled oscillator array. In chapter two, the dynamic analysis of coupled oscillator array will be revisited and extended. Three different approaches to develop the amplitude and phase dynamics will be discussed and results will be compared. Both time and frequency domain methods are adopted and the microwave oscillators are modeled by both serial and parallel resonant circuits embedded with a negative conductance.

In chapter three, classic nonlinear control theory will be used to present a better understanding of the nonlinear characteristics of the coupled oscillator array including but not limited to linearization of system, existence and uniqueness of the solution, and the phase portraits. Then Matlab implementation of phase dynamics will be presented for one-dimensional array. The design of a large two-dimensional array with 400 elements will also be discussed in this chapter, but amplitude dynamics are ignored.

Coupling coefficients are extremely crucial parameters in the design of an oscillator array. In general it is a complex number including amplitude (coupling strength) and phase (coupling phase). For simplicity, zero coupling phases are chosen. Therefore an appropriate coupling network with constant coupling strengths needs to be designed. Numerically speaking, the coupling strengths may vary from 0.1 (weak) to 4.0 (strong). For loosely coupled oscillator array, since the interactions between adjacent oscillators are generally weak, it is very difficult to control or predict the coupling coefficients precisely. Another disadvantage of the weak coupling is, for ensuring mutual locking with the proper phase relationships, tighter tolerances in the fabrication of oscillators is required for weakly coupled oscillators.

Compared with weak coupling, the oscillator arrays with strong coupling network are more robust to the randomness of the free running frequencies in coupled oscillator array. The coupling strength may be designed more precisely and conveniently when using a suitably strong coupling mechanism. Therefore, in practice we tend to choose strong coupling over weak coupling for the purpose of design and system control. Nevertheless, the mathematical model for strongly coupled oscillators is more complicated. We have demonstrated that amplitude dynamics have significant effects on system performance especially when the couplings between oscillators become stronger and stronger. Thus, amplitude dynamics may not be ignored and full sets of differential equations describing both amplitude and phase dynamics have to be solved. The numerical analysis of system dynamics becomes more complicated and difficult to study due to increasing number of coupled differential equations to be solved.

In chapter four, we will demonstrate the thorough dynamic analysis of strongly coupled oscillator array which includes the influence of the amplitude dynamics. The algorithm for solving the nonlinear differential equations describing both amplitude and phase dynamics will be developed. The effects of amplitude dynamics on main beam angle and side lobe levels will be compared for arrays with different coupling strength and operation frequency. In previous designs [5]-[15], coupled oscillator arrays have only one degree of freedom for control of phase distribution, which is the free running frequency. In this chapter, a new technique using free running amplitude as an additional degree for the oscillator array will be discussed. The free-running amplitudes and frequencies both are used as control input for achieving desired amplitude and phase distribution. The analytical solution to the free running amplitudes will be examined, and the algorithm and simulation implementation using additional degree of freedom for controlling the system dynamics will be developed. The numerical results of array factors and transient analysis of instantaneous amplitude and phase obtained from manipulating both free running amplitudes and frequencies will be demonstrated and compared with the corresponding results obtained using only one degree of freedom.

In chapter five, the influence of the randomness in free running frequencies on beam scanning angle and side lobe levels will be investigated by the Monte Carlo simulation Method. The randomness in free running frequencies will be modeled using uniform and Gaussian distributions.

1.4 Research method

The coupled oscillators are modeled by the single-tuned circuit which leads to the Van der Pol equation for certain nonlinearities. By applying the Kirchhoff's Voltage Laws and Ohm's Law, the circuit equations are written into sets of differential equations describing both instantaneous amplitude and phase dynamics. Two sets of coupled nonlinear differential equations are solved using the Euler's Method. The important issues, such as beam steering, beam shaping, effects of amplitude dynamics, randomness in free running frequencies will be investigated by Matlab implementation of mathematical model. The stability of the system dynamics will be analyzed using classic control theory.

CHAPTER 2

DYNAMIC ANALYSIS OF COUPLED OSCILLATOR ARRAYS

2.1 Introduction

The dynamic theory of mutually coupled oscillator array was inspired by the phenomenon of Injection-Locking of microwave solid-state oscillators, discussed by R. Adler [1] and K. Kurokawa [2]. Following Van der Pol's method [19], the dynamic analysis was developed in the time domain by York [5] by modeling the oscillator with a series resonant circuit and negative resistance. Later, the differential equations describing the system dynamics of coupled oscillators were developed by York and his co-workers using the frequency domain method [8], which was based on Kurokawa's analysis [3]. In [8], each oscillator was modeled by a parallel resonant circuit model embedded with a negative conductance, and it described the coupling mechanism by N-port network, which allows us to calculate the coupling parameter using Y-parameters of the N-port network. Note that both the time and frequency domain methods rely on the assumption of slowly varying amplitude and phase of an oscillator. Although they give the identical equations, the frequency domain method gives more engineering insight into the design and implementation of coupling mechanism since it is based on network concepts. Another requirement is each type of oscillator requires the corresponding coupling topology; that is, oscillators with series resonant circuit should be coupled in series, whereas parallel oscillators should be coupled in parallel.

In [9], instead of modeling the oscillator using a simple RLC circuits, a more complicated and realistic model of oscillator elements is used and the system dynamics are developed using frequency domain method. In that paper, a semi-analytical approach based on the harmonic balance (HB) was presented using the auxiliary-generator technique [20, 21] and was compared with the Full HB analysis and envelope-transient method [22].

In this chapter, the dynamic analysis of coupled oscillator array will be revisited. Three different method are discussed and results are compared. Both time and frequency domain method are adopted for oscillators modeled by parallel resonant circuit which include a negative conductance. Following that, dynamics of coupled oscillator which is modeled using a serial resonant circuit individually are investigated.

2.2 Negative Resistance Oscillator

Many materials and devices exhibit negative resistance such as IMPATT diodes and Gunn diodes. Fig. 2.1 illustrates the I-V curve of a piece of semiconductor material, demonstrating how the current through the material varies with the voltage applied across it. Various sorts of semiconductor show this effect, but the types used most often for commercial purposes are GaAs and InP.

Here we will use the example of the Gunn diode, which is essentially just a piece of doped semiconductor with two electrical contacts on opposite ends.

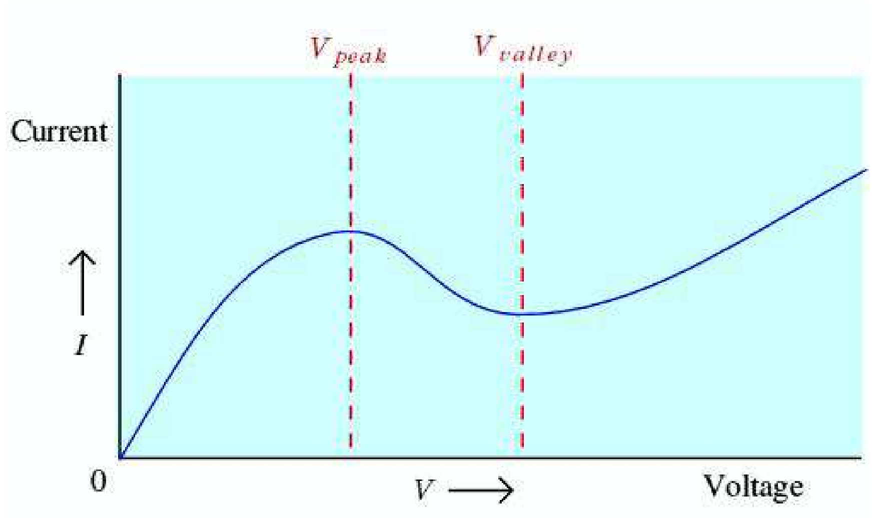

Figure 2.1: I-V curve of Gunn diodes.

In most circumstances we use the static resistance

$$R = \frac{V}{I}, \tag{2.1}$$

but the negative resistance is defined as dynamic or differential resistance

$$R_d(V) = \frac{dV}{dI}, \tag{2.2}$$

As shown in Fig. 2.1, at the threshold voltage(V_{peak}) the current reaches a maximum value. As the bias is further increased the current decreases. This is called the negative resistance region because in this voltage range the dynamic resistance $R_d(V) < 0$. Note, however, that the static resistance is always positive.

A lumped negative resistance (conductance) can be used to model the active device and is embedded in a series or parallel resonant circuit. The reactive component of the device impedance is then considered as part of the the embedded network.

2.3 Parallel Resonant Circuit

A narrow-band microwave oscillator can be modeled using either a series or parallel resonant circuit with a negative resistance embedded.

2.3.1 Time Domain Method

The parallel resonant circuit modeling a single microwave oscillator is shown in Fig. 2.2. The negative differential conductance $-G_d$ represents the nonlinear active device, which is determined by the I-V characteristics in the time domain, so $-G_d$ is frequency independent. Therefore the negative differential conductance $-G_d$ will only depend on the amplitude of its current or voltage but not the phase. The current source I_{inj} represents the injected signal from the neighboring oscillators, which is coming through the coupling network.

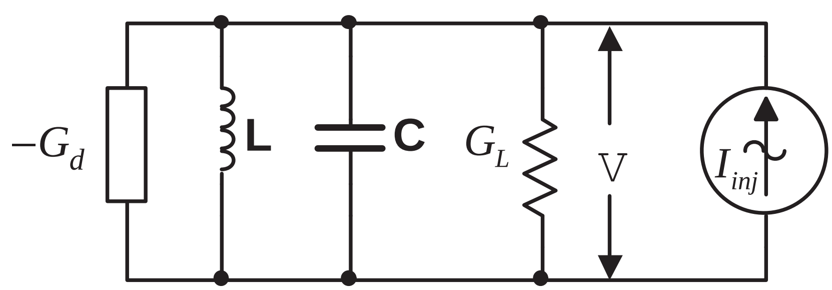

Figure 2.2: The parallel resonant circuit model for narrow-band microwave oscillators where I_{inj} denotes the injected signals from the neighboring oscillators and $-G_d$ denotes negative conductance of the device.

By the Kirchhoff's Voltage Laws and circuit analysis, the circuit equation for Fig. 2.2 is simply

$$I_{inj} = I_L + I_C + I_{-Rd} + I. \tag{2.3}$$

Using the Ohm's Law for the capacitor and inductor, we obtain

$$I_{inj} = \frac{1}{L}\int V dt + C\frac{dV}{dt} + I + (-G_d(|V|) \cdot V) \tag{2.4}$$

where V is the instantaneous voltage across the antenna and equal to

$$V = \frac{I}{G_L} \tag{2.5}$$

by the Ohm's Law.

Substituting (2.5) into (2.4), it becomes

$$I_{inj} = \frac{1}{LG_L}\int Idt + \frac{C}{G_L}\frac{dI}{dt} + I + \left(-G_d(|V|) \cdot \frac{I}{G_L}\right). \tag{2.6}$$

Multiplying $\frac{G_L}{C}$ at both ends, Eq. (2.6) can be written as

$$\frac{G_L}{C}I_{inj} = \frac{1}{LC}\int Idt + \frac{dI}{dt} + I\frac{G_L}{C}\left[1 - \frac{G_d(|V|)}{G_L}\right]. \tag{2.7}$$

The Q-factor of the parallel resonant circuit in Fig. 2.2 is defined as

$$Q = \frac{\omega_0 C}{G_L} = \frac{1}{\omega_0 G_L L}. \tag{2.8}$$

Thus

$$\frac{G_L}{C} = \frac{\omega_0}{Q}. \tag{2.9}$$

Substituting (2.9) into (2.7), we derive

$$\frac{\omega_0}{Q}I_{inj} = \frac{1}{CL}\int Idt + \frac{dI}{dt} + I\frac{\omega_0}{Q}\left[1 - \frac{G_d(|V|)}{G_L}\right]. \tag{2.10}$$

It can be shown that the resonant frequency ω_0 must be defined as

$$\omega_0 = \frac{1}{\sqrt{LC}}. \tag{2.11}$$

Substituting (2.11) into (2.10) gives

$$\frac{\omega_0}{Q} I_{inj} = \omega_0^2 \int I dt + \frac{dI}{dt} + I\frac{\omega_0}{Q}\left[1 - \frac{G_d(|V|)}{G_L}\right]. \tag{2.12}$$

which can be reorganized as

$$\frac{dI}{dt} + \omega_0^2 \int I dt + I\frac{\omega_0}{Q}\left[1 - \frac{G_d(|V|)}{G_L}\right] = \frac{\omega_0}{Q} I_{inj} \tag{2.13}$$

where ω_0 is the resonant frequency of the circuit, V is the output voltage in phasor domain, Q is the Q-factor of the parallel RLC network, and I_{inj} represents any externally injected signals from the coupling neighbors. With the Q-factor sufficiently high, the oscillator frequency will remain close to ω_0 and the amplitude and phase terms will be slowly varying functions of time (compared with the period of oscillation).

The output current can then be written as

$$I = A(t)e^{j(\omega_0 t + \phi(t))} = A(t)e^{j\theta(t)} \tag{2.14}$$

where A is the amplitude of oscillation, and θ is the instantaneous phase. The integral in (2.69) can be integrated by parts

$$\int I dt = \frac{-2jI}{\omega_0} + \frac{1}{\omega_0^2}\frac{dI}{dt} + \cdots . \tag{2.15}$$

Under the assumption of slowly varying parameters, the higher order differential terms in (2.15) can be neglected.

Following Van der Pol [19, 23], the characteristics of N-Shape negative conductance device can be approximated by the third degree parabola:

$$i = \psi(kv) = -\alpha v + \beta v^2 + \gamma v^3, \tag{2.16}$$

where both $\alpha > 0$ and $\gamma > 0$. β is an unimportant factor, since varying it will only shift position of the parabola but not affect the shape of the third degree curve. Therefore, for simplicity, we may choose $\beta = 0$ to make a symmetrical characteristic. Then the I-V equation is rewritten as

$$|I| = \psi(k\,|V|) = -\alpha\,|V| + \gamma\,|V|^3\,. \tag{2.17}$$

From (2.17), the dynamic negative conductance of the active device is derived as

$$-G_d(|V|) = \frac{d\,|I|}{d\,|V|} = -\alpha + 3\gamma\,|V|^2\,. \tag{2.18}$$

Redefining the coefficients, (2.18) may be written as

$$-G_d(A) = -G_0 + G_2 A^2, \tag{2.19}$$

where $-G_0$ is the negative conductance when a small signal is applied to the active device, and A is the amplitude of oscillation. Recalling that, in order to obtain a stable oscillation for the negative resistance oscillator, the following condition has to be satisfied

$$G_d(\alpha_0) = G_L, \tag{2.20}$$

where α_0 is the amplitude of free oscillation or free running amplitude. From Eq. (2.19) and the oscillation condition (2.20), we can write

$$\frac{-G_d(A)}{G_L} = -1 - \mu\left(\alpha_0^2 - A^2\right). \tag{2.21}$$

where μ is a positive, dimensionless quantity. To derive μ, we recognize from (2.21)

$$-G_d(A) = -G_L - \mu G_L \alpha_0^2 + \mu G_L A^2. \tag{2.22}$$

Comparing (2.22) with (2.19), we obtain

$$G_2 = \mu G_L. \tag{2.23}$$

Thus μ can be solved as

$$\mu = \frac{G_2}{G_L}. \tag{2.24}$$

Substituting (2.15) and (2.21) into (2.13) gives

$$\frac{dI}{dt} + \omega_0^2 \left[\frac{-2jI}{\omega_0} + \frac{1}{\omega_0^2} \frac{dI}{dt} \right] - I \frac{\mu\omega_0}{Q} \left(1 - \frac{A^2}{\alpha_0^2} \right) = \frac{\omega_0}{Q} I_{inj}. \tag{2.25}$$

Thus, we obtain from (2.25)

$$\frac{2dI}{dt} - 2I\omega_0 j - I \frac{\mu\omega_0}{Q} \left(1 - \frac{A^2}{\alpha_0^2} \right) = \frac{\omega_0}{Q} I_{inj}. \tag{2.26}$$

Finally, we obtain

$$\begin{aligned} \frac{dI}{dt} &= I\omega_0 j + I \frac{\mu\omega_0}{2Q} \left(1 - \frac{A^2}{\alpha_0^2} \right) + \frac{\omega_0}{2Q} I_{inj} \\ &= I \left[j\omega_0 + \frac{\mu\omega_0}{2Q} \left(1 - \frac{A^2}{\alpha_0^2} \right) \right] + \frac{\omega_0}{2Q} I_{inj} \end{aligned} \tag{2.27}$$

From (2.14) and the derivative formula, we derive

$$\begin{aligned} \frac{dI}{dt} = \frac{dAe^{j\theta}}{dt} &= \frac{dA}{dt} e^{j\theta} + Ae^{j\theta} \frac{d\theta}{dt} j \\ &= \frac{I}{A} \frac{dA}{dt} + I \frac{d\theta}{dt} j \end{aligned} \tag{2.28}$$

Substituting (2.28) into (2.27) gives,

$$\frac{1}{A} \frac{dA}{dt} + j \frac{d\theta}{dt} = j\omega_0 + \frac{\mu\omega_0}{2Q} \left(1 - \frac{A^2}{\alpha_0^2} \right) + \frac{\omega_0}{2Q} \frac{I_{inj}}{I} \tag{2.29}$$

Separating real and imaginary parts of (2.29) gives

$$\begin{aligned} \frac{dA}{dt} &= \frac{\omega_0 \mu}{2Q} \left(\alpha_0^2 - |A|^2 \right) A + \frac{\omega_0}{2Q} A Re \left\{ \frac{I_{inj}}{I} \right\} \\ \frac{d\theta}{dt} &= \omega_0 + \frac{\omega_0}{2Q} Im \left\{ \frac{I_{inj}}{I} \right\}. \end{aligned} \tag{2.30}$$

The injected signal can be written as

$$I_{inj} = \sum_{j=1}^{N} \kappa_{ij} I_j, \tag{2.31}$$

where V_j is the complex output voltage of the jth oscillator. For a system of coupled oscillators, a complex coupling coefficient κ_{ij} denotes the mutual interaction between oscillators i and j, which can be written as

$$\kappa_{ij} \equiv \epsilon_{ij} e^{-j\phi_{ij}}. \tag{2.32}$$

For some types of coupling, such as radiative interaction between antennas or transmission-line coupling circuits, the κ_{ij} can be directly related to commonly used N-port network parameters [8]. In other cases where the coupling mechanism is considerably more complicated or not well understood, such as coupling through the modes of an external cavity, simple experiments may be performed to determine the coupling parameters for a particular system [7]. Substituting (2.31) into (2.30), the system dynamics are

$$\begin{aligned} \frac{dA_i}{dt} &= \frac{\omega_0 \mu}{2Q}\left(\alpha_0^2 - |A_i|^2\right) A_i + \frac{\omega_0}{2Q} A_i Re\left\{\sum_{j=1}^{N} \kappa_{ij} \frac{I_j}{I_i}\right\} \\ \frac{d\theta}{dt} &= \omega_0 + \frac{\omega_0}{2Q} Im\left\{\sum_{j=1}^{N} \kappa_{ij} \frac{I_j}{I_i}\right\}. \end{aligned} \tag{2.33}$$

where the subscript i represents the ith oscillator. For simplicity, the Q and μ factors are assumed to be approximately the same for all of the oscillators. Taking $I_i = A_i e^{\theta_i}$ into (2.33), the amplitude and phase dynamics for an oscillator array with arbitrary coupling network are given by

$$\frac{dA_i}{dt} = \frac{\mu\omega_i}{2Q}\left(\alpha_i^2 - A_i^2\right) A_i + \frac{\omega_i}{2Q} \sum_{j=1}^{N} A_j Re\left\{\kappa_{ij} e^{j(\theta_j - \theta_i)}\right\} \tag{2.34}$$

$$\frac{d\theta_i}{dt} = \omega_i + \frac{\omega_i}{2Q}\sum_{j=1}^{N} Im\left\{\kappa_{ij}\frac{A_j}{A_i}e^{j(\theta_j-\theta_i)}\right\}$$

$$i = 1, 2, \cdots, N. \tag{2.35}$$

where κ_{ij} represents the coupling parameter between ith element and jth element, μ is an empirical nonlinearity parameter describing the oscillator and Q is the quality factor of the RLC resonant circuit. α_i and ω_i are the free running amplitude and angular frequency respectively.

2.3.2 Frequency Domain Method

In last section, we develop the amplitude and phase dynamics of coupled oscillator arrays using time domain method. In this section, we will show that the same differential equations can be derived using the frequency domain method.

The total admittance at the port of ith oscillator is defined as

$$Y_i(\omega, \bar{V}) = Y_{osc,i}(\omega, \bar{V}) + Y_{inj,i}(\omega, \bar{V}) \tag{2.36}$$

From the basic knowledge of network, we have $Y_i(\omega, \bar{V}) \equiv 0$.

Let the voltage across the ith oscillator be

$$V_i = A_i(t)e^{j[\omega_i t+\phi_i(t)]} = A_i(t)e^{j\theta_i(t)} \tag{2.37}$$

where the amplitude A_i and ϕ_i are assumed to be slow time-varying functions and ω_i is the free running angular frequency. Therefore, we have

$$\frac{d\phi_i}{dt} << \omega_i, \quad \frac{1}{A_i}\frac{dA_i}{dt} << \omega_i \tag{2.38}$$

Following Kurokawa [3], $Y_i(\omega, \bar{V})$ can be expanded using Taylor's theory around the free running frequency in radians per second ω_i

$$Y_i\left(\omega + \frac{d\phi_i}{dt} - j\frac{1}{A_i}\frac{dA_i}{dt}, \bar{V}\right) \cong Y_i(\omega_i, \bar{V}) + \left(\frac{d\phi_i}{dt} - j\frac{1}{A_i}\frac{dA_i}{dt}\right)\frac{\partial Y_i}{\partial \omega}\bigg|_{\omega_i}. \tag{2.39}$$

The approximation is used because the higher order terms of the Taylor's expansion are neglected. Since $\frac{d\phi_i}{dt} - j\frac{1}{A_i}\frac{dA_i}{dt}$ is negligible, we have

$$Y_i(\omega_i, \bar{V}) + \left(\frac{d\phi_i}{dt} - j\frac{1}{A_i}\frac{dA_i}{dt}\right)\frac{\partial Y_i}{\partial \omega}\bigg|_{\omega_i} \cong 0. \tag{2.40}$$

From (2.40), we can solve

$$-\frac{d\phi_i}{dt} + j\frac{1}{A_i}\frac{dA_i}{dt} = \frac{Y_i(\omega_i, \bar{V})}{\frac{\partial Y_i}{\partial \omega}\big|_{\omega_i}}. \tag{2.41}$$

Let us define

$$H_i(\bar{A}, \bar{\theta}) = \frac{Y_i(\omega_i, \bar{V})}{\frac{\partial Y_i}{\partial \omega}\big|_{\omega_i}}. \tag{2.42}$$

Separating the real and imaginary parts of Eq. (2.41), we have

$$\begin{aligned} \frac{dA_i}{dt} &= A_i Im\left[H_i(\bar{A}, \bar{\theta})\right] \\ \frac{d\theta_i}{dt} &= \omega_i + \frac{d\phi_i}{dt} = \omega_i - Re\left[H_i(\bar{A}, \bar{\theta})\right] \qquad i = 1, 2, \cdots, N. \end{aligned} \tag{2.43}$$

Recall that each oscillator can be modeled by a parallel resonant circuit with a load conductance, as shown in fig. 2.2. The total admittance of the oscillator and the load is

$$\begin{aligned} Y_{osc,i}(\omega, \bar{V}) &= -G_d(A_i) + G_L + j\omega C - j\frac{1}{\omega L} \\ &= G_L\left(1 - \frac{G_d(A_i)}{G_L}\right) + j\left(\omega C - \frac{1}{\omega L}\right) \end{aligned} \tag{2.44}$$

Taking (2.21) and (2.11) into (2.44) gives

$$Y_{osc,i}(\omega, \bar{V}) = -\mu G_L \left(\alpha_i^2 - A_i^2\right) + jC\left(\omega - \frac{\omega_i^2}{\omega}\right) \tag{2.45}$$

Following [4], the input admittance of the coupling network for the ith oscillator can be expressed as

$$\begin{aligned} Y_{inj,i}(\omega, \bar{V}) &= \sum_{j=1}^{N} Y_{ij}\frac{V_j}{V_i} = \sum_{j=1}^{N} Y_{ij}\frac{A_j e^{j\theta_j}}{A_i e^{j\theta_i}} \\ &= \sum_{j=1}^{N} Y_{ij}\frac{A_j}{A_i} e^{j(\theta_j - \theta_i)} \end{aligned} \tag{2.46}$$

Thus taking (2.46) and (2.45) into (2.36) gives

$$Y_i(\omega_i) = -\mu G_L \left(\alpha_i^2 - A_i^2\right) + \sum_{j=1}^{N} Y_{ij}\frac{A_j}{A_i} e^{j(\theta_j - \theta_i)} \tag{2.47}$$

Then

$$\begin{aligned} \left.\frac{\partial Y_i}{\partial \omega}\right|_{\omega_i} &= jC\left(1 - \omega_i^2\left(-\frac{1}{\omega^2}\right)\right) + \left.\sum_{j=1}^{N} \frac{\partial Y_{ij}}{\partial \omega}\frac{A_j}{A_i} e^{j(\theta_j - \theta_i)}\right|_{\omega_i} \\ &= j2C + \sum_{j=1}^{N} \frac{\partial Y_{ij}}{\partial \omega}\frac{A_j}{A_i} e^{j(\theta_j - \theta_i)}, \end{aligned} \tag{2.48}$$

Therefore

$$H_i(\bar{A}, \bar{\theta}) = \left.\frac{Y_i}{\partial Y_i / \partial \omega}\right|_{\omega_i} = \frac{-\mu\left(\alpha_i^2 - A_i^2\right) + \sum_{j=1}^{N} \frac{Y_{ij}}{G_L}\frac{A_j}{A_i} e^{j(\theta_j - \theta_i)}}{j2\frac{C}{G_L} + \frac{1}{G_L}\sum_{j=1}^{N} \frac{\partial Y_{ij}}{\partial \omega}\frac{A_j}{A_i} e^{j(\theta_j - \theta_i)}}. \tag{2.49}$$

Noticing that if the characteristics of the coupling network varies much slower around the free running angular frequency ω_i than the free running oscillator [8], the coupling network is defined as broadband and Y_{ij} is not a function of ω, thus

$$\frac{\partial Y_{ij}}{\partial \omega} \cong 0, \tag{2.50}$$

Then the sum in the denominator can be ignored, so that eq. (2.49) becomes

$$H_i(\bar{A},\bar{\theta}) = \left.\frac{Y_i}{\partial Y_i/\partial \omega}\right|_{\omega_i} = \frac{-\mu\left(\alpha_i^2 - A_i^2\right) + \sum_{j=1}^{N}\frac{Y_{ij}}{G_L}\frac{A_j}{A_i}e^{j(\theta_j-\theta_i)}}{j2\frac{C}{G_L}}. \tag{2.51}$$

Substituting $\frac{C}{G_L} = \frac{Q}{\omega_i}$ into (2.51) gives

$$H_i(\bar{A},\bar{\theta}) = \left.\frac{Y_i}{\partial Y_i/\partial \omega}\right|_{\omega_i} = j\frac{\omega_i\mu}{2Q}\left(\alpha_i^2 - A_i^2\right) + j\frac{\omega_i}{2Q}\sum_{j=1}^{N}\kappa_{ij}\frac{A_j}{A_i}e^{j(\theta_j-\theta_i)}, \tag{2.52}$$

where κ_{ij} is the complex coupling coefficient defined as

$$\kappa_{ij} = -\frac{Y_{ij}}{G_L}. \tag{2.53}$$

Defining

$$S = \sum_{j=1}^{N}\kappa_{ij}\frac{A_j}{A_i}e^{j(\theta_j-\theta_i)}, \tag{2.54}$$

we obtain

$$\begin{aligned} H_i(\bar{A},\bar{\theta}) &= j\frac{\omega_i\mu}{2Q}\left(\alpha_i^2 - A_i^2\right) + j\frac{\omega_i}{2Q}\left[Re(S) + jIm(S)\right] \\ &= j\frac{\omega_i\mu}{2Q}\left(\alpha_i^2 - A_i^2\right) + j\frac{\omega_i}{2Q}Re(S) - \frac{\omega_i}{2Q}Im(S) \end{aligned} \tag{2.55}$$

The amplitude and phase dynamics are

$$\begin{aligned} \frac{dA_i}{dt} &= A_i Im\left[H_i(\bar{A},\bar{\theta})\right] = \frac{\omega_i\mu}{2Q}\left(\alpha_i^2 - A_i^2\right)A_i + \frac{\omega_i}{2Q}A_i Re(S) \\ \frac{d\theta_i}{dt} &= \omega_i - Re\left[H_i(\bar{A},\bar{\theta})\right] = \omega_i + \frac{\omega_i}{2Q}Im(S) \\ & i = 1, 2, \cdots, N. \end{aligned} \tag{2.56}$$

Taking (2.54) into (2.56) gives

$$\begin{aligned} \frac{dA_i}{dt} &= \frac{\omega_i\mu}{2Q}\left(\alpha_i^2 - A_i^2\right)A_i + \frac{\omega_i}{2Q}\sum_{j=1}^{N}A_j Re\left[\kappa_{ij}e^{j(\theta_j-\theta_i)}\right] \\ \frac{d\theta_i}{dt} &= \omega_i + \frac{\omega_i}{2Q}\sum_{j=1}^{N}Im\left[\kappa_{ij}\frac{A_j}{A_i}e^{j(\theta_j-\theta_i)}\right] \\ & i = 1, 2, \cdots, N. \end{aligned} \tag{2.57}$$

2.4 Series Resonance Circuit

Fig. 2.4 shows the resonant circuit in series, which can be used to represent the narrow-band microwave oscillators. The negative resistance $R_d(|V|)$ is assumed to be independent of frequency and is a function of the amplitude of oscillation only. V_{inj} represents the injected signal brought by the coupled oscillators.

By the Kirchhoff's Voltage Laws and circuit analysis, the circuit equation for fig. 2.4 is simply

$$V_{inj} = V_c + V_L + V + V_{-Rd}. \tag{2.58}$$

Using the Ohm's Law for the capacitor and inductor, we obtain

$$V_{inj} = \frac{1}{C}\int idt + L\frac{di}{dt} + V + (-R_d(|V|)\cdot i) \tag{2.59}$$

where i is the instantaneous current flowing through the circuit and equal to

$$i = \frac{V}{R_L} \tag{2.60}$$

by the Ohm's Law. Substituting (2.60) into (2.59), it becomes

$$V_{inj} = \frac{1}{CR_L}\int V dt + L\frac{d\frac{V}{R_L}}{dt} + V - R_d(|V|)\frac{V}{R_L} \tag{2.61}$$

which can also be written as

$$V_{inj} = \frac{1}{CR_L}\int V dt + \frac{L}{R_L}\frac{dV}{dt} + V - \frac{R_d(|V|)}{R_L}V. \tag{2.62}$$

Multiplying $\frac{R_L}{L}$ at both ends of the equation, (2.62) can be written as

$$\frac{R_L}{L}V_{inj} = \frac{1}{CR_L}\cdot\frac{R_L}{L}\int V dt + \frac{dV}{dt} + \frac{R_L}{L}V - \frac{R_L}{L}\frac{R_d(|V|)}{R_L}V. \tag{2.63}$$

The Q-factor of this series circuit in fig. 2.4 is defined as

$$Q = \frac{\omega_0 L}{R_L} = \frac{1}{\omega_0 R_L C}. \tag{2.64}$$

Thus

$$R_L = \frac{\omega_0 L}{Q}. \tag{2.65}$$

Substituting (2.65) into (2.63), we derive

$$\frac{\frac{\omega_0 L}{Q}}{L} V_{inj} = \frac{1}{CL}\int V dt + \frac{dV}{dt} + V\frac{\frac{\omega_0 L}{Q}}{L}\left[1 - \frac{R_d(|V|)}{R_L}\right]. \tag{2.66}$$

It can be shown that the resonant frequency ω_0 must be defined as

$$\omega_0 = \frac{1}{\sqrt{LC}}. \tag{2.67}$$

Substituting (2.67) into (2.66) gives

$$\frac{\omega_0}{Q} V_{inj} = \omega_0^2 \int V dt + \frac{dV}{dt} + V\frac{\omega_0}{Q}\left[1 - \frac{R_d(|V|)}{R_L}\right]. \tag{2.68}$$

which can be rewritten as

$$\frac{dV}{dt} + \omega_0^2 \int V dt + V\frac{\omega_0}{Q}\left[1 - \frac{R_d(|V|)}{R_L}\right] = \frac{\omega_0}{Q} V_{inj} \tag{2.69}$$

where ω_0 is the resonant angular frequency of the circuit, V is the output voltage in phasor domain, Q is the Q-factor of the embedded network, and V_{inj} represents any externally injected signals from the coupled neighbors. With the Q-factor sufficiently high, the oscillator frequency will remain close to ω_0 and the amplitude and phase terms will be slowly varying functions of time (compared with the period of oscillation). The output voltage can then be written as

$$V = A(t)e^{j(\omega_0 t + \phi(t))} = A(t)e^{j\theta(t)} \tag{2.70}$$

where A is the amplitude of oscillation, and θ is the instantaneous phase. The integral in (2.69) can be integrated by parts

$$\int V dt = \frac{-2jV}{\omega_0} + \frac{1}{\omega_0^2}\frac{dV}{dt} + \cdots . \tag{2.71}$$

Under the assumption of slowly varying parameters, the higher order differential terms in (2.71) can be neglected.

Similar to (2.21), the device saturation is modeled by a quadratic function such that

$$1 - \frac{R_d}{R_l} \cong \mu\left(\alpha_0^2 - |V|^2\right) \tag{2.72}$$

where α_0 is the free-running amplitude of oscillation, and μ is an empirical nonlinearity parameter describing the oscillator. This expression is consistent with the Barkhausen Criterion for oscillation. Substituting (2.71) and (2.72) into (2.69) obtains

$$\frac{dV}{dt} = V\left[\frac{\mu\omega_0}{2Q}\left(\alpha_0^2 - |V|^2\right) + j\omega_0\right] + \frac{\omega_0}{2Q}V_{inj}. \tag{2.73}$$

Then substituting (2.70) into (2.73) and equaling the real and imaginary parts of the equation separately, the amplitude and phase dynamics are obtained as

$$\frac{dA}{dt} = \mu\frac{\omega_0}{2Q}A\left(\alpha_0^2 - |A|^2\right) + \frac{\omega_0}{2Q}ARe\left\{\frac{V_{inj}}{V}\right\} \tag{2.74}$$

$$\frac{d\theta}{dt} = \omega_0 + \frac{\omega_0}{2Q}Im\left\{\frac{V_{inj}}{V}\right\}. \tag{2.75}$$

where Re and Im denote the real and imaginary parts of the bracketed expression, respectively.

For a system of coupled oscillators, the mutual interaction between oscillators i and j is described by a complex coupling coefficient κ_{ij}, which can be written as

$$\kappa_{ij} \equiv \epsilon_{ij}e^{-j\phi_{ij}}. \tag{2.76}$$

For most arrays, the reciprocity theorem will hold so that $\kappa_{ij} = \kappa_{ji}$. In a system of N oscillators, the injected signal at the i^{th} oscillator can be written as

$$V_{inj} = \sum_{j=1}^{N} \kappa_{ij} V_j. \tag{2.77}$$

where V_i represents the output voltage of the i^{th} oscillator in phasor domain. For some types of coupling, such as radiative interaction between antennas or transmission-line coupling circuits, the κ_{ij} can be directly related to commonly used N-port network parameters [8]. In other cases where the coupling mechanism is considerably more complicated or not well understood, such as coupling through the modes of an external cavity, simple experiments may be performed to determine the coupling parameters for a particular system [7]. Substituting (2.77) into (2.73), the system dynamics are derived as

$$\frac{dV_i}{dt} = V_i \left[\frac{\mu\omega_i}{2Q} \left(\alpha_i^2 - |V_i|^2 \right) + j\omega_i \right] + \frac{\omega_i}{2Q} \sum_{j=1}^{N} \kappa_{ij} V_j. \tag{2.78}$$

where the subscript i represents the ith oscillator. For simplicity, the Q- and μ-factors are assumed to be approximately the same for all of the oscillators. Taking $V_i = A_i e^{\theta_i}$ into (2.78), the amplitude and phase dynamics for an oscillator array with arbitrary coupling network are given by [5]

$$\frac{dA_i}{dt} = \frac{\mu\omega_i}{2Q} \left(\alpha_i^2 - A_i^2 \right) A_i + \frac{\omega_i}{2Q} \sum_{j=1}^{N} A_j Re \left\{ \kappa_{ij} e^{j(\theta_j - \theta_i)} \right\} \tag{2.79}$$

$$\frac{d\theta_i}{dt} = \omega_i + \frac{\omega_i}{2Q} \sum_{j=1}^{N} Im \left\{ \kappa_{ij} \frac{A_j}{A_i} e^{j(\theta_j - \theta_i)} \right\}$$

$$i = 1, 2, \cdots, N. \tag{2.80}$$

where κ_{ij} represents the coupling parameter between i^{th} element and j^{th} element, μ is an empirical nonlinearity parameter describing the oscillator and Q is the quality factor of the RLC resonant circuit. The parameters, α_i and ω_i, are the free running amplitude and frequency respectively.

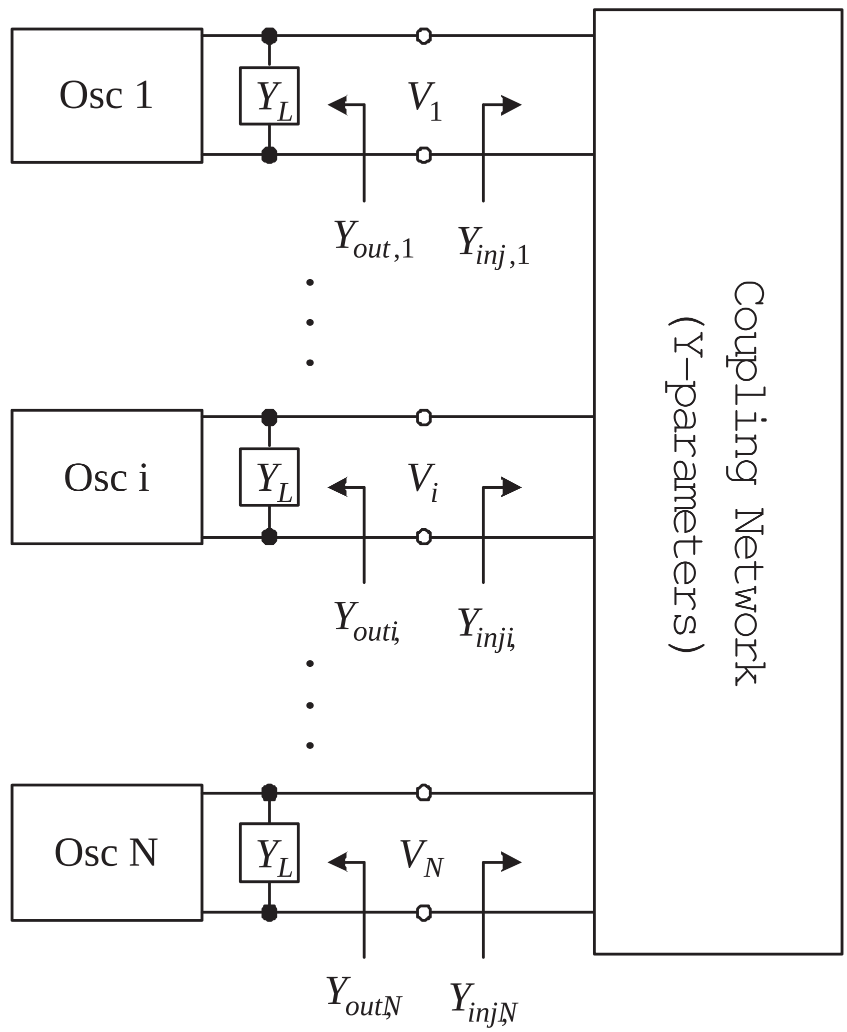

Figure 2.3: System diagram of oscillator array with arbitrary coupling network represented using Y parameter.

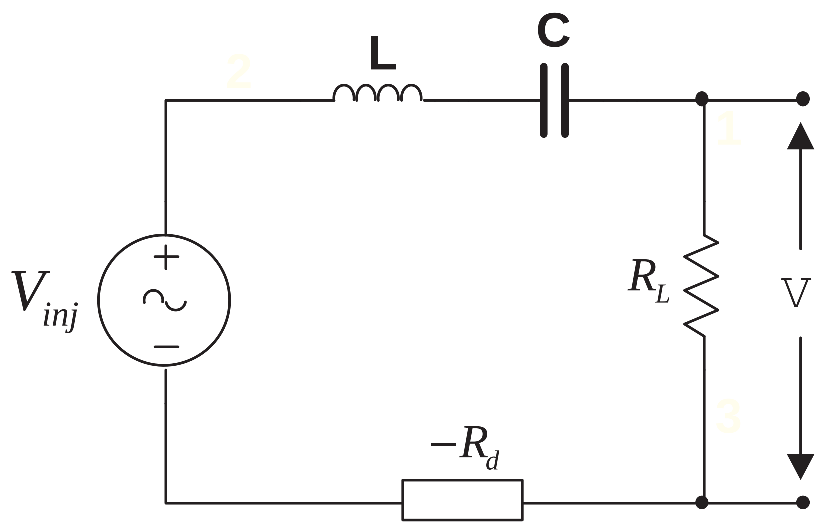

Figure 2.4: The circuit model for narrow-band microwave oscillators where V_{inj} denotes the injected signals from the neighboring oscillators and $-R_d$ denotes negative resistance of the device.

CHAPTER 3

BEAM-STEERING ANALYSIS IGNORING AMPLITUDE DYNAMICS

3.1 Application of Nonlinear Control Theory to Coupled Oscillator Array

Since there exist multiple solutions or modes which satisfy the system dynamics equations [5], it can not be guaranteed that this nonlinear system always has a stable solution. For a better understanding of the system behaviors, the stability and mode analysis were discussed in [24, 6]. This section presents a new approach to the analysis of system behaviors of coupled oscillator arrays based on classic nonlinear control theory. The stability of the system and nonlinear phenomena are investigated from a new perspective. The new theory demonstrates that there exist only one stable mode when the phase shifts are in a limited region. The state model of system dynamics is derived with phase shift $\Delta\theta$ as the state variable, and the stable equilibrium point is analytically solved. The existence and uniqueness of the solution for such a nonlinear system are also studied. The 2-D and 3-D phase portraits are shown and the qualitative behaviors of such arrays are discussed. Then practical issues in the design of coupled oscillator array are considered. The influence of the coupling parameter on the detuning accuracy of oscillators is examined. Results of Monte Carlo simulation are presented and demonstrate the influence of randomness in the free running frequencies under different coupling strengths.

3.1.1 Autonomous Systems

In mathematics, an autonomous system or autonomous differential equation is a system of ordinary differential equations which does not depend on the independent variable [25].

DEFINITION 3.1.1 *The system is an autonomous system if it can be described by the ordinary differential equations of the form*

$$\dot{\boldsymbol{x}} = f(\boldsymbol{x})$$

where $\boldsymbol{x}$ *takes values in n-dimensional Euclidean space and is usually a function of time, and also* $\dot{x}$ *denotes the derivative of* x *with respect to time variable* t.

It is distinguished from the non-autonomous systems which were described by the differential equations of the form

$$\dot{\boldsymbol{x}} = f(t, \boldsymbol{x})$$

in which f is not just function of x, but also of time.

We call

$$\dot{\boldsymbol{x}} = f(\boldsymbol{x})$$

the state equation or state-space model and refer to x as the state. If the system has an input, then

$$\dot{\boldsymbol{x}} = f(\boldsymbol{x}, \boldsymbol{u})$$

.

The nonlinear oscillator array is an autonomous system. Recall the phase dynamics is described by

$$\frac{d\theta_i}{dt} = \omega_i + \frac{\omega_i}{2Q} \sum_{j=1}^{N} Im \left\{ \kappa_{ij} \frac{A_j}{A_i} e^{j(\theta_j - \theta_i)} \right\}$$

$$i = 1, 2, \cdots, N. \tag{3.1}$$

For a linear oscillator array, in general, the coupling will be designed only between the adjacent elements and the phase of the coupling coefficients is chosen to be 0 for simplicity.

$$\kappa_{ij} = \begin{cases} \epsilon & \text{if } |i - j| = 1 \\ 0 & \text{otherwise} \end{cases} \tag{3.2}$$

Therefore, (3.1) can be simplified and written as

$$\frac{d\theta_i}{dt} = \omega_i - \frac{\omega_i \epsilon}{2Q} \sum_{\substack{j=i-1 \\ j \neq i}}^{i+1} \frac{A_j}{A_i} sin(\theta_i - \theta_j)$$

$$i = 1, 2, \cdots, N. \tag{3.3}$$

Also let's assume the oscillator array has a uniform amplitude distribution, such that $A_i = 1$. We obtained

$$\frac{d\theta_i}{dt} = \omega_i - \omega_i \epsilon^{'} \left[sin(\theta_i - \theta_{i-1}) + sin(\theta_i - \theta_{i+1}) \right]$$

$$i = 1, 2, \cdots, N. \tag{3.4}$$

where the new variable $\epsilon^{'} = \frac{\epsilon}{2Q}$.

We know that the radiation pattern of a phased antenna array is steered in a desired direction by achieving a constant phase progression along the array. The main beam scanning angle of a linear array is determined by the element-to-element phase shift $\Delta\theta_i$, not θ_i. Thus the alternative state model of the system is to choose the phase shift between the adjacent element $\Delta\theta_i$ as the state variable. Still considering (3.1), and replacing i with $i-1$ gives

$$\frac{d\theta_{i-1}}{dt} = \omega_{i-1} - \omega_{i-1}\epsilon^{'}\left[sin(\theta_{i-1}-\theta_{i-2}) + sin(\theta_{i-1}-\theta_i)\right]$$
$$i = 1, 2, \cdots, N. \tag{3.5}$$

Subtracting (3.4) by (3.5), we obtained

$$\Delta\dot{\theta}_i = \omega_i\left[1-\epsilon^{'}sin\Delta\theta_i + \epsilon^{'}sin\Delta\theta_{i+1}\right] - \omega_{i-1}\left[1-\epsilon^{'}sin\Delta\theta_{i-1} + \epsilon^{'}sin\Delta\theta_i\right]$$
$$\Delta\dot{\theta}_i = \epsilon^{'}\omega_{i-1}sin\Delta\theta_{i-1} - \epsilon^{'}(\omega_i+\omega_{i-1})sin\Delta\theta_i + \epsilon^{'}\omega_i sin\Delta\theta_{i+1} + \omega_i - \omega_{i-1}$$
$$i = 3, 4, \cdots, N-1. \tag{3.6}$$

where we defined that

$$\Delta\theta_i = \theta_i - \theta_{i-1}$$
$$\Delta\theta_{i-1} = \theta_{i-1} - \theta_{i-2}$$
$$\Delta\theta_{i+1} = \theta_{i+1} - \theta_i \tag{3.7}$$

While $i = 2$, $\Delta\theta_1 = \theta_1 - \theta_0$. since θ_0 does not exist, it means that $\Delta\theta_1$ does not exist. Thus the first equation is

$$\Delta\dot{\theta}_2 = -\epsilon^{'}(\omega_2+\omega_1)sin\Delta\theta_2 + \epsilon^{'}\omega_2 sin\Delta\theta_3 + \omega_2 - \omega_1. \tag{3.8}$$

Similarly, while $i = N$, $\Delta\theta_{N+1}$ does not exist. Therefore the last equation is

$$\Delta\dot{\theta}_N = \epsilon^{'}\omega_{N-1}sin\Delta\theta_{N-1} - \epsilon^{'}(\omega_N+\omega_{N-1})sin\Delta\theta_N + \omega_N - \omega_{N-1}. \tag{3.9}$$

Finally the state model of choosing the phase shift $\Delta\theta$ as the state variable is given as

$$
\begin{aligned}
\Delta\dot{\theta}_2 &= -\epsilon^{'}(\omega_2+\omega_1)sin\Delta\theta_2 + \epsilon^{'}\omega_2 sin\Delta\theta_3 + \omega_2 - \omega_1 \\
\Delta\dot{\theta}_i &= \epsilon^{'}\omega_{i-1}sin\Delta\theta_{i-1} - \epsilon^{'}(\omega_i+\omega_{i-1})sin\Delta\theta_i + \epsilon^{'}\omega_i sin\Delta\theta_{i+1} + \omega_i - \omega_{i-1} \\
&\vdots \\
\Delta\dot{\theta}_N &= \epsilon^{'}\omega_{N-1}sin\Delta\theta_{N-1} - \epsilon^{'}(\omega_N+\omega_{N-1})sin\Delta\theta_N + \omega_N - \omega_{N-1}
\end{aligned}
\tag{3.10}
$$

Its vector form will be simply denoted as

$$
\boldsymbol{\Delta\dot{\theta}} = f(\boldsymbol{\Delta\theta}), \tag{3.11}
$$

which shows that the alternative state model of oscillator array is also an autonomous system. Compared with the state model with variable θ, the model with variable $\Delta\theta$ is more interesting and useful for us to investigate.

3.1.2 Equilibrium Points

Before we can analyze the phenomena of the nonlinear oscillator system, there are several definitions and theorems need to be understood. The theory including part of definitions and theorems are referred from [26].

Definition 3.1.2 *A point $\boldsymbol{x} = \boldsymbol{x}^*$ in the state space is said to be an equilibrium point of* (3.11) *if it has the property that whenever the state of the system starts at $\boldsymbol{x}^*$, it will remain at $\boldsymbol{x}^*$ for all future time. For the autonomous system, the equilibrium points are the real roots of the equation*

$$
f(\boldsymbol{x}) = 0
$$

Considering the coupled oscillator array system, the equation for deriving the equilibrium points is $f(\boldsymbol{\Delta\theta}) = 0$. These equations are

$$
\begin{aligned}
0 &= -\epsilon^{'}(\omega_2+\omega_1)sin\Delta\theta_2 + \epsilon^{'}\omega_2 sin\Delta\theta_3 + \omega_2 - \omega_1 \\
0 &= \epsilon^{'}\omega_2 sin\Delta\theta_2 - \epsilon^{'}(\omega_3+\omega_2)sin\Delta\theta_3 + \epsilon^{'}\omega_3 sin\Delta\theta_4 + \omega_3 - \omega_2 \\
0 &= \epsilon^{'}\omega_{i-1} sin\Delta\theta_{i-1} - \epsilon^{'}(\omega_i+\omega_{i-1})sin\Delta\theta_i + \epsilon^{'}\omega_i sin\Delta\theta_{i+1} + \omega_i - \omega_{i-1} \\
&\vdots \\
0 &= \epsilon^{'}\omega_{N-1} sin\Delta\theta_{N-1} - \epsilon^{'}(\omega_N+\omega_{N-1})sin\Delta\theta_N + \omega_N - \omega_{N-1} \qquad (3.12)
\end{aligned}
$$

Several conclusions are obtained by examining the equation (3.12). First, the equation becomes linear if we consider $sin\Delta\theta_i$ as the variable instead of θ_i. Second, the solution of these equations or the equilibrium points are determined by the constant $\epsilon^{'}$ and the values of ω_i, where $i = 1, 2, 3 \cdots, N$. The constant $\epsilon^{'}$ is the coupling strength between adjacent elements of the oscillator array. It should be a fixed number in the design of such an array, since the couplings are difficult to control comparing with the free running frequency ω_i. Different equilibrium points of (3.11) may be obtained by choosing different sets of free running frequencies.

In the case of linear oscillator array, the desired equilibrium point is $\Delta\theta_i = \Delta\theta_{i-1} = \Delta\theta_{i+1} = \Delta\theta$. Let us choose the following set of free running frequencies

$$
\omega_i = \begin{cases} \frac{\omega_s}{1+\epsilon^{'}sin\Delta\theta_2} & \text{if } i = 1 \\ \omega_s & \text{if } 1 < i < N \\ \frac{\omega_s}{1-\epsilon^{'}sin\Delta\theta_N} & \text{if } i = N \end{cases} \qquad (3.13)
$$

Substituting $\omega_1 = \frac{\omega_s}{1+\epsilon^{'} sin\Delta\theta_2}$ and $\omega_2 = \omega_s$ into the first equation of (3.12), we obtain

$$
\begin{aligned}
0 &= -\epsilon^{'}(\omega_2+\omega_1)sin\Delta\theta_2 + \epsilon^{'}\omega_2 sin\Delta\theta_3 + \omega_2 - \omega_1 \\
\omega_2\left(1-\epsilon^{'}sin\Delta\theta_2+\epsilon^{'}sin\Delta\theta_3\right) &= \omega_1\left(1+\epsilon^{'}sin\Delta\theta_2\right) \\
\omega_s\left(1-\epsilon^{'}sin\Delta\theta_2+\epsilon^{'}sin\Delta\theta_3\right) &= \frac{\omega_s\left(1+\epsilon^{'}sin\Delta\theta_2\right)}{1+\epsilon^{'}sin\Delta\theta_2} \\
sin\Delta\theta_2 &= sin\Delta\theta_3
\end{aligned}
\tag{3.14}
$$

In next section, it will be shown that for this equilibrium point to be stable, $-\frac{\pi}{2} < \theta_i < \frac{\pi}{2}$, in which region, *sin* is a monotonic function. Therefore we may obtain

$$\Delta\theta_2 = \Delta\theta_3. \tag{3.15}$$

Similarly, by substituting $\omega_N = \frac{\omega_s}{1-\epsilon^{'} sin\Delta\theta_N}$ and $\omega_{N-1} = \omega_s$ into the last equation of (3.12), we may obtain

$$\Delta\theta_N = \Delta\theta_{N-1}. \tag{3.16}$$

Now let us examine the second equation of (3.12). By substituting $\omega_2 = \omega_3 = \omega_s$ and $\Delta\theta_2 = \Delta\theta_3$, we can easily solve

$$\Delta\theta_3 = \Delta\theta_4. \tag{3.17}$$

In a similar manner, we can obtain

$$\Delta\theta_4 = \Delta\theta_5 = \cdots = \Delta\theta_{N-1}. \tag{3.18}$$

Finally, we have

$$\Delta\theta_2 = \Delta\theta_3 = \cdots = \Delta\theta_N = \Delta\theta. \tag{3.19}$$

A special equilibrium point is obtained by choosing the free running frequency as listed in (3.13).

3.1.3 Linearization

With the definitions above, the stability of the equilibrium points for the nonlinear system is investigated by the next theorem.

Theorem 3.1.3 (Lyapunov's indirect method) *Let $\boldsymbol{x} = \boldsymbol{x}^*$ be an equilibrium point for the nonlinear system*

$$\dot{\boldsymbol{x}} = f(\boldsymbol{x})$$

where $f : D \to R^n$ is continuously differentiable and D is a neighborhood of the origin. Let

$$A = \frac{\partial f}{\partial x}(\boldsymbol{x})\bigg|_{\boldsymbol{x}=\boldsymbol{x}^*}$$

Then,

1. *The equilibrium point is asymptotically stable if $Re\lambda_i < 0$ for all eigenvalues of A.*

2. *The equilibrium point is unstable if $Re\lambda_i > 0$ for one or more of eigenvalues of A.*

The theorem suggests that the nonlinear system

$$\dot{\boldsymbol{x}} = f(\boldsymbol{x})$$

can be approximated by its linearization or the linearized system about the equilibrium point x^*

$$\dot{\boldsymbol{x}} = A\boldsymbol{x}$$

, where $A = \frac{\partial f}{\partial \boldsymbol{x}}(\boldsymbol{x} = \boldsymbol{x}^*)$.

Now consider the state equations that modeled the nonlinear system of oscillator array $\boldsymbol{\Delta\dot{\theta}} = f(\boldsymbol{\Delta\theta})$, which are repeated here as

$$
\begin{aligned}
\Delta\dot{\theta}_2 &= -\epsilon^{'}(\omega_2+\omega_1)sin\Delta\theta_2 + \epsilon^{'}\omega_2 sin\Delta\theta_3 + \omega_2 - \omega_1 \\
\Delta\dot{\theta}_i &= \epsilon^{'}\omega_{i-1}sin\Delta\theta_{i-1} - \epsilon^{'}(\omega_i+\omega_{i-1})sin\Delta\theta_i + \epsilon^{'}\omega_i sin\Delta\theta_{i+1} + \omega_i - \omega_{i-1} \\
&\vdots \\
\Delta\dot{\theta}_N &= \epsilon^{'}\omega_{N-1}sin\Delta\theta_{N-1} - \epsilon^{'}(\omega_N+\omega_{N-1})sin\Delta\theta_N + \omega_N - \omega_{N-1}
\end{aligned}
\tag{3.20}
$$

The A matrix of the linearized system can be obtained as

$$
A = \begin{bmatrix} \frac{\partial f_1}{\partial\Delta\theta_1} & \frac{\partial f_1}{\partial\Delta\theta_2} & \cdots & \frac{\partial f_1}{\partial\Delta\theta_N} \\ \cdots & \ddots & \ddots & \vdots \\ \frac{\partial f_N}{\partial\Delta\theta_1} & \frac{\partial f_N}{\partial\Delta\theta_2} & \cdots & \frac{\partial f_N}{\partial\Delta\theta_N} \end{bmatrix}. \tag{3.21}
$$

and substituting the derivatives which can be obtained from (3.20) into (3.21), we derived

$$
A = \epsilon^{'} \begin{bmatrix} -(\omega_1+\omega_2)cos\Delta\theta_2 & \omega_2 cos\Delta\theta_3 & 0 & \cdots & 0 \\ \omega_2 cos\Delta\theta_2 & -(\omega_2+\omega_3)cos\Delta\theta_3 & \omega_3 cos\Delta\theta_4 & \cdots & 0 \\ 0 & \omega_3 cos\Delta\theta_3 & -(\omega_3+\omega_4)cos\Delta\theta_4 & \cdots & 0 \\ \vdots & \vdots & \vdots & \ddots & \vdots \\ 0 & 0 & 0 & \omega_{N-1}cos\Delta\theta_{N-1} & -(\omega_{N-1}+\omega_N)cos\Delta\theta_N \end{bmatrix}. \tag{3.22}
$$

Suppose $\boldsymbol{\Delta\theta^*}$ is an equilibrium point of state equation (3.20) and $\boldsymbol{\Delta\theta^*} \equiv Constant$ which means $\Delta\theta_i = \Delta\theta_{i-1} = \Delta\theta_{i+1} = \Delta\theta$, and it can be shown that such equilibrium point can be established by controlling the free-running frequencies ω_i of the oscillators.

Substituting all the states with the single constant $\Delta\theta$, we obtained

$$A = \epsilon' \begin{bmatrix} -(\omega_1+\omega_2) & \omega_2 & 0 & \cdots & 0 \\ \omega_2 & -(\omega_2+\omega_3) & \omega_3 & \cdots & 0 \\ 0 & \omega_3 & -(\omega_3+\omega_4) & \cdots & 0 \\ \vdots & \vdots & \vdots & \ddots & \vdots \\ 0 & 0 & 0 & \omega_{N-1} & -(\omega_{N-1}+\omega_N) \end{bmatrix}. \tag{3.23}$$

Now let us try to solve the sets of ω_i for establishing the equilibrium point $\Delta\theta^* = \Delta\theta$. While $2 \leq i \leq N-1$, we have

$$\begin{aligned} \Delta\dot{\theta}_i &= \omega_i \left[1 - \epsilon' sin\Delta\theta_i + \epsilon' sin\Delta\theta_{i+1}\right] - \omega_{i-1}\left[1 - \epsilon' sin\Delta\theta_{i-1} + \epsilon' sin\Delta\theta_i\right] = 0 \\ \Delta\dot{\theta}_i &= \omega_i \left[1 - \epsilon' sin\Delta\theta + \epsilon' sin\Delta\theta\right] - \omega_{i-1}\left[1 - \epsilon' sin\Delta\theta + \epsilon' sin\Delta\theta\right] = 0 \\ \Delta\dot{\theta}_i &= \omega_i - \omega_{i-1} = 0 \\ \omega_i &= \omega_{i-1} = \omega_{syc} \end{aligned} \tag{3.24}$$

where ω_{syc} is called the synchronized frequency.

Definition 3.1.4 (Synchronized frequency) *Given all the oscillator frequencies lie within some collective locking bandwidth, they will eventually synchronize to a common frequency ω_{syc}, where $\frac{d\theta}{dt} = \omega_{syc}$ at the steady state for all i.*

While $i = 2$, we obtained

$$\begin{aligned} \Delta\dot{\theta}_2 &= \omega_2 \left[1 - \epsilon' sin\Delta\theta_2 + \epsilon' sin\Delta\theta_3\right] - \omega_1\left[1 + \epsilon' sin\Delta\theta_2\right] = 0 \\ \Rightarrow \Delta\dot{\theta}_2 &= \omega_2 \left[1 - \epsilon' sin\Delta\theta + \epsilon' sin\Delta\theta\right] - \omega_1\left[1 + \epsilon' sin\Delta\theta\right] = 0 \\ \Rightarrow \omega_1 &= \frac{\omega_2}{1+\epsilon' sin\Delta\theta} = \frac{\omega_{syc}}{1+\epsilon' sin\Delta\theta} \end{aligned} \tag{3.25}$$

Similarly, for $i = N$

$$\omega_N = \frac{\omega_{N-1}}{1 - \epsilon' sin\Delta\theta} = \frac{\omega_{syc}}{1 - \epsilon' sin\Delta\theta} \tag{3.26}$$

With the derivation above, the constant phase progression $\Delta\theta$ can be achieved by the following free-running frequencies

$$\omega_i = \begin{cases} \frac{\omega_{syc}}{1+\epsilon' sin\Delta\theta} & \text{if } i = 1 \\ \omega_{syc} & \text{if } 1 < i < N \\ \frac{\omega_{syc}}{1-\epsilon' sin\Delta\theta} & \text{if } i = N \end{cases} \tag{3.27}$$

It is noted that all the inner oscillators have the same frequency. It means that once the synchronized frequency is fixed the phase progression $\Delta\theta$ will be controlled only by the free-running frequencies of the two edge elements.

Substituting the solved free-running frequencies into (3.23), we obtained

$$A = \epsilon' cos(\Delta\theta) \begin{bmatrix} -(\omega_1 + \omega_{syc}) & \omega_{syc} & 0 & \cdots & 0 \\ \omega_{syc} & -2\omega_{syc} & \omega_{syc} & \cdots & 0 \\ 0 & \omega_{syc} & -2\omega_{syc} & \cdots & 0 \\ \vdots & \vdots & \vdots & \ddots & \vdots \\ 0 & 0 & 0 & \omega_{syc} & -(\omega_{syc} + \omega_N) \end{bmatrix} \tag{3.28}$$

which is a symmetric tri-diagonal matrix. The eigenvalues is negative if all of its diagonal elements are less than zero and that requires $cos\Delta\theta > 0$. Thus in this special case, the phase progression is limited to the range of $-\frac{\pi}{2} < \Delta\theta < \frac{\pi}{2}$ in order to make the equilibrium point $\Delta\theta$ to be stable.

Moreover the phase progression along the array is related to the main beam direction as

$$\Delta\theta = \frac{2\pi d}{\lambda_0} sin\varphi, \tag{3.29}$$

where φ is the main beam direction from broadside, d is the spacing between adjacent elements of the array and λ_0 is the wavelength with respect to the synchronized frequency. Therefore the scan angle of main beam is also limited. For example, for a linear array $d = \lambda/2$, the scan range is around $-30^o < \varphi < 30^o$ from broadside.

3.1.4 Existence and Uniqueness of Solutions

In this chapter, the existence and uniqueness of the solutions of nonlinear system will be investigated. These properties are essential for the state equation

$$\boldsymbol{\Delta}\dot{\boldsymbol{\theta}} = f(\boldsymbol{\Delta\theta})$$

to be a useful mathematical model of the oscillator array. For a deterministic system of oscillator array, we expect that if we could repeat the experiment exactly, we would exactly obtain the same phase progression at some $t > t_0$, where t_0 is the initial time.

DEFINITION 3.1.5 *A real valued function f is called Lipschitz continuous or is said to satisfy a Lipschitz condition if there exists a constant L such that*

$$\|f(t, x_2) - f(t, x_1)\| \leq L \|x_2 - x_1\|, \tag{3.30}$$

for all x_1 and x_2 in some neighborhood of x_0. The function satisfying (3.30) *is said to be Lipschitz in x, and the positive constant L is called a Lipschitz constant. [26]*

where $\|.\|$ denotes arbitrary norm of a vector.

The Lipschitz condition is defined by the non-autonomous system, however it is obvious that for autonomous system the definition is also valid. From now on we will only focus on the Lipschitz condition, Existence and Uniqueness for autonomous system, thus we will drop off the time argument t for the later definitions or theorems. Since the Lipschitz condition can be written as

$$\frac{|f(x_2) - f(x_1)|}{|x_2 - x_1|} \leq L,$$

any function $f(x)$ that has infinite slope at some point is not locally Lipschitz at that point. It can be proved that the Lipschitz condition is weaker than the continuous differentiability, as stated in the next lemma.

LEMMA 3.1.6 *If $f(t,x)$ and $[\partial f/\partial x](t,x)$ are continuous on $[a,b] \times R^n$, then f is globally Lipschitz in x on $[a,b] \times R^n$ if and only if $[\partial f/\partial x]$ is uniformly bounded on $[a,b] \times R^n$. [26]*

With the definition and derived property of Lipschitz condition, we can introduce the theorem of the Global Existence and Uniqueness.

THEOREM 3.1.7 (GLOBAL EXISTENCE AND UNIQUENESS) *Suppose that $f(x)$ is piecewise continuous in t and satisfies the Lipschitz condition*

$$\|f(x_2) - f(x_1)\| \leq L \|x_2 - x_1\|$$

$\forall x, y \in R^n, \forall t \in [t_0, t_1]$. *Then the state equation $\dot{\boldsymbol{x}} = f(\boldsymbol{x})$, with $x(t_0) = x_0$, has a unique solution over $[t_0, t_1]$. [26]*

The sets of differential equations modeling the phase dynamics of the oscillator array $\boldsymbol{\Delta\dot{\theta}} = f(\boldsymbol{\Delta\theta})$ is given by (3.20). The Jacobian matrix $A = \left[\frac{\partial \vec{f}}{\partial \Delta\vec{\theta}}\right]$ is given by

$$A = \epsilon' \begin{bmatrix} -(\omega_1+\omega_2)cos\Delta\theta_2 & \omega_2 cos\Delta\theta_3 & 0 & \cdots & 0 \\ \omega_2 cos\Delta\theta_2 & -(\omega_2+\omega_3)cos\Delta\theta_3 & \omega_3 cos\Delta\theta_4 & \cdots & 0 \\ 0 & \omega_3 cos\Delta\theta_3 & -(\omega_3+\omega_4)cos\Delta\theta_4 & \cdots & 0 \\ \vdots & \vdots & \vdots & \ddots & \vdots \\ 0 & 0 & 0 & \omega_{N-1}cos\Delta\theta_{N-1} & -(\omega_{N-1}+\omega_N)cos\Delta\theta_N \end{bmatrix}. \qquad (3.31)$$

We need to introduce the matrix norm $\left\|\frac{\partial \vec{f}}{\partial \vec{\Delta\theta}}\right\|$ to find a bound for all vectors $\vec{\Delta\theta}$ in R^n.

$$\left\|\frac{\partial \vec{f}}{\partial \vec{\Delta\theta}}\right\|_\infty = \epsilon^{'} max \left\{ \begin{array}{c} \left|-(\omega_1+\omega_2)cos\Delta\theta_2\right| + \left|\omega_2 cos\Delta\theta_3\right|, \\ \left|\omega_2 cos\Delta\theta_2\right| + \left|-(\omega_2+\omega_3)cos\Delta\theta_3\right| + \left|\omega_3 cos\Delta\theta_4\right|, \\ \vdots \\ \left|\omega_{N-1} cos\Delta\theta_{N-1}\right| + \left|-(\omega_{N-1}+\omega_N)cos\Delta\theta_N\right| \end{array} \right\} \tag{3.32}$$

It can be simplified as

$$\left\|\frac{\partial \vec{f}}{\partial \vec{\Delta\theta}}\right\|_\infty = \epsilon^{'} max \left\{ \begin{array}{c} \omega_1 + 2\omega_2, \\ 2\omega_2 + 2\omega_3, \\ \vdots \\ 2\omega_{N-1} + \omega_N \end{array} \right\} \tag{3.33}$$

Since ω_i, $i = 1, 2, \cdots, N$, are all real positive constant, $\frac{\partial \vec{f}}{\partial \vec{\Delta\theta}}$ is bounded for $\Delta\theta \in R^n$ and the differential equations will be globally Lipschitz. Thus the solution for a deterministic system of oscillator array exist and is unique.

3.1.5 Phase Portrait

A second-order autonomous system is described by two scalar differential equations

$$\dot{x}_1 = f_1(x_1, x_2) \tag{3.34}$$

$$\dot{x}_2 = f_2(x_1, x_2) \tag{3.35}$$

Since its solution trajectories can be represented by curves in the 2-D plane, the second-order systems play an important role in the study of nonlinear systems. The x_1-x_2 plane is generally called the phase plane or state plane. The solution trajectory starts from a certain initial state $x_0 = (x_{10}, x_{20})$, then passes through all the solution states for $t > 0$. If we repeat the process many times, the family of all trajectories or solution curves is called the phase portrait of (3.34).

For 1-D linear oscillator array, the constant phase progression is desired for beam scanning. Thus it is more suitable to use the phase difference between the adjacent element $\Delta\theta_i$ as the state variable than the instantaneous phase θ_i. The state model of choosing the phase shift $\Delta\theta$ as the state variable is given by (3.10). The order number of oscillator array system is equal to $N-1$. The oscillator array of three elements can be considered as a second-order system if we choose phase shift $\Delta\theta$ as the state variable.

The two differential equations for three elements oscillator array are written as

$$\begin{aligned}\Delta\dot{\theta}_2 &= -\epsilon^{'}(\omega_2+\omega_1)sin\Delta\theta_2+\epsilon^{'}\omega_2 sin\Delta\theta_3+\omega_2-\omega_1.\\ \Delta\dot{\theta}_3 &= \epsilon^{'}\omega_2 sin\Delta\theta_2-\epsilon^{'}(\omega_3+\omega_2)sin\Delta\theta_3+\omega_3-\omega_2.\end{aligned}\tag{3.36}$$

To find the equilibrium points, we set $\Delta\dot{\theta}_2=\Delta\dot{\theta}_3=0$ and solve for $\Delta\theta_2$ and $\Delta\theta_2$:

$$\begin{aligned}0 &= -\epsilon^{'}(\omega_2+\omega_1)sin\Delta\theta_2+\epsilon^{'}\omega_2 sin\Delta\theta_3+\omega_2-\omega_1.\\ 0 &= \epsilon^{'}\omega_2 sin\Delta\theta_2-\epsilon^{'}(\omega_3+\omega_2)sin\Delta\theta_3+\omega_3-\omega_2.\end{aligned}\tag{3.37}$$

Eq. (3.37) is useful to solve the equilibrium points.

The phase portrait is demonstrated using a design example, in which the synchronized frequency of $10GHz$ and the quality factor $Q=10$ are chosen. Following [6, 8], it is assumed that the couplings only exist between the nearest neighbors and the coupling phase is zero for simplicity. The coupling strength $\epsilon=2$ is chosen and it relates to relatively strong coupling [8]. The array spacing between antenna elements is half wavelength, $d=\lambda/2$. The desired main beam scanning angle is $\psi=16°$ from broadside. From (3.13), the frequencies of the oscillators on the edges are required to be detuned at $9.29GHz$ and $10.83GHz$, respectively. The diagram of oscillator array with the nearest neighbor couplings is given by Figure 3.1.

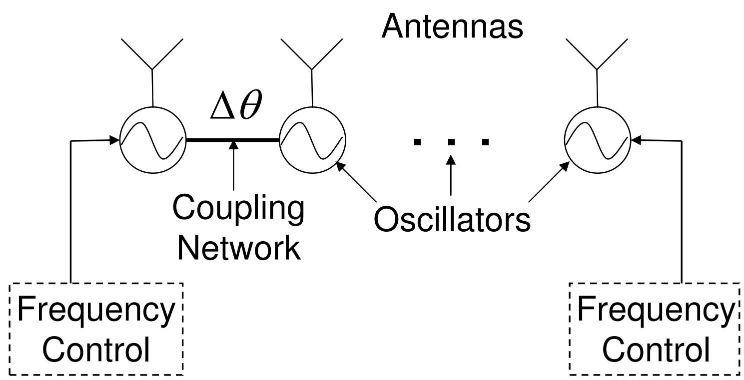

Figure 3.1: Diagram of phased array using coupled oscillators.

Figure 3.2 shows the phase portrait of a three element oscillator array without any bounding box. The small circles represent the initial state $\boldsymbol{\Delta\theta(0)} = [\Delta\theta_2(0), \Delta\theta_3(0)]^T$ with elements randomly chosen from -2π to 2π for each simulation. The red crosses represent the desired equilibrium point. Analytically, the equilibrium points can be solved by

$$\begin{bmatrix} sin\Delta\theta_2 \\ sin\Delta\theta_3 \end{bmatrix} = \begin{bmatrix} -\epsilon^{'}(\omega_2 + \omega_1) & \epsilon^{'}\omega_2 \\ \epsilon^{'}\omega_2 & -\epsilon^{'}(\omega_3 + \omega_2) \end{bmatrix} \begin{bmatrix} \omega_1 - \omega_2 \\ \omega_2 - \omega_3 \end{bmatrix} \tag{3.38}$$

Due to the periodic characteristic of the equilibrium points implied by (3.38), the nine red crosses represent the same equilibrium point, which corresponds to the desired phase shifts, $\Delta\theta_2 = \Delta\theta_3 = 49.6°$ in the region of $[0, 2\pi)$. Therefore, there exists only one stable equilibrium point for this nonlinear system, whose behavior is similar to a stable node. Moreover, the stable equilibrium point is associated

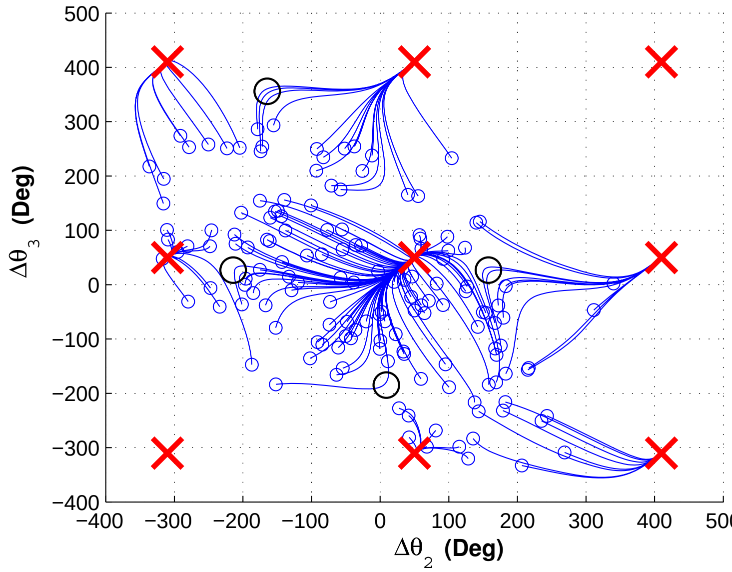

Figure 3.2: 2-D Phase portraits for 3 element oscillator array without bounding box.

with the desired phase shifts of 49.6° at the steady state. It is interesting to note that behaviors of saddle points are also observed in the phase portrait. For this three element oscillator array, these are attributed to the unstable equilibrium points $(\Delta\theta_2 = 49.6, \Delta\theta_3 = 130.4°)$, $(\Delta\theta_2 = 130.4°, \Delta\theta_3 = 49.6°)$ or $(\Delta\theta_2 = 130.4°, \Delta\theta_3 = 130.4°)$. It can also be verified by solving the eigenvalues of the Jacobian matrix, A, given by (3.28). Although the unstable equilibrium points exist, in practice the ever-present noise in the oscillator can cause the trajectories to diverge away from them and converge to the stable equilibrium point.

Figure 3.3 shows three-dimensional phase portraits for a four element oscillator array with the same associated parameters. Similar behavior of the stable equilibrium point is observed. Due to its periodic characteristics, the bounding box of the phase portrait is selected to be $-180° < \Delta\theta_i(0) < 180°$, $i = 2, 3, 4$. Limited but sufficient

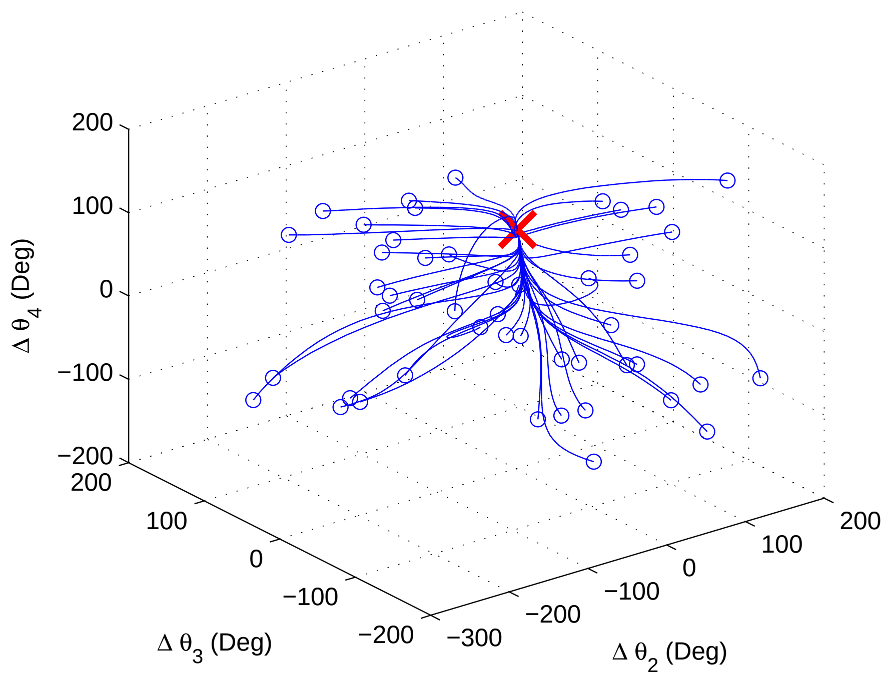

Figure 3.3: 3-D phase portraits for 4 element oscillator array with bounding box.

trajectories are shown in this 3-D phase portraits in order to provide better visibility of the convergence of states and clear observation of the location of the desired equilibrium point. In the case of a four element oscillator array, we still observe that only one stable equilibrium point exists and the states converge to this equilibrium point no matter what the initial states are. The phase portrait of an oscillator array with more than four elements can not be displayed graphically, but this theory is also true for a N element oscillator array. For those cases, instead of the phase portrait the mean value of $\Delta\theta_i$ may be computed for a similar investigation.

3.2 Linear Oscillator Array

The beam scanning technique was theoretically proposed, and experimentally applied to loosely coupled oscillator array using a four elements microstrip patch array by Liao and York [6]. The oscillators were radiatively coupled via free space and the substrate. The coupling parameters, including the coupling strength and coupling phase, were measured by an imaging technique described in [7]. Since the radiative coupling is weak and hard to control, the separation of oscillators has to be precisely adjusted for obtaining a zero coupling phase.

In their reports, free running frequencies of oscillators achieving the constant phase progression were obtained but the following assumptions were also made:

1. The solutions of free running frequency are only applicable to the case of uniform amplitude distribution.

2. Nearest neighbor coupling is assumed in the approach.

3. Amplitude dynamics are ignored since under the weak coupling amplitudes will remain at their free running values.

In this section, instead of using Liao and York's solution, a new solution of free running frequencies is derived and implemented, which can be applied to the oscillator array with arbitrary amplitude distribution. Moreover, these solutions may be applied to an oscillator array with an arbitrary coupling scheme which include non-nearest neighbor couplings. A beaming scanning technique for oscillator array with both uniform and triangular amplitude distributions is demonstrated. The amplitude dynamics are also ignored in this chapter, as in Liao's paper, but will be explored in details later.

3.2.1 Solution of Free Running Frequencies

In the assumption of weak coupling, with $\kappa_{ij} << 1$, the amplitude of the oscillators will remain close to their free-running values ($A_i \approx \alpha_i$), and the phase dynamics of the system will be described predominantly by

$$\frac{d\theta_i}{dt} = \omega_i + \frac{\omega_i}{2Q} \sum_{j=1}^{N} Im \left\{ \kappa_{ij} \frac{\alpha_j}{\alpha_i} e^{j(\theta_j - \theta_i)} \right\}$$
$$i = 1, 2, \cdots, N. \tag{3.39}$$

Since the conditions of weak coupling and uniform distribution are assumed, the amplitude dynamics may be ignored. At the steady state, it can be easily shown that all the oscillators will become synchronized to a common frequency $\frac{d\theta_i}{dt} = \omega$, which is given as

$$\omega = \omega_i \left[1 + \frac{1}{2Q} \sum_{j=1}^{N} Im \left\{ \kappa_{ij} \frac{\alpha_j}{\alpha_i} e^{j(\theta_j - \theta_i)} \right\} \right]$$
$$i = 1, 2, \cdots, N. \tag{3.40}$$

From (3.40), the free running frequency of each element can be solved as

$$\omega_i = \omega \cdot \left[1 + \frac{1}{2Q} \sum_{j=1}^{N} Im \left\{ \kappa_{ij} \frac{\alpha_j}{\alpha_i} e^{j(\theta_j - \theta_i)} \right\} \right]^{-1}$$
$$i = 1, 2, \cdots, N. \tag{3.41}$$

The relationship between the constant phase progression along the array, $\Delta\theta$, and the main beam angle ϕ for a linear array is given by

$$\Delta\theta = \frac{2\pi d}{\lambda_0} sin\phi \tag{3.42}$$

where d is the space between the adjacent elements and λ_0 is the wavelength in free space. The free running frequencies achieving a constant phase progression $\Delta\theta$ and arbitrary amplitude distribution at the steady state may be found as

$$\omega_i = \omega \cdot \left[1 + \frac{1}{2Q} \sum_{j=1}^{N} Im \left\{ \kappa_{ij} \frac{A_j}{A_i} e^{j(\Delta\theta_{ji})} \right\} \right]^{-1}$$
$$i = 1, 2, \cdots, N, \tag{3.43}$$

Furthermore, (3.43) can be simplified to its matrix form as

$$\omega_i = \omega \cdot \left(1 + \frac{1}{2Q} \cdot Im \left\{ \begin{bmatrix} \kappa_{i1} & \kappa_{i2} & \cdots & \kappa_{iN} \end{bmatrix} \begin{bmatrix} \frac{\alpha_1}{\alpha_i} e^{j\Delta\theta_{1i}} \\ \frac{\alpha_2}{\alpha_i} e^{j\Delta\theta_{2i}} \\ \vdots \\ \frac{\alpha_N}{\alpha_i} e^{j\Delta\theta_{Ni}} \end{bmatrix} \right\} \right)^{-1}$$
$$i = 1, 2, \cdots, N, \tag{3.44}$$

where

$$\Delta\theta_{ji} = \theta_j - \theta_i = (j - i)\Delta\theta \tag{3.45}$$

3.2.2 Computer Implementation

For the weakly coupled oscillator array, it is worth noting that the amplitude dynamics can be ignored. The primary computational feature of this Matlab code is simulation process of the system dynamics. This is a small part of the code, but the most heavily used part. Prior to the system dynamics, the free-running frequencies must be computed and some constants should also be evaluated and stored before the system dynamics simulation begins. The time-invariant parameters include the Q factor of the Oscillator, number of elements, coupling matrix, synchronized frequency, array spacing, main beam direction, and amplitude distribution. The program written using matlab code consists of the following major steps:

- Define the required parameters of design criteria such as time stepping, synchronized frequency, coupling parameters, array spacing, amplitude distribution for suppression of the SLL and etc.
- Calculate the free-running frequencies using (3.44) from the design criteria.
- At each time step, the instant phases are calculated for all elements and then update the previous values with them.
- Post-processing including generating the radiation pattern using the steady amplitude and phase, plotting the transient phases, plotting steady phases and etc.

A code structure implementing the above requirement is suggested by the simplified flowchart given in Fig. 3.4.

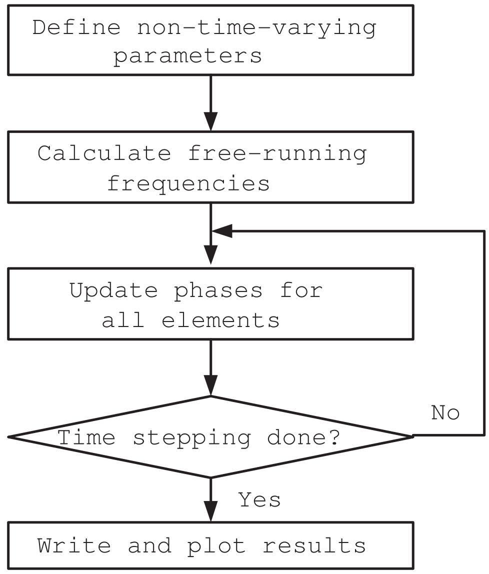

Figure 3.4: Flowchart for loosely coupled oscillator array.

The calculation of the instantaneous phase is illustrated as following. The phase dynamics for the ith oscillator at time step k may be written as

$$\frac{d\theta_i(k)}{dt} = \omega_i + \frac{\omega_i}{2Q}\sum_{j=1}^{N} Im\left\{\kappa_{ij}\frac{A_j}{A_i}e^{j(\theta_j(k)-\theta_i(k))}\right\}$$
$$i = 1, 2, \cdots, N, \tag{3.46}$$

where the subscript i denotes the spatial index number and k denotes the temporal index number. Equation (3.46) is identical with eq. (2.80) but shows the temporal index. Since amplitude dynamics are ignored, here, the amplitudes remain at their initial values so the temporal index for them is suppressed in eq. (3.46).

The nonlinear coupled different equations (3.46) describing the phase dynamics are solved using the Euler method, which is a first order numerical procedure for solving ordinary differential equations (ODEs) with a given initial value. The derivative of instantaneous phases around time index k may be approximated by the finite difference

$$\frac{d\theta_i(k)}{dt} \cong \frac{\theta_i(k+1) - \theta_i(k)}{h}, \tag{3.47}$$

for a very small value of h, where it is defined as the time stepping

$$h = t_{k+1} - t_k. \tag{3.48}$$

It is important to choose an appropriate value of time stepping. It is normal to have time stepping no greater than 1/10 of the period of oscillation. Substituting (3.47) into (3.46), the updated phase $\theta_i(k+1)$ for the ith element at time step k is solved as

$$\theta_i(k+1) = \theta_i(k) + h \cdot f(i,k) \tag{3.49}$$

where

$$f(i,k) = \omega_i + \frac{\omega_i}{2Q} \sum_{j=1}^{N} Im \left\{ \kappa_{ij} \frac{A_j}{A_i} e^{j(\theta_j(k) - \theta_i(k))} \right\} \qquad i = 1, 2, \cdots, N, \tag{3.50}$$

Therefore the equation (3.49) shows that the updating phase for the i^{th} element is calculated from the previous phases of coupled oscillators.

As an initial condition, all phases are randomly chosen from 0 to 2π. The pseudo-code in matlab for initializing is

$$\theta_i(k=1) = 2\pi \cdot rand(N,1), \tag{3.51}$$

where N is the number of oscillators.

3.2.3 Uniform Amplitude Distribution

In order to verify our solution of free running frequency and compare with the results of Liao and York. We took the design which was demonstrated in their paper which included:

- Synchronized frequency: 10Ghz
- Coupling strength $|\kappa|$: 0.1(Strong)
- Coupling phase ϕ: 0 deg
- Array spacing d: 0.5λ

With zero coupling phase and ignoring the amplitude dynamics, the equation describing phase dynamics reduces to

$$\frac{d\theta_i}{dt} = \omega_i + \frac{\omega_i}{2Q} \sum_{j=1}^{N} |\kappa_{ij}| \frac{\alpha_j}{\alpha_i} sin(\theta_j - \theta_i) \qquad i = 1, 2, \cdots, N. \tag{3.52}$$

The free running frequency also reduces to

$$\omega_i = \omega \cdot \left[1 + \frac{1}{2Q} \sum_{j=1}^{N} |\kappa_{ij}| \frac{\alpha_j}{\alpha_i} sin(\theta_j - \theta_i) \right]^{-1} \qquad i = 1, 2, \cdots, N. \tag{3.53}$$

Since Liao assumed $\alpha_i = 1.0$ for equally excited amplitude distribution, the free running frequency can be further reduced to

$$\omega_i = \omega \cdot \left[1 + \frac{1}{2Q} \sum_{j=1}^{N} |\kappa_{ij}| \, sin(\theta_j - \theta_i) \right]^{-1} \qquad i = 1, 2, \cdots, N. \tag{3.54}$$

The coupling parameter between the adjacent elements is equal to 0.1. Accordingly, as the coupling strength will decrease rapidly with distance, the coupling amplitude $|\kappa_{ij}|$ is assumed to be zero for all $|i-j| \neq 1$. Therefore, for a four element, loosely coupled oscillator array with $Q = 10$ and $|\kappa| = 0.1$, the free running frequencies are obtained as

$$\boldsymbol{\omega} = \left[\begin{array}{cccc} 9.962 & 10.000 & 10.000 & 10.038 \end{array} \right] \text{ (GHz)} \tag{3.55}$$

in order to have a maximum beam pattern at 16 degree from broadside. The synchronized frequency is chosen as 10GHz. Fig. 3.5 shows the diagram of the oscillator array.

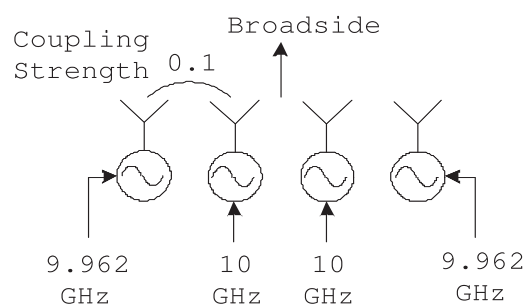

Figure 3.5: Diagram of four elements loosely coupled oscillator array with $Q = 10$, $|\kappa| = 0.1$ and $f_{syn} = 10$Ghz

A numerical simulation of the coupled array has been implemented. A time evolution of the array has been carried out using randomly chosen initial phases. From fig. 3.6(a), the three phase differences between the adjacent elements converge to the same value after $50ns$. This implies a constant phase progression has been achieved by manipulating the free running frequencies of oscillators. Radiation patterns of the

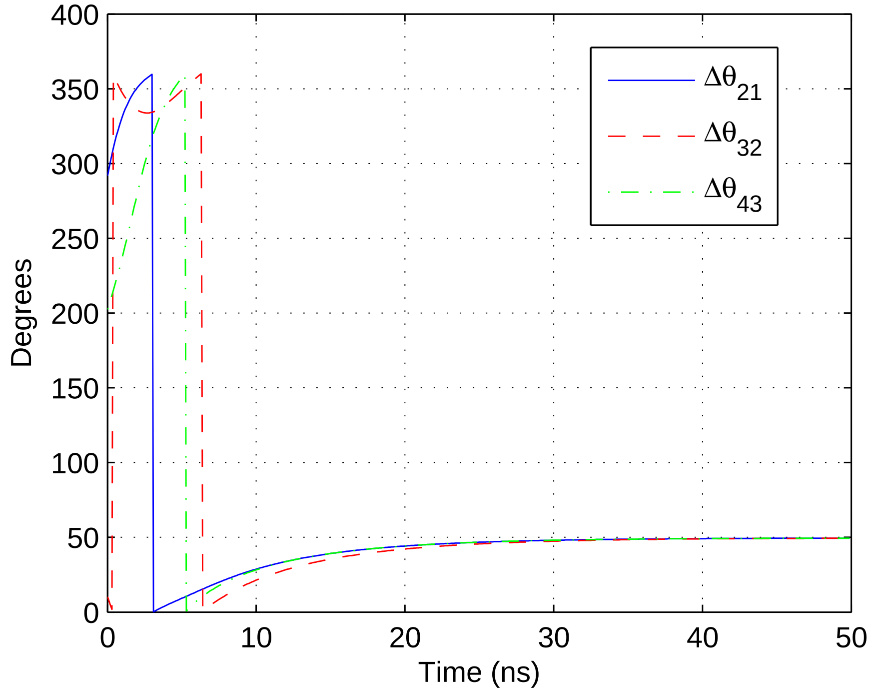

(a)

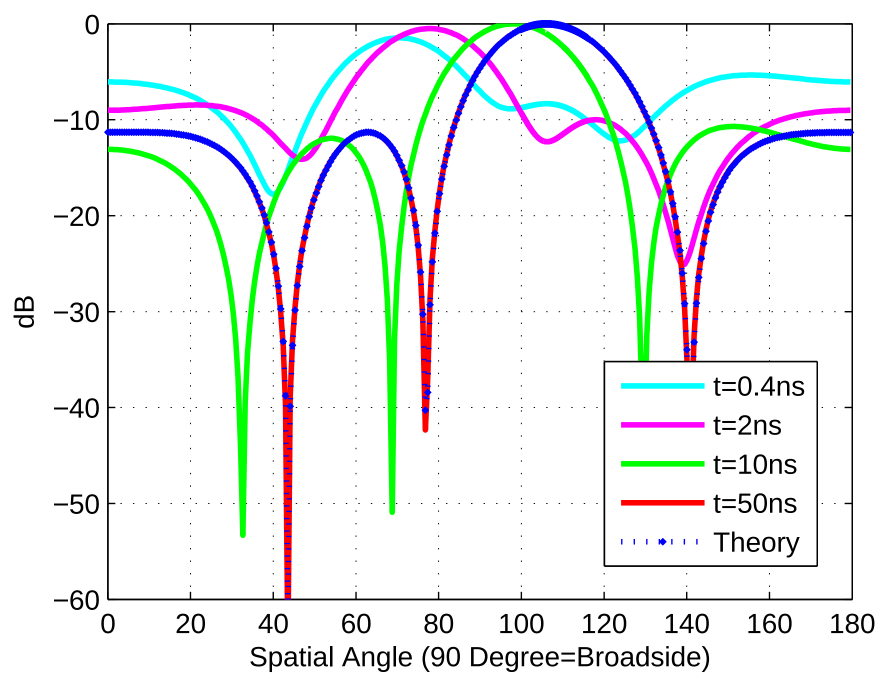

(b)

Figure 3.6: Phase difference and array pattern. (a) Phase difference between adjacent elements versus time. (b) Normalized radiation pattern of the oscillator array in convergence.

oscillator array of different times during convergence are shown in fig. 3.6(b). 90 degrees correspond to broadside. These patterns were calculated using the instantaneous phases. In the steady state, the main beam direction settled to 15.94°, while the desired scan angle was 16° off broadside.

3.2.4 Triangular Amplitude Distribution to Control the Sidelobe Level (SLL)

The linear arrays with uniform amplitude distribution have a side lobe level(SLL) of $\approx -13.5dB$. For many applications, lower side lobe levels are demanded. By adjusting the current amplitude of an array, the beam shape and side lobe levels(SLLs) can be controlled [27]. For a linear oscillator array with uniform amplitude distribution, the main beam can be steered by detuning the free running frequencies of the two oscillators on the edges as demonstrated. Note that the nearest neighbor coupling and zero coupling phase are required in this case. If a non-uniform triangular amplitude distribution is used in such a coupled oscillator array, the desired constant phase shift and main beam angle can not be achieved by only detuning the free running frequencies of the edge elements, even though all the oscillators will simultaneously synchronize to the same frequency at the steady state. For example, considering the oscillator array with triangular amplitude distribution, the array factor of such an array is plotted in Figure 3.7 and compared with the theoretical array factor. It is observed that the main beam angle deviates significantly from the desired angle and the shape of array factor is distorted when detuning only the frequencies of the edge elements as shown in this figure.

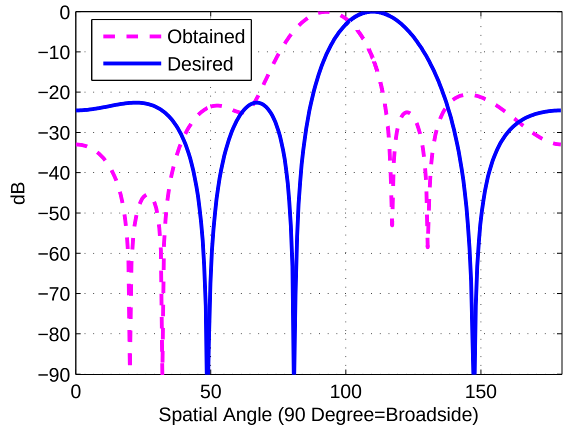

Figure 3.7: The obtained array factor of a seven element coupled oscillator oscillator with triangular amplitude distribution when detuning only the free running frequencies of the edge elements. The desired array factor is shown for comparison.

The weakly coupled linear oscillator array of 9 element with a triangular amplitude distribution will be discussed in this section, which is a larger array compared to the one demonstrated in last section. The triangular amplitude distribution is shown in 3.2.4 and listed by (3.56).

$$\boldsymbol{\alpha} = \begin{bmatrix} 0.2000 \\ 0.4000 \\ 0.6000 \\ 0.8000 \\ 1.0000 \\ 0.8000 \\ 0.6000 \\ 0.4000 \\ 0.2000 \end{bmatrix} \tag{3.56}$$

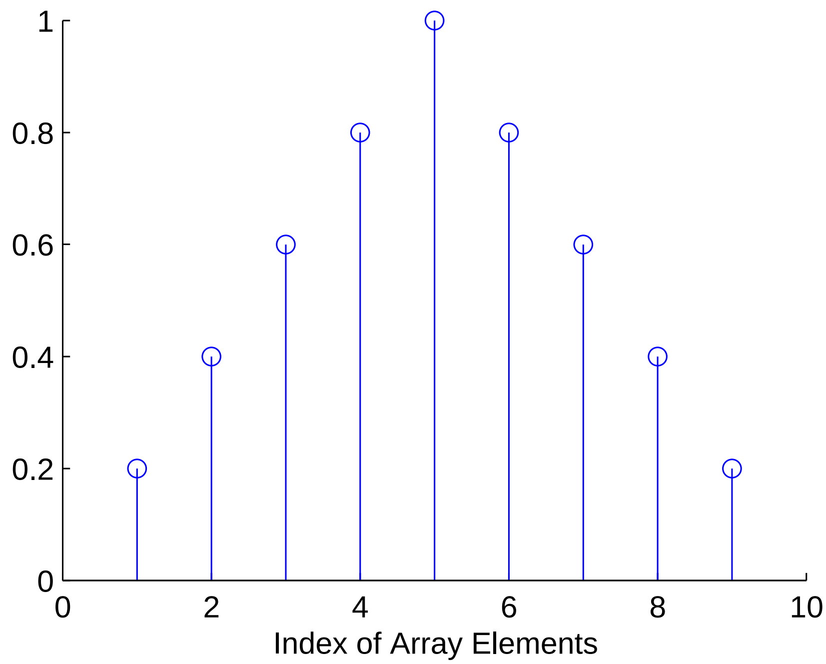

Substituting (3.56) into (3.44), the free running frequencies are found to be

$$\boldsymbol{\omega} = \begin{bmatrix} 9.924 \\ 9.962 \\ 9.975 \\ 9.981 \\ 10.00 \\ 10.019 \\ 10.025 \\ 10.038 \\ 10.077 \end{bmatrix} \text{(GHz)} \tag{3.57}$$

All other design parameters remain the same, as in the case of uniform amplitude distribution, including the coupling strength is 0.1.

Figure 3.8(a) and 3.8(b) show the convergence of phases between adjacent elements and beam pattern respectively. The side lobe level of the convergent pattern for this triangular amplitude oscillator array is around -24dB which is much lower than the uniform amplitude's -14dB SLL. The beam direction from the simulation results is found to be 15.74 degree for real time $t = 200ns$.

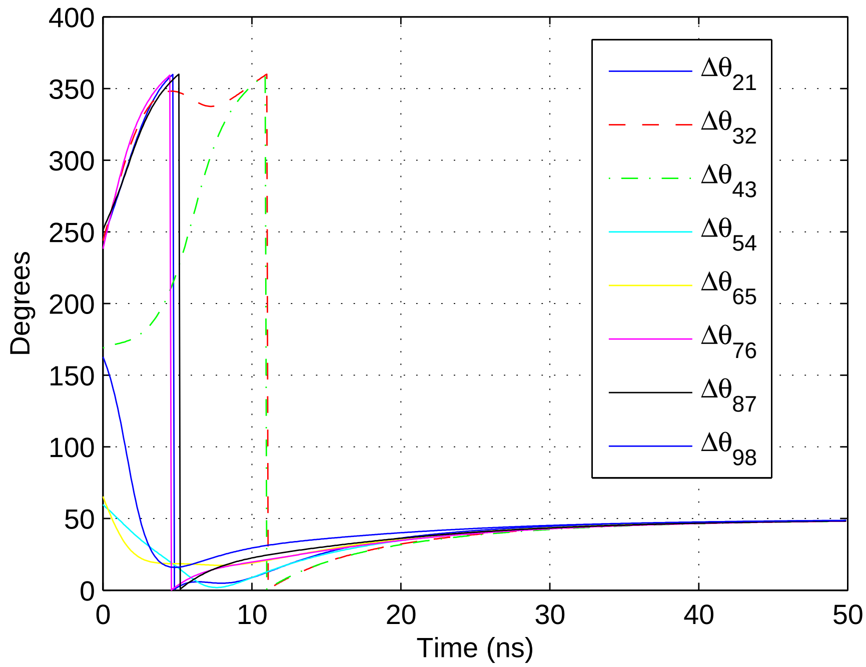

(a)

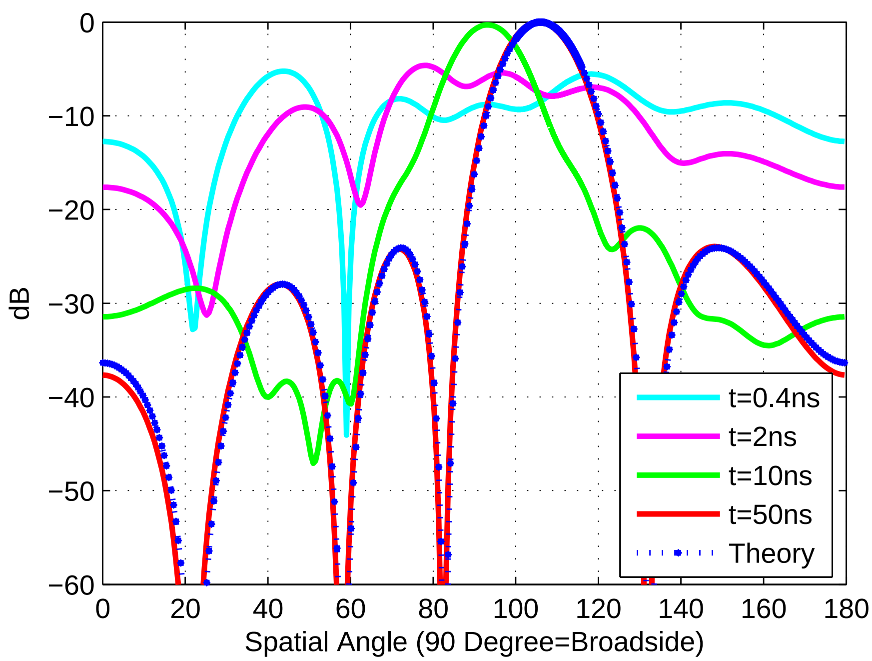

(b)

Figure 3.8: Triangle amplitude distribution with lower SLL (a)Phase difference between adjacent elements versus time. (b)Beam pattern of the oscillator array in convergence for triangle amplitude distribution..

3.3 Planar Oscillator Array

The planar array is comprised of individual radiators positioned along a rectangular grid. They are more versatile than the linear array and can be used to scan the main beam toward any point in the space. The dynamic analysis for oscillator planar array is more complicated than the linear oscillator array. In this section, we will demonstrate the beam scanning technique for planar phased array using coupled oscillators.

3.3.1 Two Dimension Model of the Phase Dynamics

As a matrix may be converted into a vector by rearranging each rows into one single row, the planar array may also be considered as a linear array at some time. Recall that, nonlinear differential equations describing phase dynamics for a one-dimensional coupled oscillator array are given by

$$\frac{d\theta_i}{dt} = \omega_i + \frac{\omega_i}{2Q}\sum_{j=1}^{N} Im\left\{\kappa_{ij}\frac{A_j}{A_i}e^{j(\theta_j-\theta_i)}\right\}$$
$$i = 1, 2, \cdots, N. \tag{3.58}$$

With the uniform amplitude distribution, likewise the linear coupled oscillator array, the amplitude dynamics can be approximately ignored and the phase dynamics will be dominated to describe the system dynamics of the planar oscillator array.

With ignoring amplitude dynamics, it implies that $\frac{A_j}{A_i} \approx 1$. The complex coupling parameter is $\kappa_{ij} = \epsilon e^{-j\phi}$, therefore, (3.58) can be written as

$$\frac{d\theta_i}{dt} = \omega_i + \frac{\epsilon\omega_i}{2Q}\sum_{j=1}^{N} sin(\theta_j - \theta_i - \phi)$$
$$i = 1, 2, \cdots, N. \tag{3.59}$$

In the previous chapters, we have successfully demonstrated that (3.59) is a good mathematical model for the linear oscillator array. Unfortunately, those differential equations of one dimensional form are not suitable to model the planar oscillator array, especially the coupling network. Therefore, the two-dimension mathematical model were suggested in [15]. The 2-D model of the system dynamics can be derived simply by replacing the index i of 1-D coupled oscillator array with 2-D indices m, n,

$$\frac{d\theta_{m,n}}{dt} = \omega_{m,n} + \frac{\epsilon\omega_{m,n}}{2Q}\sum_{i=1}^{M}\sum_{j=1}^{N} sin(\theta_{i,j} - \theta_{m,n} - \phi)$$
$$i = 1, 2, \cdots, M. \qquad j = 1, 2, \cdots, N. \tag{3.60}$$

Fig. 3.9 shows that the diagram of a planar array. Note that, θ_y denotes the constant phase progression along the rows, given by $\theta_y = \theta_{m,n+1} - \theta_{m,n}$. The constant phase progression along the columns is $\theta_x = \theta_{m+1,n} - \theta_{m,n}$, where the Δ signs are ignored for simplification of the formula, m is the index number along the rows, and n is the index number along the columns.

Assuming the nearest neighbor couplings as shown in fig. 3.10, the phase dynamics of the two dimensional form of the planar coupled oscillator array can be written as

$$\begin{aligned} \tfrac{d\theta_{m,n}}{dt} = \omega_{m,n} + \tfrac{\epsilon\omega_{m,n}}{2Q}\,[sin(\theta_{m,n+1} - \theta_{m,n} - \phi) + sin(\theta_{m,n-1} - \theta_{m,n} - \phi) + \\ sin(\theta_{m+1,n} - \theta_{m,n} - \phi) + sin(\theta_{m-1,n} - \theta_{m,n} - \phi)] \\ m = 1, 2, \cdots, M \\ n = 1, 2, \cdots, N \end{aligned} \tag{3.61}$$

where ϵ is the coupling strength, and Q is the quality factor of the resonance circuit.

The interior elements of the planar array will be coupled with four adjacent elements. The edge elements will be coupled with their three adjacent elements and the corner elements will couple with only the two adjacent elements. Eq. (3.61) with the four sin terms are the phase dynamics for the interior elements, noting that for the

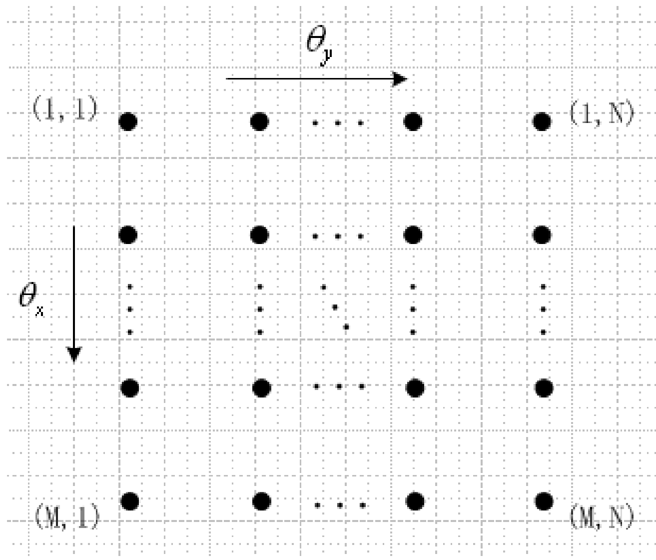

Figure 3.9: Diagram of a planar array.

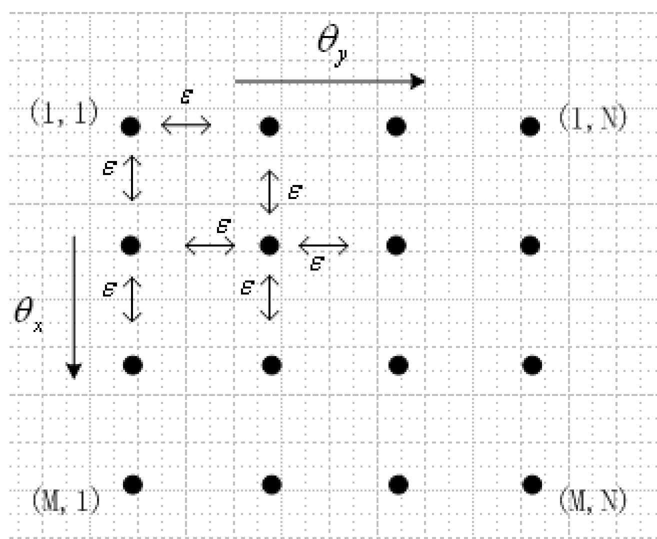

Figure 3.10: The illustration of the coupling network for a 4 by 4 planar array.

other elements while $m = 0$ or $n = 0$ the corresponding sin term will vanish. For example considering the two left edge elements, the phase dynamic equations for it will be

$$\frac{d\theta_{m,n}}{dt} = \omega_{m,n} + \omega_{m,n}\epsilon^{'} \left[sin(\theta_{m,n+1} - \theta_{m,n} - \phi) + sin(\theta_{m+1,n} - \theta_{m,n} - \phi) + sin(\theta_{m-1,n} - \theta_{m,n} - \phi)\right] \tag{3.62}$$

where $\epsilon^{'} = \epsilon/(2Q)$. Since the element $m, n-1$ does not exist, the corresponding coupling should be zero, and the phase dynamics only contain three terms of the sin function.

3.3.2 Solution of Free Running Frequencies

The beam steering for planar oscillator array may also be achieved by manipulating the free running frequencies of the oscillators. Similar to the 1-D coupled oscillator array, it is assumed that the steady state and the synchronization phenomenon for the planar coupled oscillator array will be achieved, as given by

$$\begin{aligned} \omega_s = \omega_{m,n} + \tfrac{\epsilon\omega_{m,n}}{2Q}\left[sin(\theta_{m,n+1} - \theta_{m,n} - \phi) + sin(\theta_{m,n-1} - \theta_{m,n} - \phi) + \right. \\ \left. sin(\theta_{m+1,n} - \theta_{m,n} - \phi) + sin(\theta_{m-1,n} - \theta_{m,n} - \phi)\right] \\ m = 1, 2, \cdots, M \\ n = 1, 2, \cdots, N, \end{aligned} \tag{3.63}$$

where ω_s is the synchronized frequency at the steady state. By eq. (3.63), the relationship between the free running frequencies and the phase distributions along both x and y direction of array has been established.

Fig. 3.11 shows the coordinates and the geometry configuration of the planar array. The 2-D Array is placed in the x-y plane and the main beam is pointing at (θ, ϕ). It is worthy to note that θ used here does not represent the instantaneous phase of oscillator but the beam angle of the planar array. The constant phase shifts

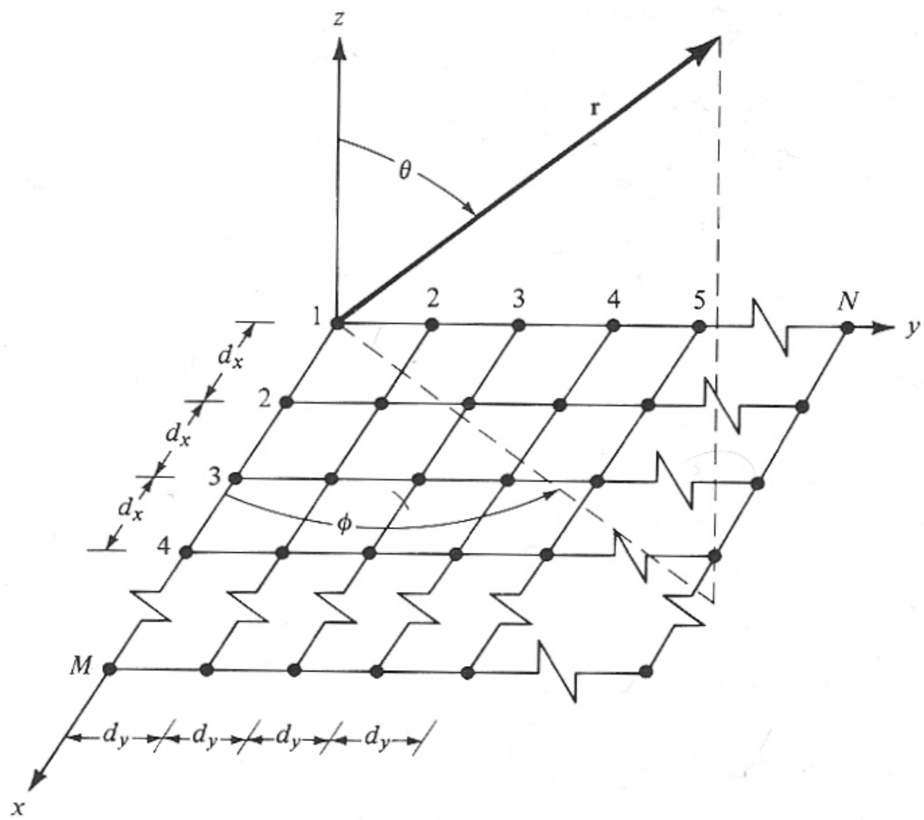

Figure 3.11: Coordinate system for planar array.

θ_x along x axis and θ_y along y axis are required to scan the beam in certain direction. The relationship between the desired beam angle (θ, ϕ) and the phase shifts are

$$\theta_x = -kd_x sin\theta_0 cos\phi_0$$
$$\theta_y = -kd_y sin\theta_0 sin\phi_0 \tag{3.64}$$

From (3.63) and (3.64), we may solve the free-running frequencies of the planar oscillator array for achieving the desired phase shifts as following.

- Corner Elements

$$\omega_{1,1} = \frac{\omega_s}{1+\epsilon' \left[sin(\theta_x - \phi) + sin(\theta_y - \phi)\right]}$$
$$\omega_{1,N} = \frac{\omega_s}{1+\epsilon' \left[sin(\theta_x - \phi) - sin(\theta_y + \phi)\right]}$$
$$\omega_{M,1} = \frac{\omega_s}{1+\epsilon' \left[sin(\theta_y - \phi) - sin(\theta_x + \phi)\right]}$$
$$\omega_{M,N} = \frac{\omega_s}{1-\epsilon' \left[sin(\theta_y + \phi) + sin(\theta_x + \phi)\right]} \tag{3.65}$$

- Edge Elements

$$\omega_{1,n} = \frac{\omega_s}{1+\epsilon' \left[sin(\theta_x - \phi) - 2cos\theta_y sin\phi\right]}$$
$$n = 2, 3, \cdots, N-1$$

$$\omega_{M,n} = \frac{\omega_s}{1-\epsilon' \left[sin(\theta_x + \phi) + 2cos\theta_y sin\phi\right]}$$
$$n = 2, 3, \cdots, N-1$$

$$\omega_{m,1} = \frac{\omega_s}{1+\epsilon' \left[sin(\theta_y - \phi) - 2cos\theta_x sin\phi\right]}$$
$$m = 2, 3, \cdots, N-1$$

$$\omega_{m,N} = \frac{\omega_s}{1 - \epsilon' \left[sin(\theta_y + \phi) + 2cos\theta_x sin\phi\right]}$$
$$m = 2, 3, \cdots, N-1 \tag{3.66}$$

- Interior Elements

$$\omega_{m,n} = \frac{\omega_s}{1 - 2\epsilon' sin(\phi) \left[cos\theta_x + cos\theta_y\right]}$$
$$m = 2, 3, \cdots, N-1$$
$$n = 2, 3, \cdots, N-1 \tag{3.67}$$

3.3.3 Uniform Amplitude Distribution

The instantaneous array factor of the planar array is calculated as

$$AF(\theta, \phi) = \sum_{m=1}^{M} \sum_{n=1}^{N} e^{j\theta_{m,n}} e^{j((m-1)kd_x sin\theta cos\phi + (n-1)kd_y sin\theta sin\phi)} \tag{3.68}$$

where $k = \frac{2\pi}{\lambda}$ is the wave number, $\theta_{m,n}$ is the instantaneous phase at the (mth, nth) element, and d_x and d_y are the spacing between the elements along x and y directions. Thus the array factor can be calculated from the instantaneous phases while the instantaneous amplitudes are uniform.

The beam scanning technique of oscillator planar array is illustrated by the 6 by 6 elements array of uniform amplitude distribution. The design criteria are shown below:

- Quality factor: $Q = 10$
- Coupling strength: $\epsilon = 2$
- Synchronization frequency: $f_{syc} = 10GHz$

- Array spacing: $dx = 0.4\lambda$ and $dy = 0.4\lambda$
- Main beam direction: $\theta = 20$ deg, and $\phi = 120$ deg

Fig. 3.13 shows the 1-D array patterns, which are calculated from the instantaneous phase after reaching the steady state at $t = 4ns$. The main beam angle is found at $\theta = 19.9$ and $\phi = 120.3$. The free running frequencies used to achieve the beam scanning are listed in fig. 3.12. Fig. 3.14(a) shows the 2-D pattern for the 6 by 6 elements oscillator array.

A large 20 by 20 elements array is also simulated with the same design criteria, and its array pattern is shown in fig. 3.14(b). It takes much longer for it to converge than the 6-by-6 array. The calculated beam angle is at $\theta = 19.5$ and $\phi = 120.3$ at real time of $t = 30ns$.

10.2679	9.6000	9.6000	9.6000	9.6000	9.0137
10.7268	10.0000	10.0000	10.0000	10.0000	9.3654
10.7268	10.0000	10.0000	10.0000	10.0000	9.3654
10.7268	10.0000	10.0000	10.0000	10.0000	9.3654
10.7268	10.0000	10.0000	10.0000	10.0000	9.3654
11.2287	10.4348	10.4348	10.4348	10.4348	9.7458

Figure 3.12: Free running frequencies achieving beam scanning technique.

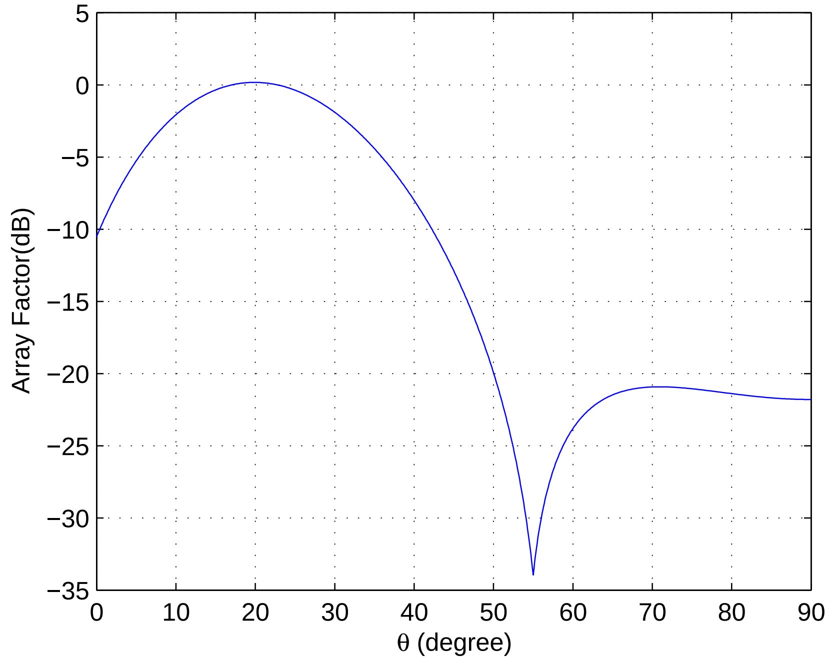

(a)

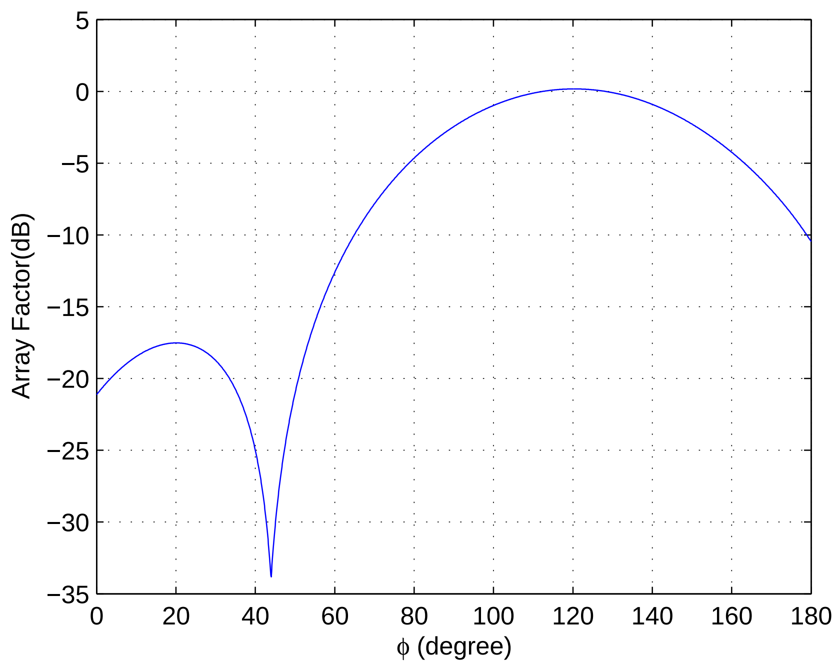

(b)

Figure 3.13: 1-D array pattern of a 4 by 4 planar array (a) E-plane pattern with $\phi = 120$. (b) H-plane pattern with $\theta = 20$.

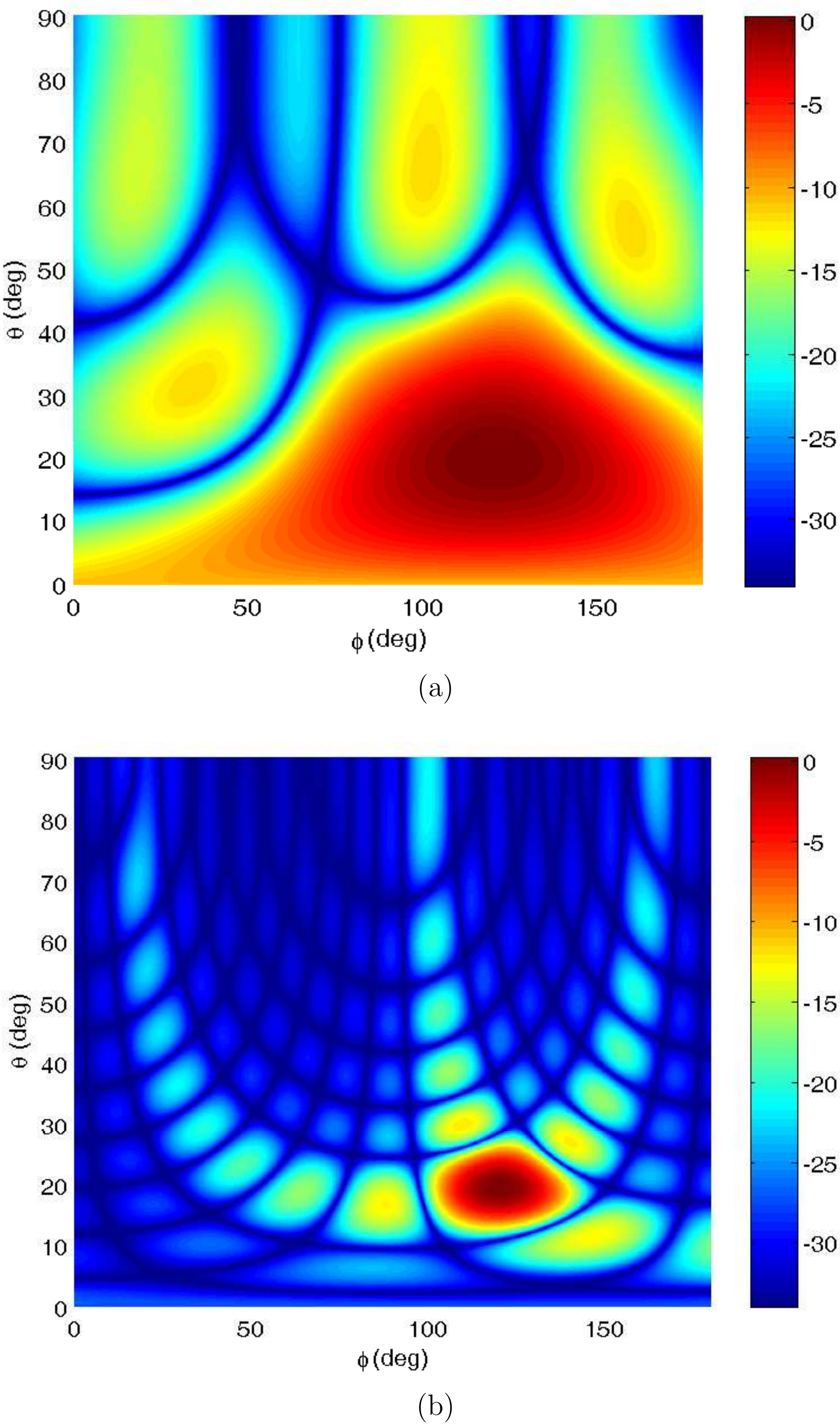

Figure 3.14: 2-D array pattern (a) 6 by 6. (b) 20 by 20.

CHAPTER 4

BEAM-STEERING ANALYSIS INCLUDING AMPLITUDE DYNAMICS

By modeling the oscillator by a negative resistance, and an RLC circuit, the dynamics of coupled oscillator array were described by equation (2.79). A specified phase distribution is required to scan the beam in the desired direction for phased array regardless of using phase-shifter or oscillator, and the amplitude distribution determines the Side Lobe Levels (SLLs). Although lower SLLs are desired in some applications, it is essential that the main beam scanning angle be as accurate as possible. As implied by Eq. (2.79), the amplitude dynamics have only a second-order influence on the phase dynamics. Therefore amplitude dynamics have been simply ignored by most of the previous studies [5, 6, 8, 28]. For instance, in a weakly coupled oscillator array, the variations of oscillator amplitudes are very small so they may be ignored under certain conditions. The important advantage of ignoring amplitude dynamics under weak coupling is that the modeling of system dynamics of coupled oscillator array is significantly simplified. In chapter 2, it has been shown that a simple set of differential equations for the phase dynamics would be sufficient to predict the mutual synchronization, mode stability, and the steady state phase relationship in the system of weakly coupled oscillators [5].

Although the weakly coupled oscillator arrays have successfully been demonstrated in the power-combining concept, such as arrays exploiting radiative coupling between antennas, which is not very useful in practice. One important reason is that the coupling coefficients are extremely crucial parameters in the design of an oscillator array, but since the interactions between adjacent oscillators are generally weak it is very difficult to control or predict the coupling coefficients precisely. Another reason is, to ensure mutual locking with the proper phase relationships, tighter tolerances in the fabrication of oscillators is required for weakly coupled oscillators. Therefore, the oscillator arrays with strong coupling effects would be more interesting to us. However, the dynamic analysis of strongly coupled oscillator array becomes more complicated when compared to a weakly coupled array. Some results have been reported about the coupled-oscillator array with an arbitrary N-port strong coupling network [8]. When the oscillators are strongly coupled, the amplitude dynamics become important and deserve great attention. Furthermore, as the coupling strength is increased, the coupling network itself will perturb the oscillator frequencies and hence the steady-state phase distribution.

A few attention has been given to the amplitude dynamics [17, 9, 18]. In [17, 18], beam shaping in COAs was introduced and side lobe reduction was demonstrated. In this chapter, we are interested in the analysis of a beam-steering technique using a coupled oscillator array which includes the amplitude dynamics. The nonlinear differential equations describing amplitude and phase dynamics are coupled and implemented. Since each oscillator is modeled by one dimensional nonlinear differential equation in the time domain, the algorithm will be interwoven in both space and time. For example, the new value of instantaneous amplitude for a single oscillator is calculated from the previous value of both instantaneous amplitudes and phases of all its coupling neighbors in free space. Although including the amplitude dynamics will make the analysis much more complicated, the results should be more practical and accurate compared with those obtained when ignoring the amplitude dynamics.

4.1 Dynamic Analysis

4.1.1 Beam Steering Control

In chapter 2, using three different methods, we have shown the amplitude and phase dynamics for coupled oscillator array with an arbitrary coupling network are given as

$$\begin{aligned} \frac{dA_i}{dt} &= \frac{\mu\omega_i}{2Q}\left(\alpha_i^2 - A_i^2\right)A_i + \frac{\omega_i}{2Q}\sum_{j=1}^{N} A_j Re\left\{\kappa_{ij}e^{j(\theta_j-\theta_i)}\right\} \\ \frac{d\theta_i}{dt} &= \omega_i + \frac{\omega_i}{2Q}\sum_{j=1}^{N} Im\left\{\kappa_{ij}\frac{A_j}{A_i}e^{j(\theta_j-\theta_i)}\right\} \\ & i = 1, 2, \cdots, N. \end{aligned} \tag{4.1}$$

where $\kappa_{ij} = |\kappa_{ij}|\, e^{-j\phi_{ij}}$ represents the coupling parameter between ith element and jth element, μ is an empirical nonlinearity parameter describing the oscillator, A_i is the instantaneous amplitude of oscillator and Q is the quality factor of an RLC resonant circuit. The variables α_i and ω_i are the free running amplitude and frequency respectively.

A code structure that implements both the amplitude and phase dynamics is suggested by the simplified flowchart in Figure 4.1. The sets of differential equations describing both amplitude and phase dynamics are solved in the simulation. Since more coupled nonlinear differential equations will be solved, the computation time increases.

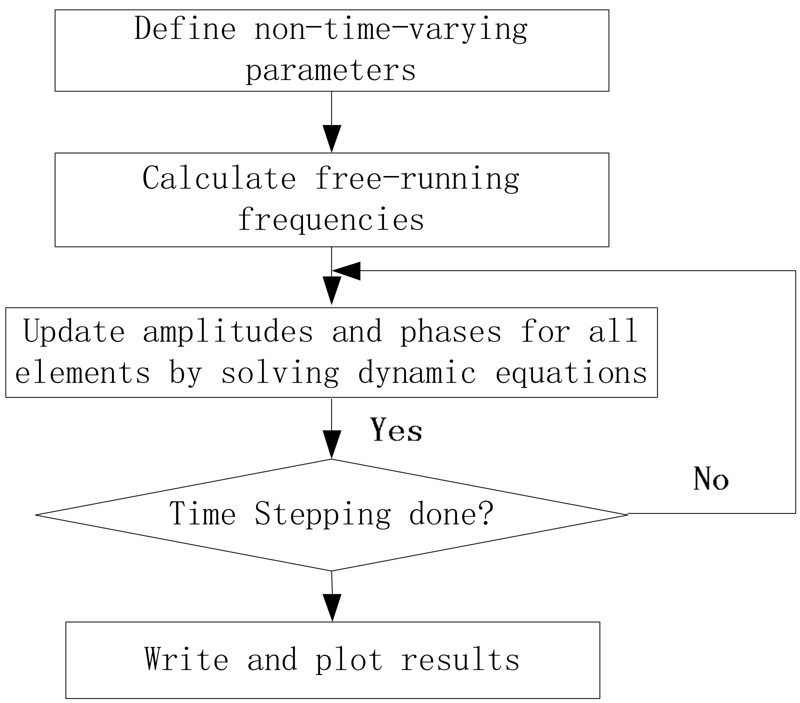

Figure 4.1: Flowchart of computer implementation solving both amplitude and phase dynamics.

At the steady state, it can be shown that all the oscillators will become synchronized to a common frequency $\frac{d\theta_i}{dt} = \omega$, provided that the free running frequencies are within the locking range. From Eq. (4.1), the synchronized frequency is

$$\omega = \omega_i \left[1 + \frac{1}{2Q} \sum_{j=1}^{N} Im \left\{ \kappa_{ij} \frac{A_j}{A_i} e^{j(\theta_j - \theta_i)} \right\} \right]$$

$$i = 1, 2, \cdots, N. \tag{4.2}$$

From (4.2), the free running frequency of each element can be solved as

$$\omega_i = \omega \cdot \left[1 + \frac{1}{2Q} \sum_{j=1}^{N} Im \left\{ \kappa_{ij} \frac{A_j}{A_i} e^{j(\theta_j - \theta_i)} \right\} \right]^{-1}$$

$$i = 1, 2, \cdots, N, \tag{4.3}$$

which are used to control the amplitude and phase distribution of oscillators. By using the free running frequencies (4.3) as an input, both desired phase progression and amplitude distribution can be achieved.

The relationship between the constant phase progression along the array $\Delta\theta$ and the main beam-steering angle ψ for a linear array is given by

$$\Delta\theta = \frac{2\pi d}{\lambda_0} sin\psi, \tag{4.4}$$

where d is the antenna spacing, and λ_0 is the wavelength in free space. Therefore, the free running frequencies achieving a constant phase progression $\Delta\theta$ and arbitrary amplitude distribution at the steady state is found as

$$\omega_i = \omega \cdot \left[1 + \frac{1}{2Q} \sum_{j=1}^{N} Im \left\{ \kappa_{ij} \frac{A_j}{A_i} e^{j(\Delta\theta_{ji})} \right\} \right]^{-1}$$

$$i = 1, 2, \cdots, N, \tag{4.5}$$

where

$$\Delta\theta_{ji} = \theta_j - \theta_i = (j - i)\Delta\theta \tag{4.6}$$

Since amplitude dynamics are included, the instantaneous amplitude A_i or A_j will not remain at the free running values α_i. Notice that the formulations of Eq. (2.79) implies that the calculations are interleaved in both space and time. The following amplitude or phases are calculated based upon the most recent values of A_i and θ_i. The amplitude and phase of each oscillator are also coupled to its neighboring oscillator.

4.1.2 Saturation Rate of Single Oscillator

The nonlinear parameter μ has a significant influence on the oscillator arrays. One way to examine the characteristics of the nonlinear parameter μ is to perform a transient analysis of the system dynamics for a free running oscillator.

When no coupling network is present, following (2.34) and (2.35), the amplitude and phase dynamics of single oscillator were described by

$$\begin{aligned} \frac{dA(t)}{dt} &= \frac{\mu\omega_0}{2Q}\left(\alpha^2 - A(t)^2\right)A(t) \\ \frac{d\theta(t)}{dt} &= \omega_0 \end{aligned} \tag{4.7}$$

Assume the example of a coupled oscillator array using the following values for associated parameters

$$\begin{aligned} \alpha &= 1 \\ \omega_0 &= 10GHz \\ Q &= 10 \\ \mu &= 5, 10, 20 \end{aligned} \tag{4.8}$$

No input or source was used for system because the oscillator is in the free running state. However, an initial small perturbation is required for the amplitude to start the oscillations. For a real system, this perturbation can be represented by bias startup or low noise reference.

The output voltage of oscillation is defined as

$$V_{out} = A(t)cos\left[\theta(t)\right] = Re\left\{A(t)e^{j\theta(t)}\right\}. \tag{4.9}$$

Figure 4.2 shows the transient analysis of free running oscillation for different μ values. From this figure, we observe that the values of μ determines the rate of amplitude saturation. The free running oscillator reaches its steady state faster for a larger μ value. At steady state, the oscillator has the free running amplitude of $\alpha = 1$ and free running frequency of $f = 10Ghz$.

4.1.3 Uniform Amplitude Distributions

The effects of amplitude dynamics were illustrated using a nine elements array with the spacing $d = \lambda_0/2$, where λ_0 is the wavelength of synchronized frequency at the steady state. The following values for associated parameters and design criteria were chosen:

- Synchronized frequency: 10Ghz or 4Ghz
- Coupling strength $|\kappa|$: 0.1(Weak), 2 or 4(Strong)
- Coupling phase ϕ: 0 deg
- Main beam angle: 16°

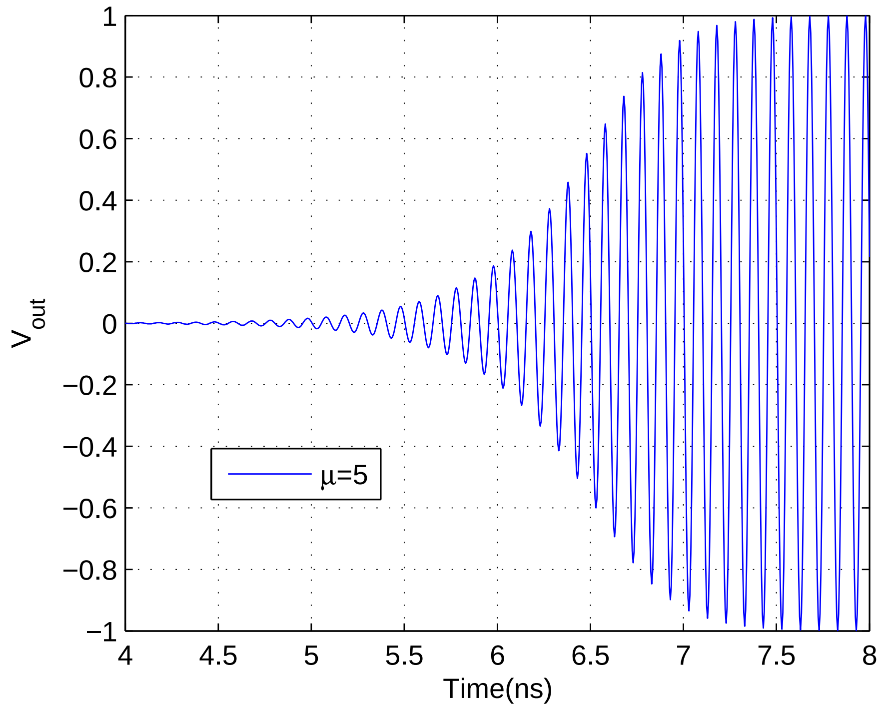

(a)

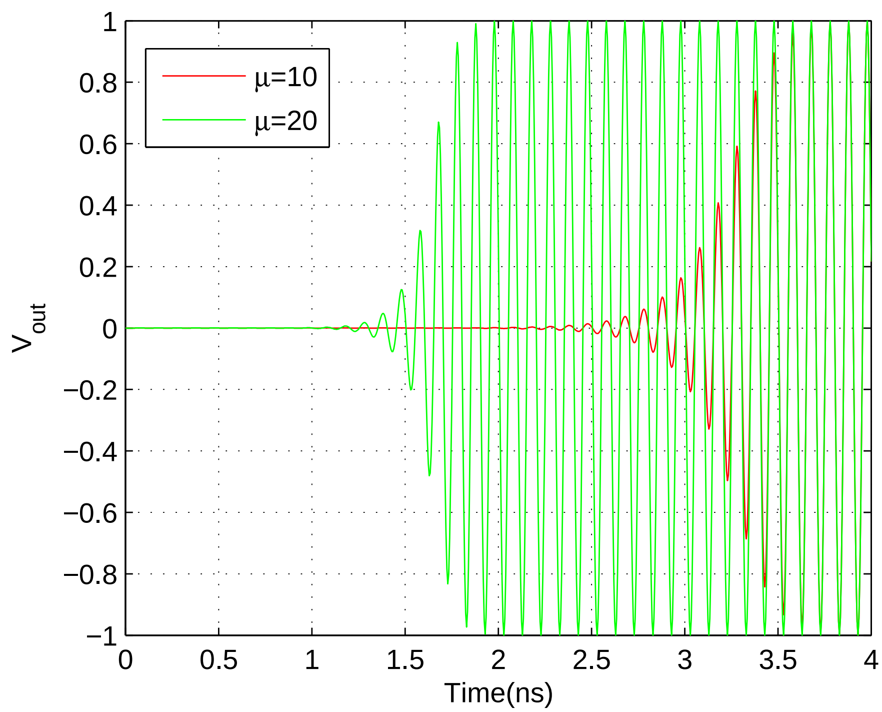

(b)

Figure 4.2: The output of oscillator V_{out} versus time for different values of μ.

- Quality Factor: $Q = 10$

It is worthy to note that since the amplitudes are uniformly distributed, we may assume the oscillators have identical values of μ and Q. Regarding the coupling network, the nearest neighbor coupling with $|\kappa_{ij}| = 0$ for all $|i - j| \neq 1$ is assumed and the zero coupling phase is assumed for simplicity. Furthermore, the coupling strength is assumed to be identical and reciprocal for every two adjacent array elements. The coupling coefficient matrix is given as

$$\boldsymbol{\kappa} = \begin{bmatrix} 0 & |\kappa| & 0 & \cdots & 0 \\ |\kappa| & 0 & |\kappa| & \cdots & 0 \\ 0 & |\kappa| & 0 & \cdots & 0 \\ \vdots & \vdots & \vdots & \ddots & \vdots \\ 0 & 0 & 0 & |\kappa| & 0 \end{bmatrix}. \tag{4.10}$$

The performance of the oscillator arrays are evaluated by the main beam errors and side lobe levels, whose values are obtained from the array factor at the steady states. The main beam error, denoted by $\Delta\psi$, is defined as the absolute value of difference between the actual main beam angle ψ obtained from the numerically solved array factors and the desired angle ψ_0,

$$\Delta\psi = |\psi - \psi_0|. \tag{4.11}$$

The side lobe level (SLL) of antenna array is defined as the the maximum at the first side lobe on the array factors.

Extensive simulation results demonstrate that the nonlinear parameter μ plays an important role in the system dynamics. The effects of the amplitude dynamics on the array factor is strongly associated with the value of nonlinear parameter μ. Figure 4.3 shows the main beam error plotted versus nonlinear parameter μ. Different

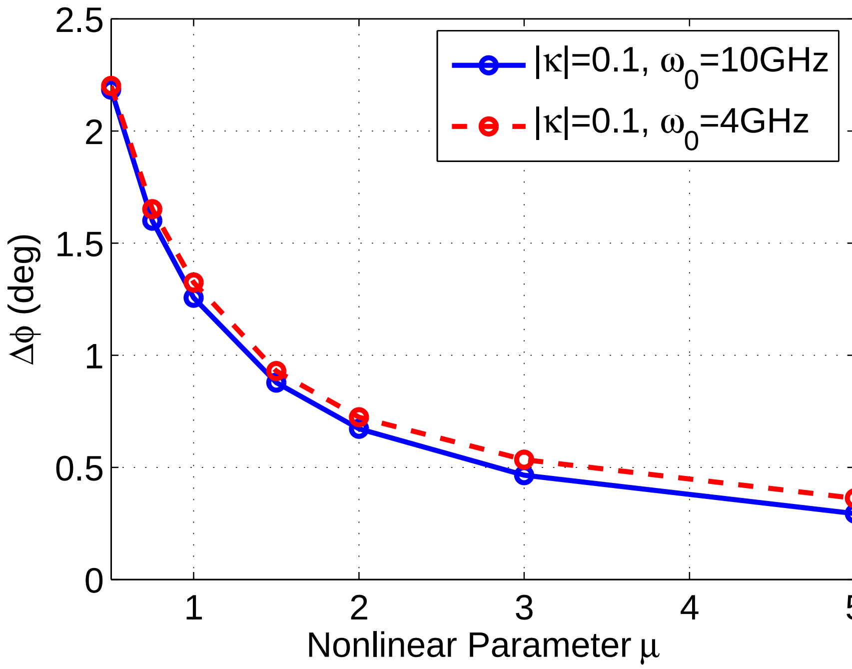

(a)

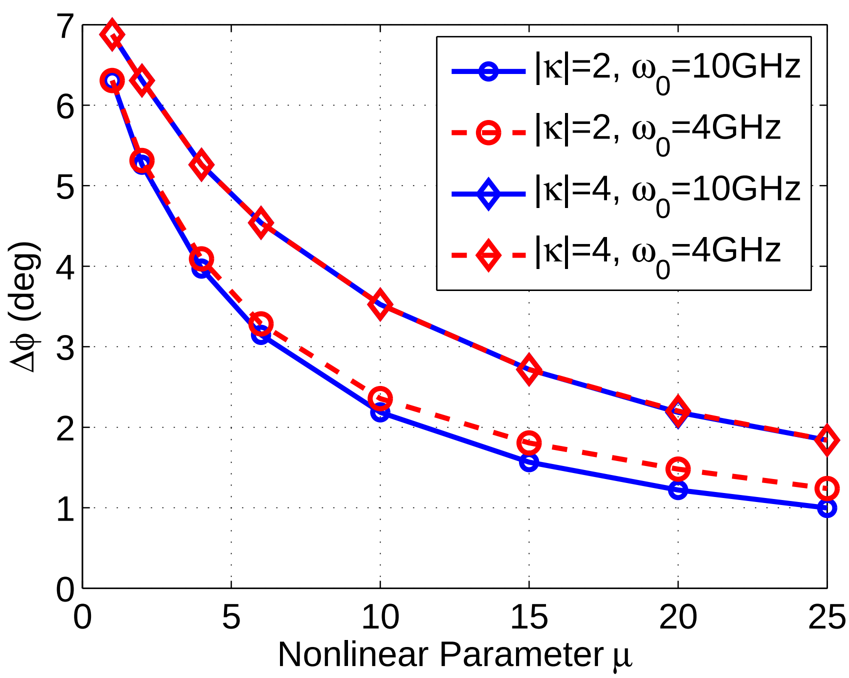

(b)

Figure 4.3: Main Beam Error with different μ. (a)Weakly coupled oscillator array. (b)Relatively strongly coupled oscillator array.

synchronized frequencies ω_0 and coupling strengths are considered. Clearly, as the nonlinear parameter μ becomes larger, the main beam error decreases. This figure also implies that for the same coupling strength and value of μ, the main beam error decreases as the synchronized frequency increases from 4GHz to 10Ghz. As shown in Figure 4.3(b, when the the coupling strength increases to 4.0, the main beam errors of oscillator array with 4GHz and 10GHz synchronized frequency are very close. Therefore, for fixed coupling strength, the larger μ value produces a smaller main beam error. If a strongly coupled oscillator is required, it is even more important to choose or design oscillator with larger μ.

Table 4.1 shows the effects of amplitude dynamics on main beam error and side lobe level with $\mu = 5$ for different oscillator arrays. While ignoring the amplitude dynamics, perfect agreement between the analytical and numerical results are obtained for the main beam scanning angle and side lobe levels. However when the amplitude dynamics are considered, errors are observed for the main beam scanning angle which tend to increase as the coupling strength increases. It is interesting to note that the side lobe levels are almost identical for different design of oscillator arrays, and very close to the theoretical values of array with uniform amplitude.

The solved free-running frequencies are listed in table 4.2. The free running frequencies do not vary for different values of μ. However as shown in this table, different free running frequencies are required for different coupling strengths, and for different synchronized frequencies.

$\lvert\kappa\rvert$	ω_0(GHz)	Ignore Amp. Dynamics		Include Amp. Dynamics		Final Time
		$\Delta\psi$	SLL	$\Delta\psi$	SLL	
0.1	4	0^o	$-12.9dB$	0.36^o	$-12.4dB$	$250ns$
	10	0^o	$-12.9dB$	0.3^o	$-12.7dB$	$250ns$
2	4	0^o	$-12.9dB$	3.7^o	$-12.4dB$	$20ns$
	10	0^o	$-12.9dB$	3.55^o	$-12.7dB$	$20ns$
4	4	0^o	$-12.9dB$	4.9^o	$-12.6dB$	$20ns$
	10	0^o	$-12.9dB$	4.9^o	$-12.6dB$	$20ns$

Table 4.1: Comparison of Simulation Results with $\mu = 5$.

Index	$\lvert\kappa\rvert = 0.1$		$\lvert\kappa\rvert = 2$		$\lvert\kappa\rvert = 4$	
	4G	10G	4G	10G	4G	10G
1	3.985	9.962	3.717	9.292	3.471	8.678
2	4	10	4	10	4	10
$\vdots$	$\vdots$	$\vdots$	$\vdots$	$\vdots$	$\vdots$	$\vdots$
8	4	10	4	10	4	10
9	4.015	10.038	4.330	10.825	4.719	11.797

Table 4.2: Free-running frequencies(Ghz) scanning the main beam at 16 degree off broadside for different oscillator array. Numerical solution are obtained from eq. (4.5).

4.2 Non-uniform Amplitude Distribution for Side Lobe Reduction

The coupled oscillator array with uniform amplitude distribution was discussed and analyzed while considering the amplitude dynamics. The numerical and graphical solutions were used to illustrate the influence of amplitude dynamics on the array factors. In this section, oscillator arrays with uniform spacing but non-uniform amplitude distribution will be considered. As is known from traditional phased array theory, the shape of main beam and level of side lobes is controllable by manipulating the amplitudes of an array. Patterns with lower side lobe level are of interest in many applications.

For an coupled oscillator array, the amplitude of oscillation of an individual element source determines the current amplitude of the radiating element. In order to obtain a stable oscillation for the negative resistance oscillator, the following oscillation condition has to be satisfied

$$G_d(\alpha_0) = G_L, \tag{4.12}$$

where α_0 is the amplitude of free oscillation or free running amplitude, G_L denotes the load conductance, and G_d denotes the conductance of active device. From (2.19), the negative conductance with the stable oscillation amplitude is given as $-G_0 + G_2\alpha^2$. Substituting this equation into (4.12) gives

$$G_L = -G_0 + G_2\alpha^2, \tag{4.13}$$

where G_0 and G_2 are device-dependent parameters, and they can be determined from the I-V characteristic curve of the active device. Therefore, one direct way to achieve the desired amplitude of oscillation without using additional control circuitry is to adjust the load conductance G_L, or resistance R_L.

In the last section, we showed that the influence of amplitude dynamics on array factors and demonstrated the significance of the nonlinear parameter μ in the analysis of system dynamics. Since the amplitude were uniformly distributed, we assumed that oscillators have the same value of μ. In chapter 2, we showed that when modeling the oscillator with parallel resonant circuit, the nonlinear parameter μ is given by

$\mu = \frac{G_2}{G_L}$, where G_2 is the nonlinear device-dependent parameter. Noticing that the value of μ is associated with G_L and hence the free running amplitude, it is unreliable to make the same assumption for non-uniform amplitude distribution.

However we may define a new parameter for non-uniform amplitude distribution, which does not associate with free running amplitude. This parameter must also be a dimensionless quantity. Recalling the Q-factor of the parallel resonant circuit in Fig. 2.2 is defined as

$$Q = \frac{\omega_0 C}{G_L} = \frac{1}{\omega_0 G_L L}. \tag{4.14}$$

We can define

$$\epsilon = \frac{\mu}{Q} = \frac{G_2}{G_L}\omega_0 G_L L = \omega_0 G_2 L. \tag{4.15}$$

The parameter ϵ is a truly dimensionless quantity which is not associated with the free running amplitude. We can assume that the oscillators have identical values of the nonlinear parameter, ϵ.

4.2.1 Triangular Amplitude Distribution

The triangular amplitude distribution for reducing side lobe level is chosen as

$$\alpha = [\ 0.2 \quad 0.4 \quad 0.6 \quad 0.8 \quad 1.0 \quad 0.8 \quad 0.6 \quad 0.4 \quad 0.2]. \tag{4.16}$$

The influence of amplitude dynamics is investigated by a nine element oscillator array with the spacing of $d = \lambda_0/2$. It is assumed that the oscillators have identical ϵ values which is given by Eq. (4.15). The following values for associated parameters and design criteria were chosen:

- Synchronized frequency: 10Ghz

- Coupling strength $|\kappa|$: 0.1(Weak), 2(Strong)

- Coupling phase ϕ: 0 deg

The nonlinear parameter ϵ determines the rate of convergence of the coupled oscillators. The system of coupled oscillators with lower ϵ parameter converge slower. Moreover, it will be demonstrated that when the value of ϵ is too low, the coupled oscillator array will fail to converge and fall into an unstable state. As shown in Figure 4.4(a), the phase shifts fail to converge to the constant value required for beam scanning when $\epsilon = 0.2$. In such case, an irregular array pattern will be obtained. However the convergence of the constant phase shift between element is achieved when $\epsilon = 2$ as shown in Figure 4.4(b). Similarly, transient analysis of phase shifts for larger coupling strength of $|\kappa| = 2$ is shown in Figure 4.5. Comparing with weak coupling, higher value of nonlinear parameter ϵ is required for strongly coupled oscillator array.

Amp. Distribution	$\lvert\kappa\rvert$	Ignore Amp. Dynamics		Include Amp. Dynamics		Time
		$\Delta\psi$	SLL	$\Delta\psi$	SLL	
Uniform	0.1	0.09^o	$-12.9dB$	0.26^o	$-12.8dB$	$200ns$
	2.0	0^o	$-12.9dB$	1.2^o	$-12.8dB$	$20ns$
Triangular	0.1	0^o	$-24.1dB$	1.36^o	$-23.2dB$	$200ns$
	2.0	0^o	$-24.1dB$	6.0^o	$-21.1dB$	$20ns$

Table 4.3: Comparison of Simulation Results.

The results comparison between including and ignoring the influence of amplitude dynamics are shown in table 4.3. $\Delta\psi$ denotes the main beam error defined by Eq. (4.11) as the absolute value of difference between the actual main beam angle ψ

Figure 4.4: Transient analysis of phase shifts between the adjacent element for weak coupling strength of $\epsilon = 0.1$. (a)$\mu = 0.2$. (b)$\mu = 2$.

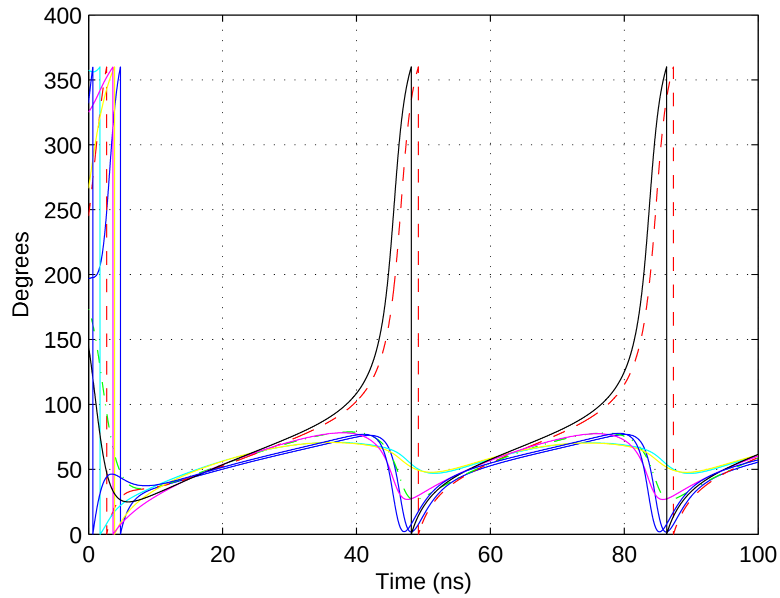

(a)

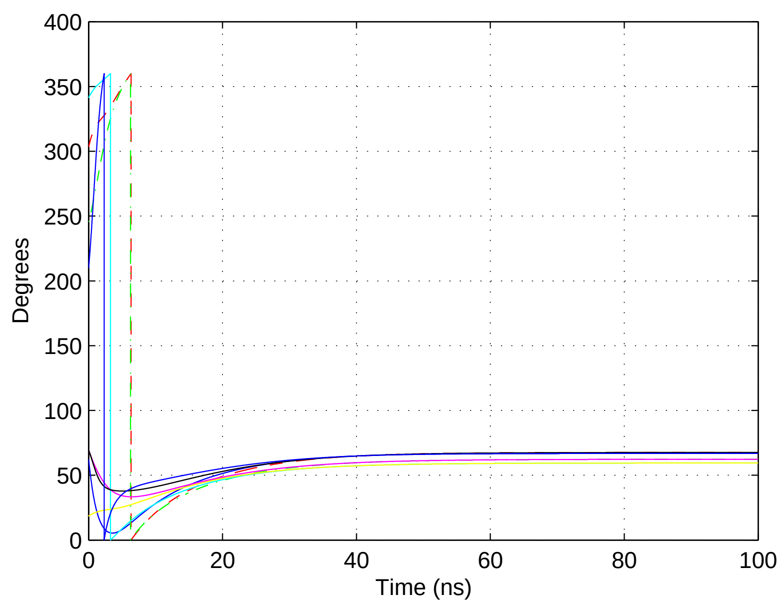

(b)

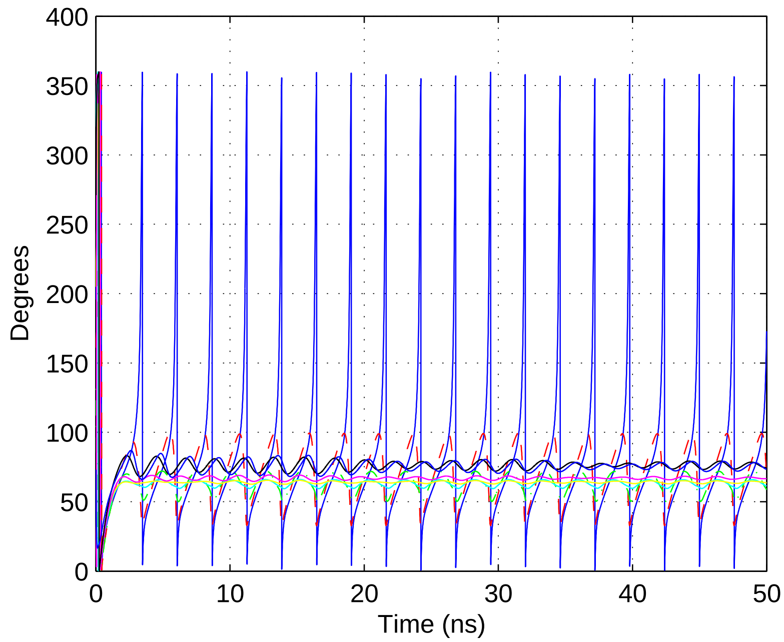

(a)

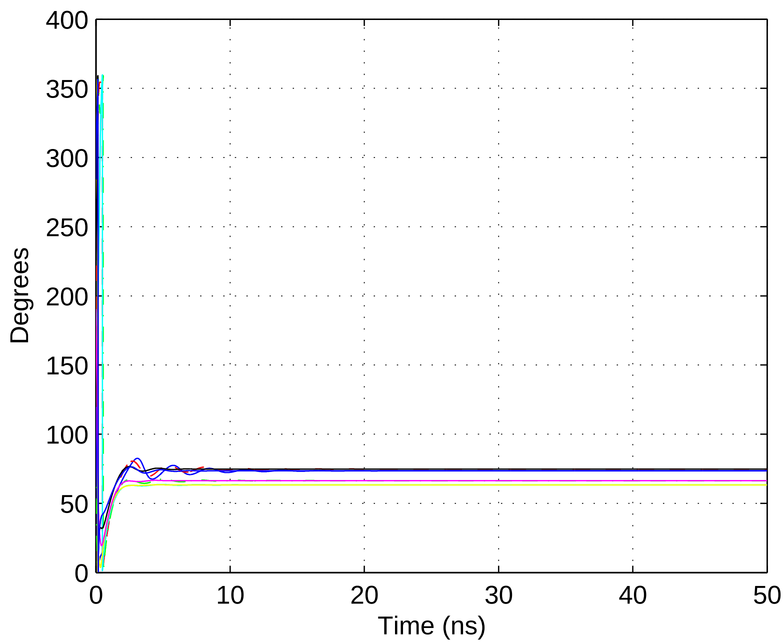

(b)

Figure 4.5: Transient analysis of phase shifts between the adjacent element for strong coupling of $\epsilon = 2$. (a)$\mu = 16$. (b)$\mu = 20$.

obtained from the numerically solved array factors and the desired angle ψ_0. The main beam error $\Delta\psi$ and side lobe levels are obtained from fig. 4.6. When the amplitude dynamics are ignored, the instantaneous amplitudes are assumed to remain at their free running values. With this assumption, the numerical solutions for main beam angle and side lobe level agree with the theoretical predictions.

Both main beam error and side lobe levels increase when the effects of amplitude dynamics are included, especially when a triangular amplitude distribution is employed. From this table, the main beam error increases by approximately 5 times relative to their values when using uniform amplitude distribution. Therefore, the amplitude dynamics are very significant when a under non-uniform amplitude distribution is employed for side lobe reduction. It may be adequate to use the nonlinear differential equations describing phase dynamics to model the system if a uniform amplitude distribution is used, or the oscillator are weakly coupled with each other.

The results are numerically calculated at $t = 200ns$ for weak coupling and $t = 20ns$ for strong coupling where t is the real time in the dynamics analysis. It can be shown that the steady state is achieved with those amount of time.

4.2.2 Dolph-Chebyshev Oscillator Array(DCOA)

In many application, such as point-to-point communications and direction finding, it is desirable to obtain a narrow main beam and the lowest side lobe level. The trade off between the bandwidth and side lobe level can be optimized by using the Chebyshev window for amplitude distribution. This method was recognized by Dolph [29] in 1946 and such an array is named after him as Dolph-Chebyshev Array.

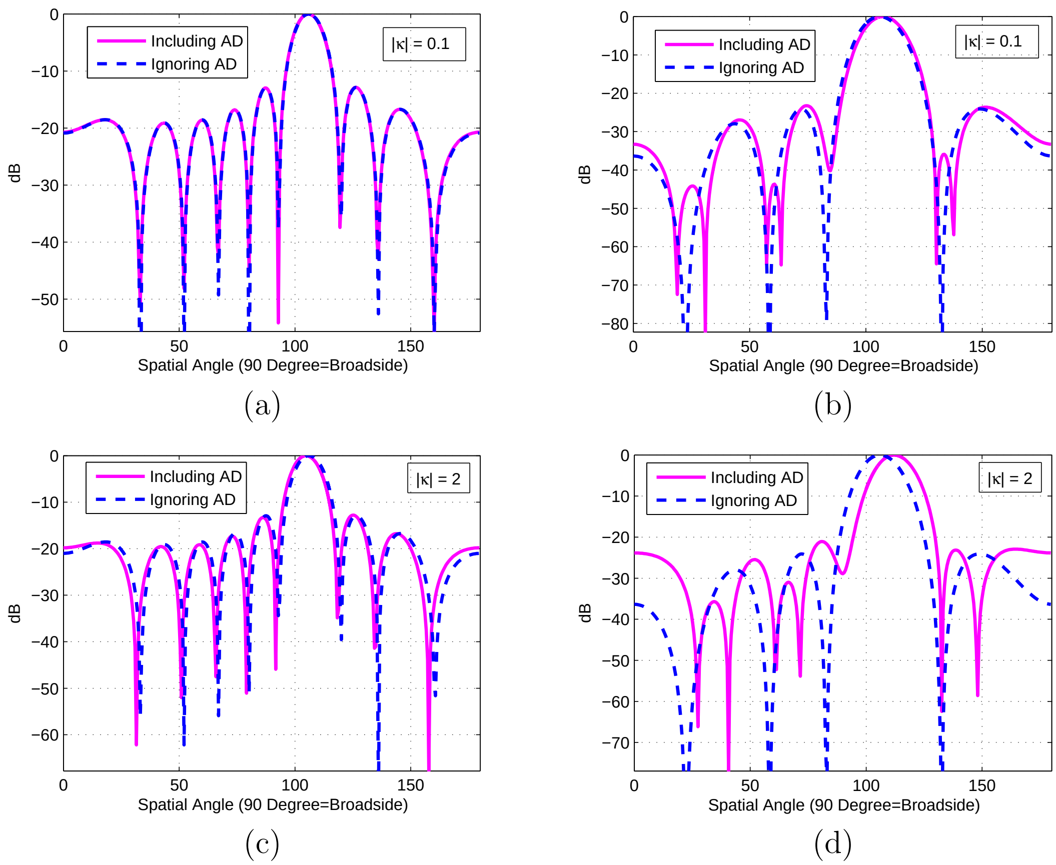

Figure 4.6: Array factors including or ignoring the effects of amplitude dynamics(AD). (a) Weakly coupled oscillator array of $|\kappa| = 0.1$ with uniform amplitude distribution. (b) Weakly coupled oscillator array of $|\kappa| = 0.1$ with triangular amplitude distribution. (c) Relatively strongly coupled oscillator array of $|\kappa| = 2.0$ with uniform amplitude distribution. (d) Relatively strongly coupled oscillator array of $|\kappa| = 2.0$ with triangular amplitude distribution.

Table 4.4 shows that the side lobe level decreased from $-12.8dB$ to $-24.1dB$ but the 3dB(or Half Power) bandwidth increases to 15.4^o for changing uniform to triangular amplitude distribution. In general, as the current amplitude is tapered more toward the edges of the array, the side lobes tend to decrease and the bandwidth increases [27][pp151].

Amplitude Excitation	HP Bandwidth	Side Lobe Level (SLL)
Uniform	11.8^o	$-12.8dB$
Triangular	15.4^o	$-24.1dB$
Dolph-Chebyshev	14.1^o	$-25.0dB$

Table 4.4: Bandwidth and side lobe level for two different amplitude distribution.

The Dolph-Chebyshev is optimum in the sense that, for the given sidelobe level of 25 dB, it has the narrowest width of all three amplitude distribution at the expense of equal sidelobe levels. Conventionally, the side lobe level of the Dolph-Chebyshev array(DCOA) can be specified as any value, but for the phase-shifterless array of coupled oscillator this may be impossible to achieve. As shown in fig. 4.6, the array factor from simulation results failed to converge to the theoretical pattern when non-uniform amplitude distribution are used. The side lobe level is reduced but at the expense of larger main beam error. We predict that there may be a tradeoff between the error of main scanning angle and side lobe level in the design of oscillator array. Although the side lobe level can be specified arbitrarily as a design requirement, when the lower side lobe level is specified, the oscillator array becomes more sensitive. In other words, the system dynamics becomes more complicated and difficult to control by using only the free-running frequencies.

Results

To investigate the theoretical predictions, we still choose the same nine element strongly coupled oscillator array. The following values for associated parameters and design criteria were chosen:

- Synchronized frequency: 10Ghz
- Coupling strength $|\kappa|$: 2(Strong)
- Coupling phase ϕ: 0 deg
- Nonlinear parameter ϵ: 1.0, 1.5, and 2.0
- Array spacing d: 0.5λ

Due to the essential impact of the empirical parameter ϵ on the system performance, different values are chosen. The free-running frequencies for achieving different side lobe level under strong coupling are found and listed in table 4.5.

SLL	Free-running Frequencies(GHz)								
20	9.277	9.746	9.695	9.852	10	10.153	10.324	10.268	10.845
25	9.034	9.476	9.612	9.812	10	10.196	10.421	10.586	11.197
30	8.875	9.281	9.532	9.774	10	10.237	10.517	10.839	11.605
35	8.538	9.126	9.458	9.738	10	10.276	10.608	10.060	12.066
40	8.299	8.994	9.389	9.706	10	10.312	10.695	11.260	12.577

Table 4.5: Calculated Free-running frequencies(GHz) of strongly coupled oscillator array for different side lobe levels. $|\kappa| = 2$.

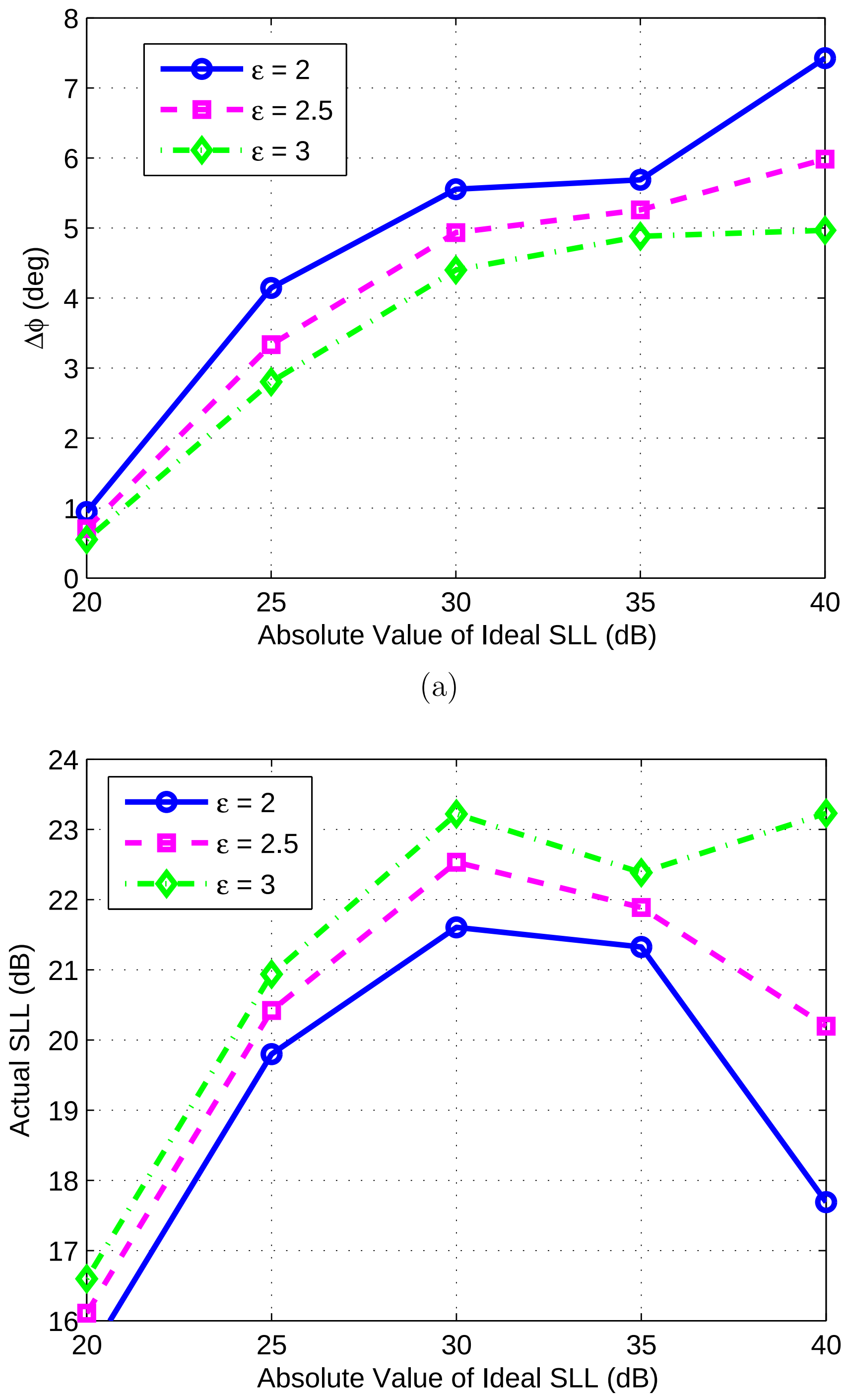

(a)

(b)

Figure 4.7: Results obtained after real time of $t = 20ns$ for strongly coupled Dolph-Chebyshev Oscillator Array(DCOA) with different desired side lobe levels. Single degree of freedom is used. (a) Main beam errors. (b) Side lobe levels.

The tradeoff between the SLL and the main beam error for the Dolph-Chebyshev Oscillator Array(DCOA) is illustrated in fig. 4.7(a) using the same nine element array with strong coupling network. As the specified side lobe levels decrease, the deviation between the desired and derived side lobe level becomes larger. The lowest side lobe level achieved is around $-23dB$ when the desired SLL was $-35dB$ with nonlinear parameter $|\epsilon| = 3.0$. For the desired side lobe level of -40dB, due to the presence of amplitude dynamics, the main beam error increases from 31% to 47% as the nonlinear parameter ϵ decreases from 3.0 to 2.0. While the desired SLL is -20dB, the main beam error is 6% for $\epsilon = 2.0$ and 3% for $\epsilon = 3.0$. Thus as the desired SLL are decreased, the difficulty of controlling the oscillator array increases.

Fig. 4.7(b) demonstrates the actual SLLs with different ideal SLLs. We observe that the actual SLL decreases more slowly than the predicted. Although the desired the side lobe level is -40dB, the realized SLL is only around -22dB but the main beam error is more than 36%. The main beam errors and the side lobe levels are obtained from the array factor calculated from the steady state amplitude and phase of array elements. The simulation results under strong coupling are obtained at $t = 20ns$, at which the steady states have been achieved.

In conclusion, there is an important tradeoff between the main beam error and the SLL for the Dolph-Chebyshev Oscillator Array(DCOA). Lower SLLs are obtained at the expense of the large main beam errors. It will be helpful to have a large value of nonlinear parameter ϵ, which can reduce this expense in this tradeoff.

4.3 Coupled Oscillator Array with Additional Degree of Freedom

The dynamics analysis derived in (2.79) implies that amplitude dynamics only have second order influence on the phase dynamics. However it is inadequate to use the differential equations describing the phase dynamics to model the system at certain conditions. As shown in table 4.3, when amplitude dynamics are included, the main beam errors increases 1.36° under weak coupling and 6.0° under strong coupling with triangular amplitude distribution. The side lobe levels under effects of amplitude dynamics are also higher than those when ignoring the effects. If oscillator array uses weak coupling network, the effects of amplitude dynamics are less intense and it may be adequate to model using only phase dynamics.

In this section, an additional degree of freedom other than the free running frequencies is developed to control the amplitude and phase dynamics simultaneously so that lower main beam errors and side lobe levels can be obtained. The conclusion is that the free running amplitude may be considered as the additional degree of freedom.

4.3.1 Amplitude Dynamics and Free-Running Amplitude

The free running frequencies were used to control the phase dynamics and establish the constant phase progression to achieve beam scanning. Because of the effects of amplitude dynamics, the assumption that the amplitude of oscillators will remain the same as free running amplitude $A_i \approx \alpha_i$ is invalid. Thus, instead of using (3.39), the phase dynamics under coupling of amplitude dynamics should be described by

$$\frac{d\theta_i}{dt} = \omega_i + \frac{\omega_i}{2Q} \sum_{j=1}^{N} Im \left\{ \kappa_{ij} \frac{A_j}{A_i} e^{j(\theta_j - \theta_i)} \right\}$$
$$i = 1, 2, \cdots, N, \tag{4.17}$$

where κ_{ij} represents the coupling parameter between i^{th} element and j^{th} element, and Q is the quality factor for the RLC resonant circuit. α_i and ω_i are the free running amplitude and frequency respectively. The free-running frequencies then are solved as

$$\omega_i = \omega \cdot \left(1 + \frac{1}{2Q} \cdot Im \left\{ \boldsymbol{\kappa}_i \times \frac{\boldsymbol{A} \cdot e^{\boldsymbol{\Delta\theta}_i}}{A_i} \right\} \right)^{-1} \tag{4.18}$$

In (4.18), the free running frequencies were obtained from the differential equations for phase dynamics by requiring the free-running phase to satisfy certain phase progression and amplitude distributions along the oscillator array. In other words, these free running frequencies were used as the sole degree of freedom to control and/or predict the system dynamics (both phase and amplitude dynamics). While including amplitude dynamics, the amplitudes will vary over time and the phase dynamics will be influenced by the effects of the coupling with the amplitude dynamics. Therefore, the system dynamics can not be analyzed accurately with only the differential equations describing the phase dynamics. Two sets of coupled nonlinear differential equations describing both amplitude and phase dynamics have to be solved in this case. In the last section, the simulation results are obtained showed that only one degree of freedom is not sufficient to precisely control and/or predict both phase and amplitude dynamics of coupled oscillator arrays. With a sole degree of freedom, the phase progression will not be uniform at a steady state, and array factors with shifted main beam angle were obtained.

Thus, it is our goal to seek additional degrees of freedom to describe, control and predict the system dynamics for both weakly and strongly coupled oscillator arrays. Similar to the free running frequency, the free running amplitude has the potential to be considered as the extra degree of freedom to control and predict the amplitude dynamics and establish certain amplitude distributions for reducing sidelobe levels.

For the coupled oscillator arrays with arbitrary coupling networks, the amplitude dynamics are described by

$$\frac{dA_i}{dt} = \frac{\mu\omega_i}{2Q}\left(\alpha_i^2 - A_i^2\right)A_i + \frac{\omega_i}{2Q}\sum_{j=1}^{N} A_j Re\left\{\kappa_{ij}e^{j(\theta_j-\theta_i)}\right\}$$
$$i = 1, 2, \cdots, N. \tag{4.19}$$

Once the steady state is achieved, the amplitudes for all elements will remain constant. Hence their derivatives should be zero. Therefore, the free running amplitudes of oscillators required to achieve certain amplitude distributions and phase progressions could be solved as follows:

$$0 = \frac{\mu\omega_i}{2Q}\left(\alpha_i^2 - A_i^2\right)A_i + \frac{\omega_i}{2Q}\sum_{j=1}^{N} A_j Re\left\{\kappa_{ij}e^{j(\theta_j-\theta_i)}\right\}$$
$$\alpha_i = \sqrt{A_i^2 - \frac{1}{\mu A_i}\sum_{j=1}^{N} A_j Re\left\{\kappa_{ij}e^{j(\theta_j-\theta_i)}\right\}}. \tag{4.20}$$

By using the free-running amplitudes as the extra degree of freedom, it is predicted that the system dynamics of both weakly and strongly coupled oscillator arrays will be more controllable and robustic. Furthermore, the questions related to the advantages and improvement using free-running amplitude as the extra degree of freedom have to be answered. Examples are shown to compare the system dynamics using the free-running amplitudes to those without using them.

4.3.2 Computer Implementation

The computer implementation using two degrees of freedom is more complicated than just using free running frequencies. First of all, the amplitude dynamics can not be ignored and has to be implemented together with the phase dynamics, and updated at every time increment. When the second degree of freedom is going to be used, the free-running amplitudes need to be calculated before the implementation of system dynamics.

The program written using matlab code consists of the following major steps:

- Define the required parameters including time step, synchronized frequency, coupling parameters, array spacing, amplitude distribution for suppressing the SLL and etc.
- Calculate the free-running frequencies using (4.3) and the free-running amplitude using (4.20).
- Calculate the instant phases and amplitudes for all elements by solving the non-linear differential equations, then update them.
- Post-processing including generation of the array factor using the steady amplitudes and phases, the transient analysis of amplitudes and phases, plotting steady amplitudes and phases and other important plots or figures.

A code structure that will implement the above requirement is suggested by the simplif in Fig. 4.8.

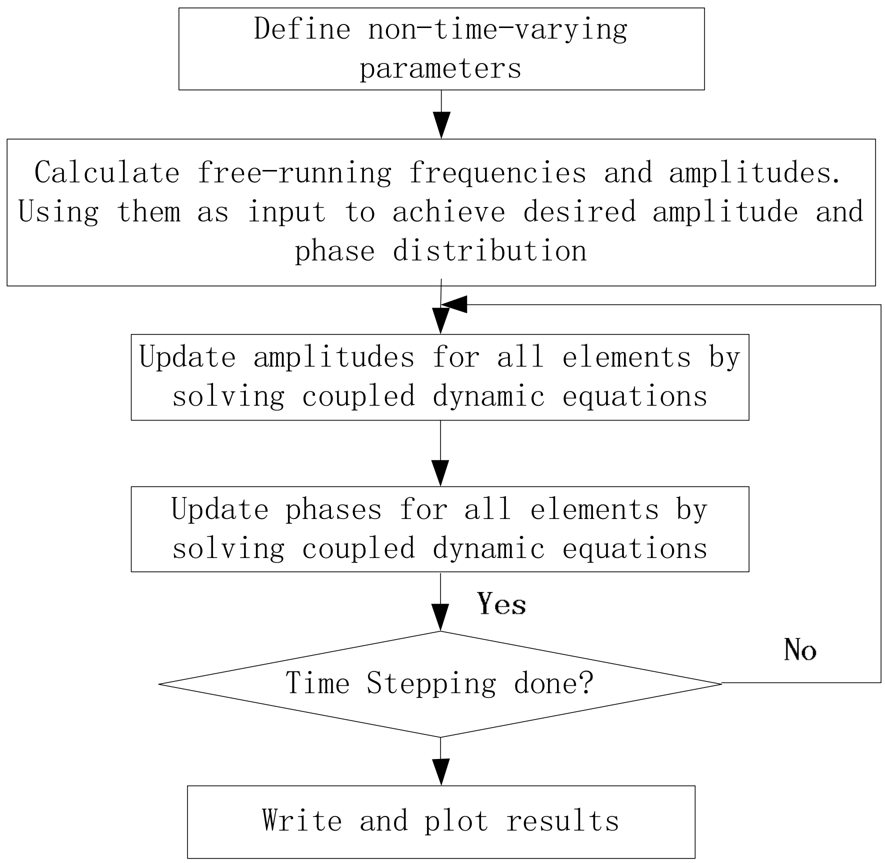

Figure 4.8: Flowchart for strongly coupled oscillator array with two degrees of freedom.

4.3.3 Triangular Amplitude Distribution with Reduced Main Beam Error

In the previous section, we have demonstrated that when a triangular amplitude distribution is employed, the main beam error is higher than when employing a uniform amplitude distribution. The effects of amplitude dynamics are more significant for strongly coupled oscillators. For weakly coupled oscillators, the interaction between elements are weak, so that the amplitudes of the oscillators do not change much from their free running values. In that case, the amplitude dynamics may be disregarded and it is adequate to describe the system dynamics simply by the differential equations of phase dynamics.

When the amplitude dynamics become more crucial, the sets of differential equations describing both amplitude and phase dynamics have to be solved to obtain more accurate simulation results. With the influence of amplitude dynamics, the amplitudes of sinusoidal waves will be also varying over time. Although the amplitudes are desired to converge and achieving the steady state of the array system, it is not guaranteed that they will. We have derived the free running amplitude in the last section, and it demonstrates the additional degree of freedom. Some adjustments on the free running amplitudes of oscillators can be made for amplitude dynamics to converge. The adjusted free-running amplitudes could be used as the additional degree of freedom for controlling the system dynamics like the free running frequencies.

Let us consider a nine-element, strongly coupled oscillator array with triangular amplitude distribution. Zero coupling phase and nearest neighbor coupling are still assumed, and coupling strengths are given by

$$|\kappa_{ij}| = \begin{cases} 2 & \text{if } |i-j| = 1 \\ 0 & \text{otherwise} \end{cases} \tag{4.21}$$

In the simulation, the quality factor of $Q = 10$ and nonlinear parameter of $\mu = 18$ are chosen. The synchronization frequency is 10Ghz. The antenna array is spaced $d = 0.5\lambda$ between adjacent elements. The array is designed to scan the main beam at 16°. At the steady state, the array should have a triangular amplitude distribution to reduce the SLL given by

$$\boldsymbol{\alpha} = \begin{bmatrix} 0.4 & 0.8 & 1.2 & 1.6 & 2.0 & 1.6 & 1.2 & 0.8 & 0.4 \end{bmatrix}, \tag{4.22}$$

and also shown in fig. 3.2.4.

Substituting (4.22) into (4.2) and (4.20), the free-running frequencies and the free-running amplitudes were obtained respectively as

$$\boldsymbol{\omega} = \begin{bmatrix} 8.678 \\ 9.292 \\ 9.517 \\ 9.633 \\ 10.0 \\ 10.396 \\ 10.535 \\ 10.825 \\ 11.797 \end{bmatrix} \text{(GHz), and } \boldsymbol{\alpha} = \begin{bmatrix} 0.2054 \\ 0.7226 \\ 1.1499 \\ 1.5628 \\ 1.9763 \\ 1.5628 \\ 1.1499 \\ 0.7226 \\ 0.2054 \end{bmatrix}. \tag{4.23}$$

Fig.4.9 shows the distribution of solved free running frequencies and amplitudes from equation (2.79) and (2.80). Fig.4.10 shows the transient analysis of an oscillator array comparing one and two degrees of freedom. In fig.4.10(b), using the solved free running amplitudes as additional degree of freedom, the amplitudes exactly converged to the preset values given by (4.22). Apparently, fig. 4.10(a) shows that they failed

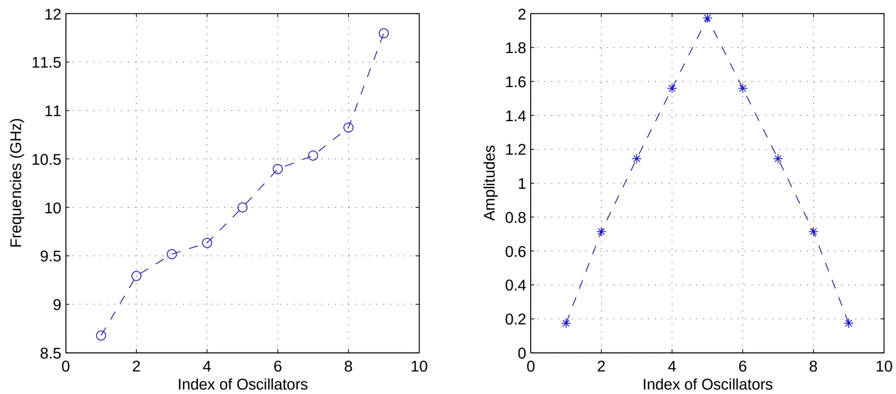

Figure 4.9: Results of a numerical integration of (2.79) and (2.80) for a nine-element oscillator array with triangular amplitude distribution, $\mu = 18$, $|\kappa| = 2$, and $f_{syn} = 10GHz$. (a) Free-running frequencies solved by (4.2) (b) Free-running amplitudes solved by (4.20).

to converge to the preset triangular amplitude values without using free running amplitudes to control the system dynamics.

Fig. 4.10(c) and 4.10(d) plot the phase difference between every element and its next adjacent element versus time. Since the phase difference of the antenna array determines the main beam scanning angle, its settling time is a crucial parameter for the oscillator array. Comparing the two figures 4.10(c) and (d), the phase difference shown with using the free running amplitudes as the addition degree of freedom converged twice as quickly as when using one degree of freedom. At the steady state, the array factor of oscillator array controlled by additional degrees of freedom completely matches the ideal array factor as shown in fig. 4.11(b). Clearly, the main beam shifted away from the theoretical angle without using the additional degree of freedom . The main beam error, SLL and convergence time have been calculated using the two different free running amplitudes, and listed in Table 4.6. From the

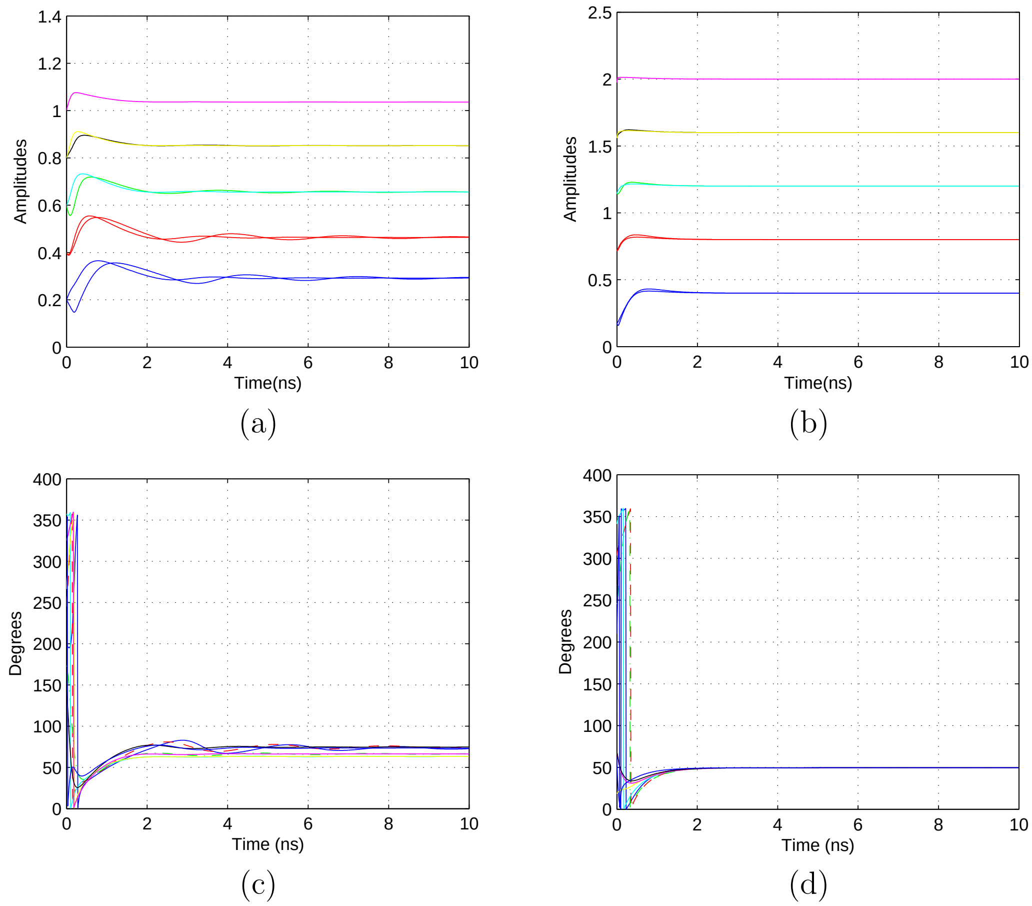

Figure 4.10: Transient analysis of system dynamics of equations (2.79) (2.80) for a nine-element oscillator array with triangular amplitude distribution, $\mu = 18$, $|\kappa| = 2$, and $f_{syn} = 10GHz$ (a) Amplitudes with only one degree of freedom (b) Amplitudes with additional degree of freedom. (c) Phase difference with one degree of freedom (d) Phase difference with additional degree of freedom.

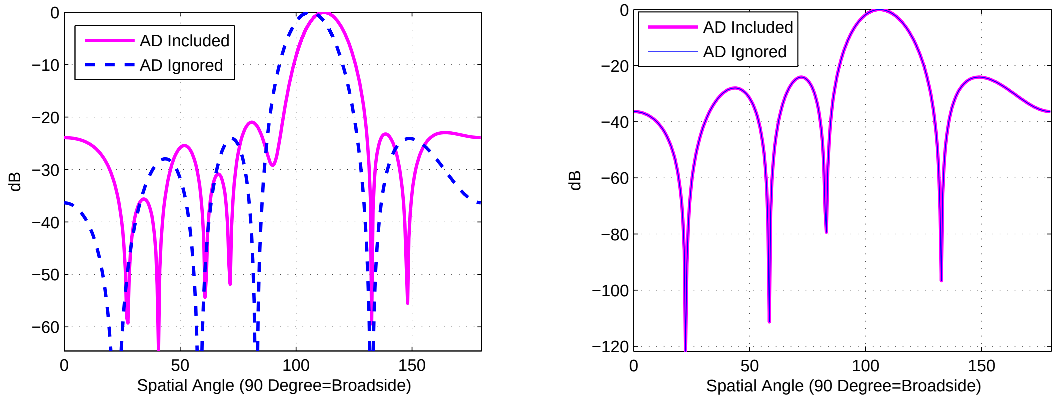

(a) (b)

Figure 4.11: Array factor analysis for a nine-element oscillator array with triangular amplitude distribution, $\mu = 18$, $|\kappa| = 2$, and $f_{syn} = 10GHz$ (a) Normalized array factor using only free-running frequencies as degrees of freedom (b) Normalized array factor using both free-running frequencies and amplitudes as degrees of freedom.

comparison, we notice that the advantages of using the free running amplitudes as an additional degree of freedom are obvious, since there are no main beam error and the side lobe levels are reduced.

Degree of Freedom	Beam Error	Side Lobe Level (SLL)	Convergence Time
One	6.1^o	$-21dB$	$1.5\mu s$
Two	0^o	$-24.1dB$	$0.6\mu s$

Table 4.6: Results comparison for one and two degree of freedom.

CHAPTER 5

ANALYSIS OF RANDOMNESS OF FREE RUNNING FREQUENCIES IN COUPLED OSCILLATOR ARRAYS

In previous chapters, we demonstrated that it is possible to achieve a constant phase progression by controlling the free running frequencies in a linear oscillator array using an appropriate coupling mechanism. Consequently, manipulation of the phase shift between the neighboring elements aims the main beam at the desired radiation angle. With a uniform amplitude distribution, the constant phase progression is simply achieved by detuning the free running frequencies of the edge element. With non-uniform amplitude distribution, the free running frequencies of all elements except the center element need to be adjusted for establishing the constant phase shift.

However due to the intrinsic differences between devices and circuits as a result of fabrication tolerance, there exists an unwanted random deviation in the free running frequencies from the desired values. This problem of randomness is considered practically important, since the deviation of the free running frequencies may cause a severe error in the phase shift, and hence the main beam direction of the oscillator array. Such a problem has been considered for certain cases [30, 31]. The theory described in [31] was applied to the dynamic analysis of the coupled oscillator array with nearest neighbor coupling, identical amplitudes, and zero coupling phases by York [5]. Recently, the results of a statistical study were presented and provided understanding of the relationships among random free-running frequency distribution, phase shift error, and beam-pointing error in a one-dimensional (1-D) oscillator array [16].

In this chapter, the discussion of the influence of the random distribution of free running frequencies on the main beam scanning angle and the progressive phase shift will be further extended to the cases of different coupling strengths using Monte Carlo Simulation. The influence of the randomness of free running frequencies is investigated for oscillator arrays with different coupling strengths when amplitude dynamics are considered. The influence on the synchronization frequency and array patterns at the steady state is also demonstrated. The randomness of free running frequencies is statistically modeled by using both Uniform and Gaussian distributions. It is noted that the oscillator arrays with uniform amplitude are only considered in the analysis, due to the fact that these arrays has been widely developed and tested in practice.

5.1 Dynamic Analysis

The dynamic equations of a general N-element coupled oscillator array with arbitrary coupling network are given by

$$\frac{dA_i}{dt} = \frac{\mu\omega_i}{2Q}\left(\alpha_i^2 - A_i^2\right)A_i + \frac{\omega_i}{2Q}\sum_{j=1}^{N} A_j Re\left\{\kappa_{ij}e^{j(\theta_j-\theta_i)}\right\}, \tag{5.1}$$

$$\frac{d\theta_i}{dt} = \omega_i + \frac{\omega_i}{2Q}\sum_{j=1}^{N} Im\left\{\kappa_{ij}\frac{A_j}{A_i}e^{j(\theta_j-\theta_i)}\right\}, \tag{5.2}$$

$$i = 1, 2, \cdots, N,$$

where A and θ are the instantaneous current amplitude and phase, while α and ω are the free running amplitude and angular frequencies respectively. The nonlinear parameter in Eq. (5.1), μ, describes the rate of saturation of the active device, and Q is the quality factor of the oscillator. The complex coupling coefficient, $\kappa_{ij} = |\kappa|_{ij}\, e^{-j\phi_{ij}}$, describes the mutual coupling between oscillators i and j, where $|\kappa|$ and ϕ represent the coupling strength and phase respectively [5, 8].

From the phase dynamic equation, a general solution of the free running frequencies can be solved as

$$\omega_i = \omega_{syc}\cdot\left[1 + \frac{1}{2Q}\sum_{j=1}^{N} Im\left\{\kappa_{ij}\frac{A_j}{A_i}e^{j(\Delta\theta_{ji})}\right\}\right]^{-1} \qquad i = 1, 2, \cdots, N, \tag{5.3}$$

where

$$\Delta\theta_{ji} = \theta_j - \theta_i = (j-i)\Delta\theta. \tag{5.4}$$

ω_{syc} is the synchronization frequency of all oscillators at the steady state. Equation (5.3) establishes a relationship between the free running frequencies and the phase progression along the array. By detuning the free running frequencies of the coupled oscillators, constant phase shifts can be achieved, hence, allowing the main beam scanning at the desired angle.

In practice, due to fabrication tolerances, there will be inherent differences between active devices and circuits. Therefore, these differences will make problems of the randomness of free running frequencies of oscillators. For coupled oscillator arrays, the randomness can cause phase shift error which, in turn, will cause an error in the main beam scanning angle (EMBSA). The EMBSA can be defined as

$$\Delta\psi = |\psi - \psi_0|, \tag{5.5}$$

where ψ is the actual main beam angle obtained from the numerically solved array factors and ψ_0 is the desired angle.

Both uniform and Gaussian distributions have been used to model the randomness of free running frequencies [5, 16], but it has not been identified which distribution agrees more with the practical phenomena. In this chapter, the influence of the randomness of both the uniform and the Gaussian distribution model is investigated. Assuming a Gaussian distribution, the free running frequency of the ith oscillator can be written as

$$\omega_i = \omega_{syc} \cdot \left[1 + \frac{1}{2Q}\sum_{j=1}^{N} Im\left\{\kappa_{ij}\frac{A_j}{A_i}e^{j(\Delta\theta_{ji})}\right\}\right]^{-1} + N(0, \sigma^2)$$
$$i = 1, 2, \cdots, N, \tag{5.6}$$

where σ^2 denotes variance of ω_i. Similarly, the randomness of the uniform distribution with zero mean is modeled by adding the random deviation in the free running frequency. Note that fabrication tolerances can also affect the quality factor Q and the coupling coefficient $|\kappa|$, but these effects are combined and modeled in the free running frequencies.

5.2 Shift of Synchronization Frequency

The phase dynamics of the oscillator array are described by Eq. (5.1). Ideally, the free running frequencies of all oscillators become synchronized to a single frequency at the steady state when there is no random distribution on the free running frequencies. In order to illustrate such synchronization phenomenon, a six-element coupled oscillator array is used as an example. The associated parameters of this example are

- Quality factor: $Q = 10$
- Coupling strength: $\epsilon = 2$
- Synchronization frequency: $f_{syc} = 10GHz$
- Array spacing: $dx = 0.5\lambda$
- Main beam direction: $\theta = 16$ deg
- Uniform amplitude distribution

First, the ideal cases of no randomness of free running frequencies are examined. Note that the amplitude of each oscillator is assumed to be identical. Since the amplitudes are uniformly distributed, only the free running frequencies of two edge elements need to be detuned for achieving the desired main beam scanning angle of 16 degree. The solved free running frequencies are plotted versus element index in Figure 5.1.

An intuitive way of observing this synchronization phenomenon and obtaining synchronized frequency is to plot the signal waveform and examine the period of

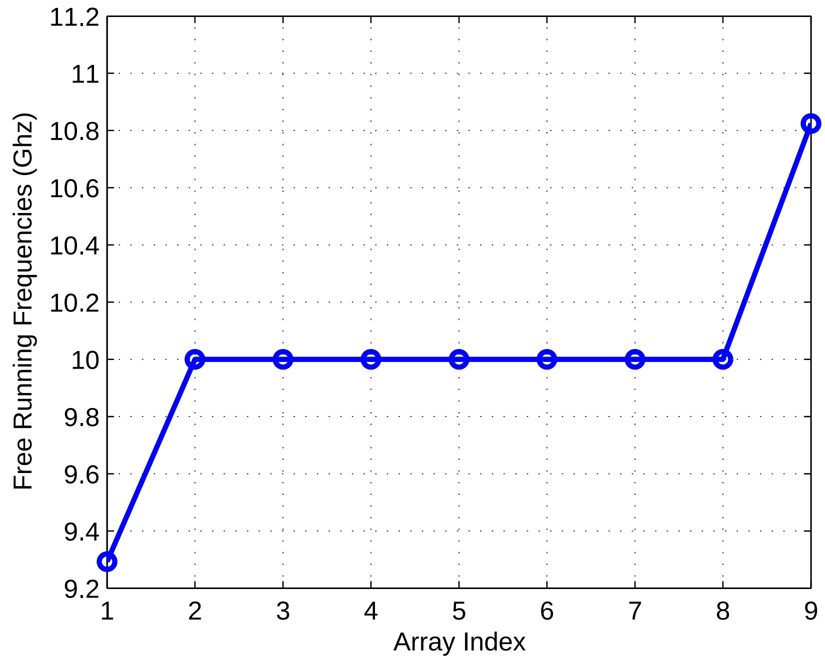

Figure 5.1: Free running frequencies for achieving beam angle of 16 degree.

the signal. Figure 5.2 shows the voltage waveforms of the left-edge element in the time domain for both start-up state 5.2(a) and steady state 5.2(b). These waveforms are obtained by solving the coupled differential equations given by (5.1) in the time domain using Euler's method. The free running frequencies of $9.292Ghz$ can be calculated from the time difference of period shown in Figure 5.2(a). Figure 5.2(b) shows the waveform of the same oscillator at the steady state, and the oscillation frequency is found as $10Ghz$ from the time difference of period. Similarly, synchronization frequencies of $10Ghz$ can be obtained for the right-edge oscillator. As shown in Figure 5.3, the oscillators are all synchronized at the same operational frequency of $10Ghz$

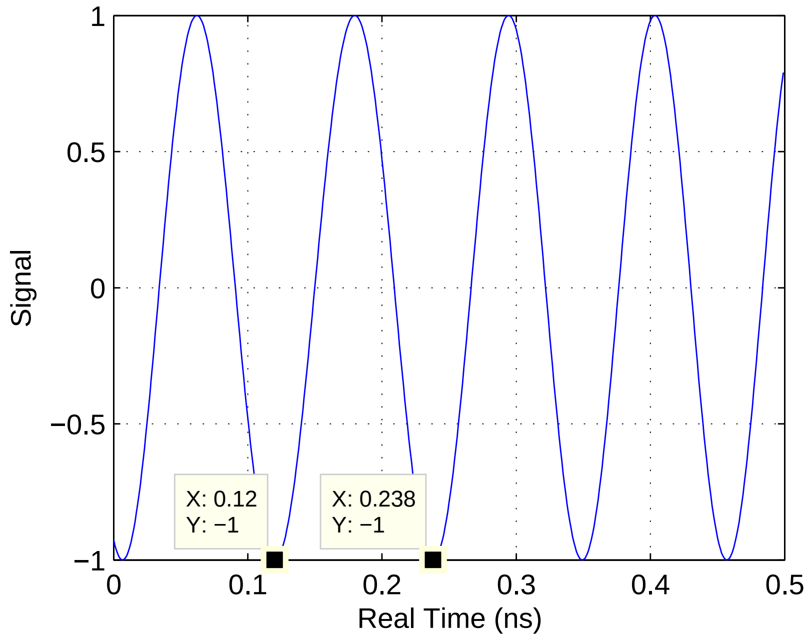

(a)

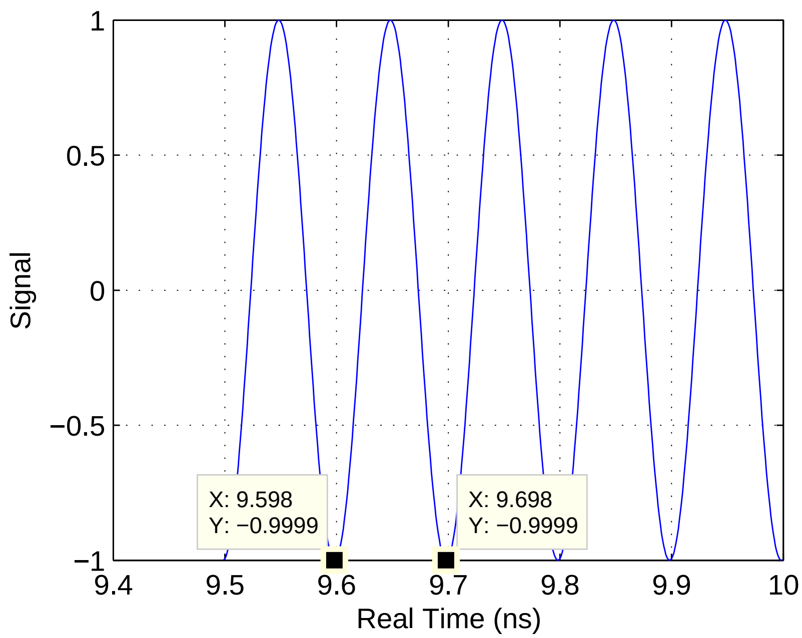

(b)

Figure 5.2: Signal waveform of edge element (Left). (a) Start-up. (b) Steady State.

at the steady state without the random deviations in the original distribution of the free running frequencies.

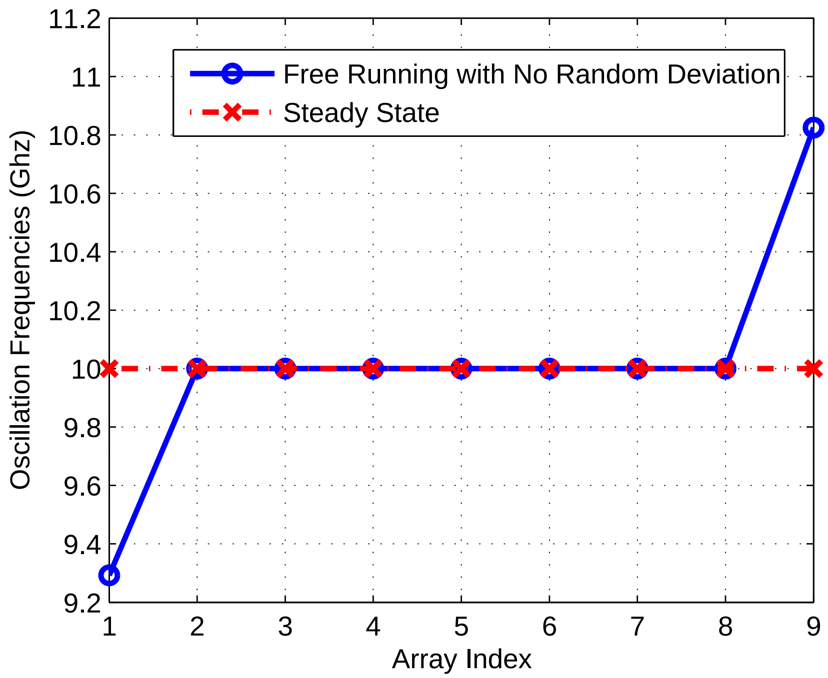

Figure 5.3: Free running frequencies and synchronization frequencies.

However, in practice, the randomness will be in the free running frequency, and will the oscillators still synchronize to the ideal frequency of $10Ghz$ under that influence? Suppose the randomness of the free running frequency is uniformly distributed as shown in Figure 5.4. The free running frequency of a single oscillator with randomness is modeled to be uniformly distributed between $f_0 - f_{err}$ and $f_0 + f_{err}$, where f_0 is the original free running frequency of the oscillator, and f_{err} represents the max deviation of the actual frequency from its original value.

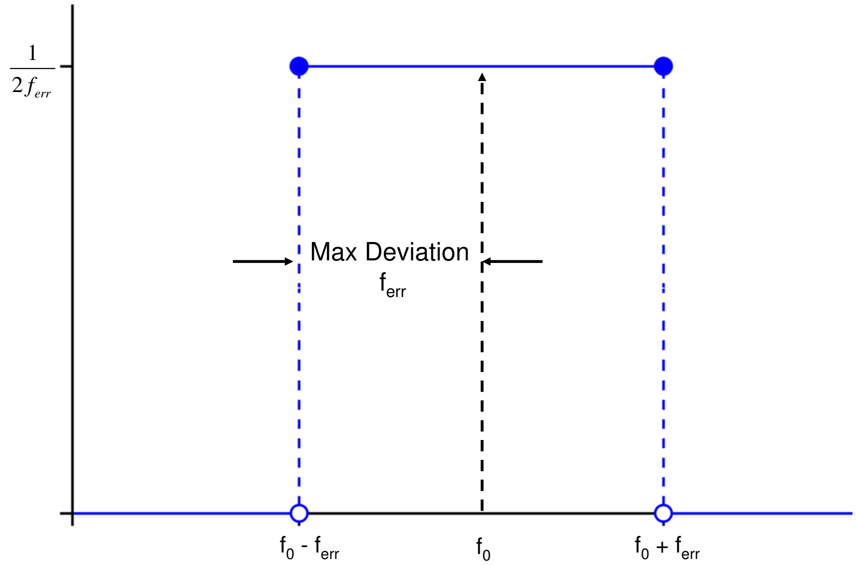

Figure 5.4: Uniform distribution model of randomness of free running frequencies of oscillators.

The coupled oscillator array with the same associated parameters is used to study the influence of the randomness of free running frequencies on the synchronization frequency. The uniform distribution is employed to model the randomness of the free running frequency with the assumption that the maximum actual deviation from the ideal frequency, f_{err}, is equal to $50Mhz$. Figure 5.5, 5.6, 5.7, and 5.8 show the free running frequencies (FRF) and the synchronization frequencies of coupled oscillator array with four different coupling strengths of 0.5, 1, 2, and 4 respectively. For oscillator arrays with coupling strengths of 0.5 and 1, the frequencies at the steady state are not synchronized to the same frequency but have random deviations. Examining results for oscillator arrays with larger coupling strengths of 2, as shown in figure 5.7, the synchronization phenomena are still observed. Due to the influence of randomness of free running frequencies, the synchronized frequency shifts from the desired frequency of $10GHz$ to $9.97GHz$. Furthermore, when the coupling strength increases to 4, oscillators are synchronized without any shifting as there is no influence of the randomness of free running frequency. It demonstrates that the randomness of the free running frequency will result in a random shift in the synchronized frequency. As the variance of the uniform distribution increases, the random shift of the synchronized frequency becomes larger.

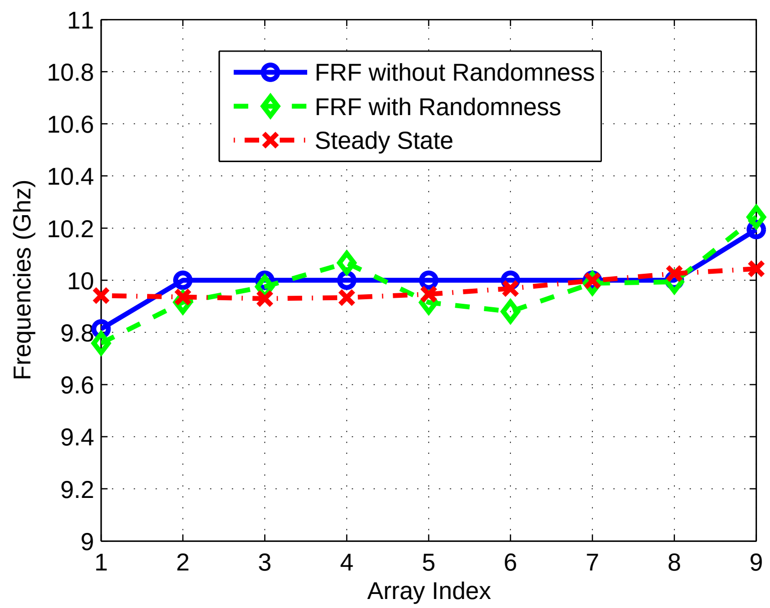

Figure 5.5: Free running and synchronized frequencies achieving beam angle of 16 degree. $|\kappa| = 0.5$.

Simulation results demonstrates that the coupling parameter is very important in the design of an oscillator array, and this was also validated by previous experimental results [5, 7]. The coupling strength influences the relationship between the main

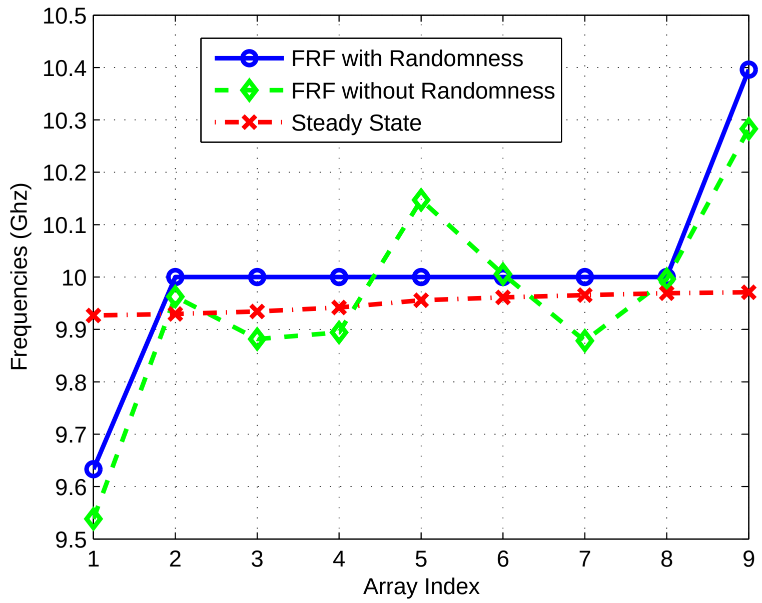

Figure 5.6: Free running and synchronized frequencies achieving beam angle of 16 degree. $|\kappa| = 1$.

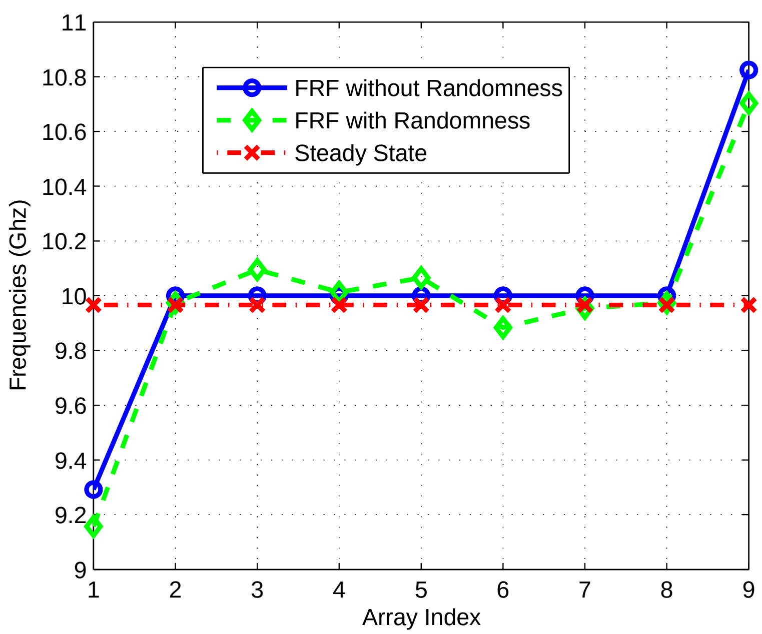

Figure 5.7: Free running and synchronized frequencies achieving beam angle of 16 degree. $|\kappa| = 2$.

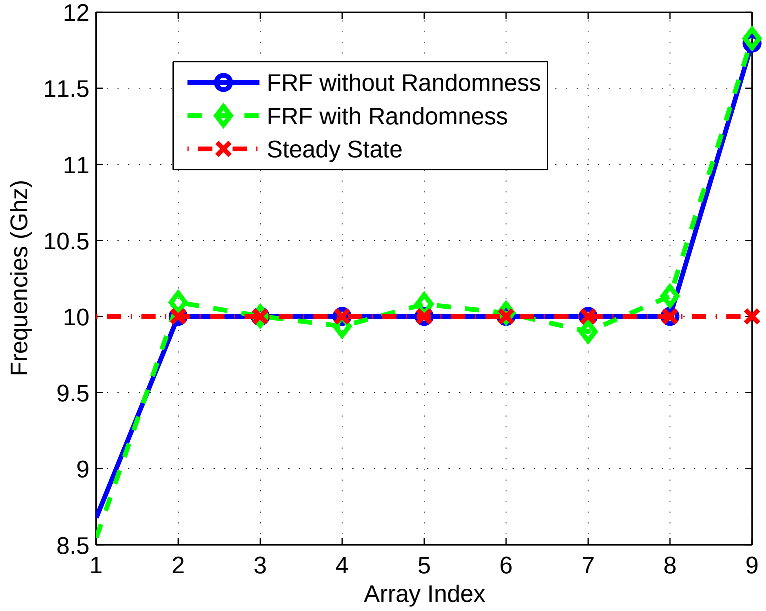

Figure 5.8: Free running and synchronized frequencies achieving beam angle of 16 degree. $|\kappa| = 4$.

beam scanning angle and the distribution of the free running frequency of coupled oscillators. An accurate characterization of the coupling parameter would be very valuable, but it is difficult to develop. Some of the previous experiments use radiative coupling between the antenna elements [7, 6] which is defined as weak coupling. In these experiments, the coupling strength is controlled by the physical distance between the antennas. In [8], a general characterization of the coupling parameter ϵ' was described, and a six-element oscillator array coupled by one-wavelength transmission line was designed and tested. Based on this model, several transmission line coupled oscillator arrays were built [32, 33, 34, 15, 14]. It is noted that the transmission line coupling typically corresponds to "strong" coupling as characterized by the coupling parameter, κ [8], and the radiative coupling was related with "weak" or "loose" coupling.

Comparing the weak coupling of $\epsilon^{'} = 0.5$ (figure 5.5) with the stronger coupling of $\epsilon^{'} = 4$ (figure 5.8), a small detuning of the free running frequencies can achieve the same amount of relatively large main beam angle, in this case, 16° from broadside. Thus same random deviations in the free running frequencies will cause a larger error in the main beam scanning angle when using loose coupling between the oscillators. In the case of weak coupling, oscillators with the capability of more accurate frequency detuning are required in order to obtain better resolution of the main beam scanning angle. Typically, such oscillators are complicated and difficult to fabricate. If a stronger coupling network can be employed, the frequency detuning range becomes larger and hence the array will achieve a good beam scanning resolution without tight requirements of accurate control of the free running frequencies.

5.3 Monte Carlo Simulation

In the practical design of a coupled oscillator array, another issue is that random variations in the free running frequency exist for a real oscillator due to fabrication tolerances. Therefore, the oscillators and their free running frequencies in such an array may not be completely identical as desired. Such deviations in the free running frequencies can cause a significant error of the main beam scanning angle (EMBSA). The effects of randomness in free running frequency on the main beam scanning angle are investigated here by Monte Carlo simulations. Note that fabrication tolerances affect the quality factor Q and the coupling coefficient $|\kappa|$ also, but these effects are combined and modeled in the free running frequencies. Both uniform and Gaussian distributions have been used to model the randomness in the free running frequencies [5, 16], but it has not been identified which distribution agrees more with the practical phenomena.

In the simulation, the associated parameters for design examples are

- Quality factor: $Q = 10$
- Synchronization frequency: $f_{syc} = 10GHz$
- Array spacing: $dx = 0.5\lambda$
- Main beam direction: $\theta = 18$ deg
- Uniform amplitude distribution

Four different coupling strengths of 0.2, 0.5, 2, and 4 are considered. The flow chart of the Monte Carlo simulation is shown in Figure 5.9. Pseudo-random number generator is used for the simulations. Two different random distribution of free running frequencies are considered: Uniform and Gaussian. The computation is repeated 10 thousand times for each coupling strength and statistical model. The time stepping h is chosen as 10^{-10} for coupling strength of ϵ =0.2 or 0.5, and 10^{-11} for coupling strength of ϵ =2 or 4.

5.3.1 Uniform Distribution

The variance of free running frequency with the uniform distribution is determined by the max deviation f_{err} and proportional with it. Monte Carlo methods are a class of computational algorithms that rely on repeated random sampling to compute their results. For the same simulation using the same computer, it takes longer time when

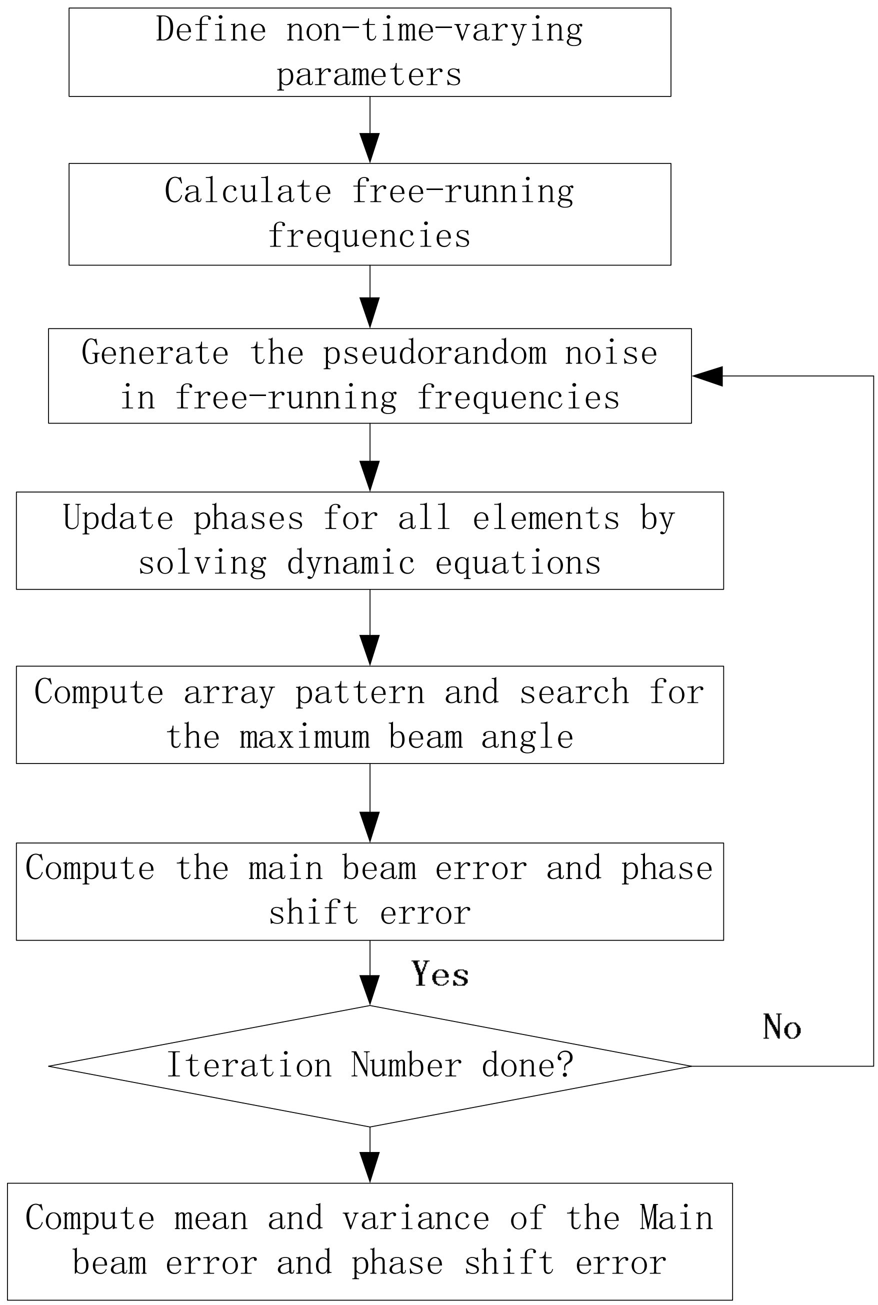

Figure 5.9: Flow chart of coupled oscillator simulation with randomness in free running frequency.

more random sample is repeated. Due to the limitation of the computer memory and speed, 10 thousand random samples are generated and simulated in this case. It should be noted that 1000 time steps are solved and the minimal angle of calculated array factor is 0.003 degree. The number of time steps determines the real time the program simulates under certain coupling strength. For example, if the time stepping of $h = 10^{-10}$ is chosen, the real time simulated in the study is equal to $100ns$. Since the steady state may be not completely achieved in $100ns$, the EMBSAs could be slightly larger than values at the steady state. Also, it is noted that the minimal angle will not affect the accuracy of results of EMBSAs unless the mean beam scanning error is lower than 0.003 degree.

Figure 5.10(a) shows the mean of main beam error plotted versus the max frequency deviation f_{err} for four different coupling strengths. As the deviation of free running frequencies increases, the error of mean beam angle becomes larger. It demonstrates that the oscillator arrays with strong couplings behave more robustly than with weakly coupled array under the influence of the randomness of the free running frequency. Figure 5.10(b) shows the variance of the main beam error for ten thousand samples. Figure 5.11 shows the mean and variance of the phase shift for each random model. Similar trends are observed for the phase shift comparing with the results for EMBSAs.

5.3.2 Gaussian Random Model

Gaussian distribution is also studied since the randomness of free running frequency is associated with several random processes within the fabrication process.

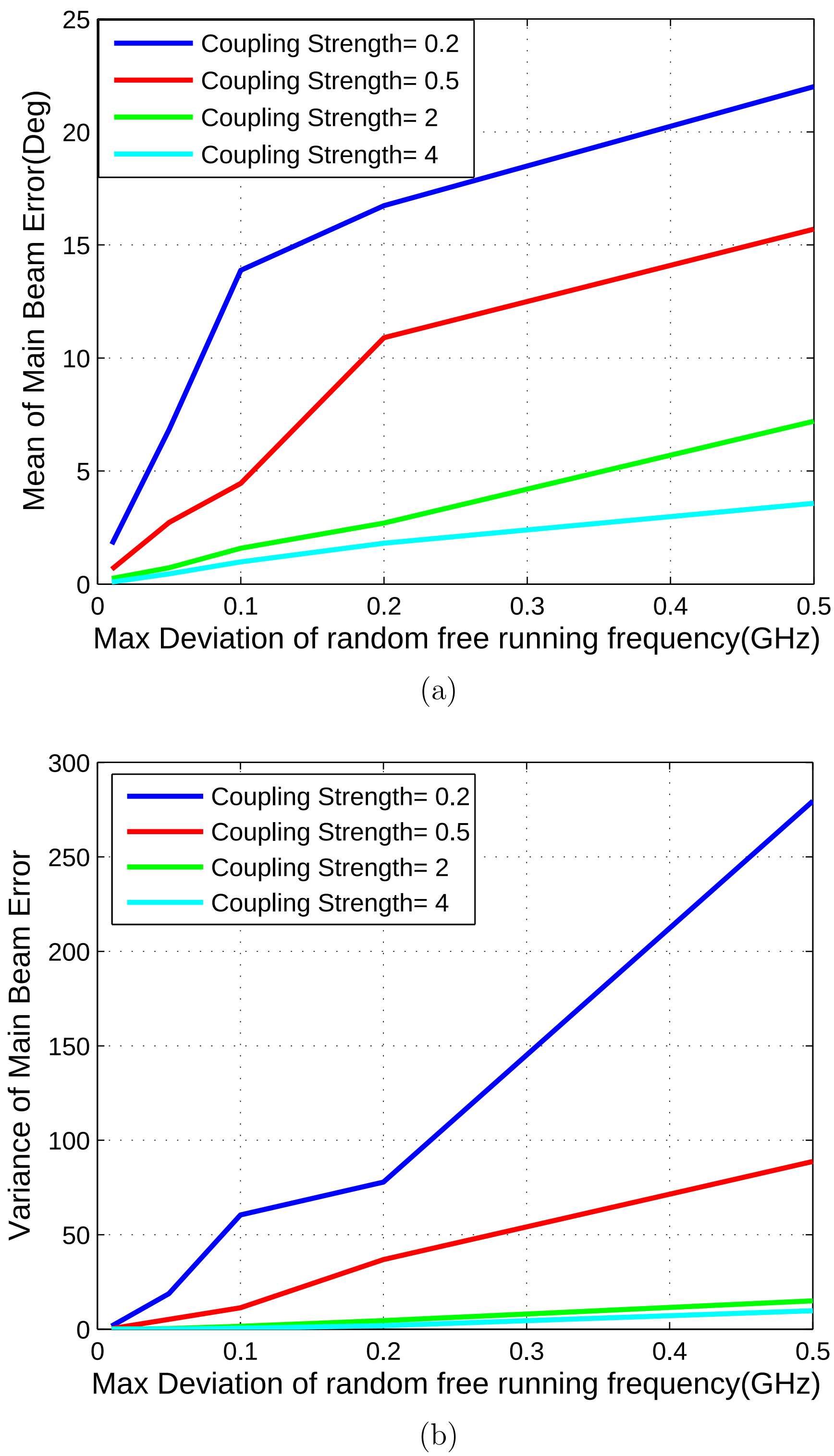

Figure 5.10: Error of main beam angle (a) Mean. (b) Variance.

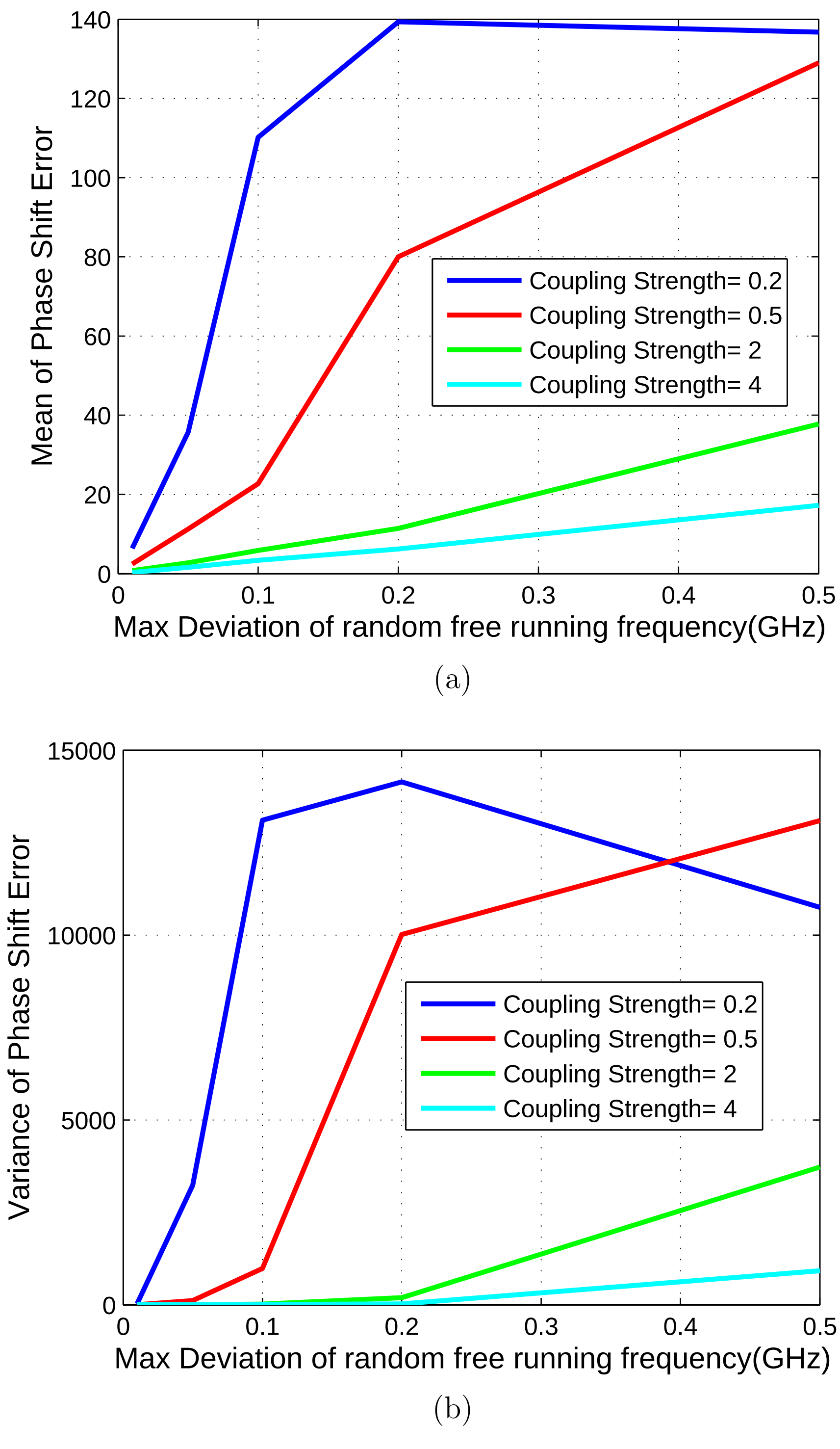

Figure 5.11: Error of phase shift along the array (a) Mean. (b) Variance.

These phenomena can be approximated by Gaussian distributions due in part to the central limit theorem. The free running frequencies with Gaussian randomness are shown in figure 5.12.

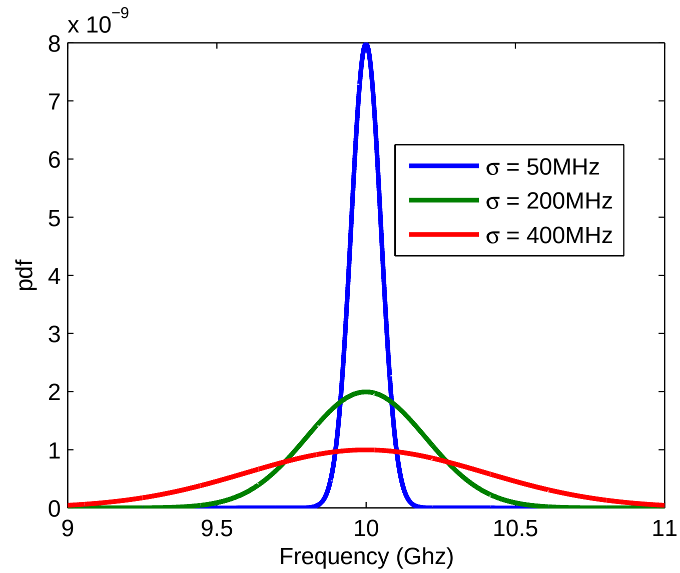

Figure 5.12: Gaussian random model of free running frequency with different standard deviation.

As used for the uniform random model, the same design example of the coupled oscillator array is used for investigating the influence of the randomness with Gaussian distribution. The mean and variance of the EMBSA due to different random deviations in the free running frequencies are shown in figure 5.13 using Monte Carlo simulation. Four different coupling strengths are considered. As shown in figure 5.13(a), the average error of main beam angle decreases when the coupling becomes stronger, and they drop quickly as the deviation in the free running frequency increases. Similar to the case of uniform randomness, it is inferred that oscillator arrays with strong coupling are more robust than the same arrays with weak coupling under the influence of the randomness of free running frequencies. Moreover, as the random deviation of free running frequency becomes larger, the robustness of the strongly coupled oscillator array is especially obvious.

Figure 5.14 shows the average array patterns for the corresponding cases. The theoretical model [27] of microstrip patch resonating at $10GHz$ is used in the computation of the total pattern. For the average array factors, more obvious distortion can be noticed for weak coupling than strong coupling, which results by adding up the shifted array factor for each simulation. It is noted that the element pattern has no influence on the mean of EMBSA, but it does attenuate heavily the side lobe levels as shown in Figure 3.5.

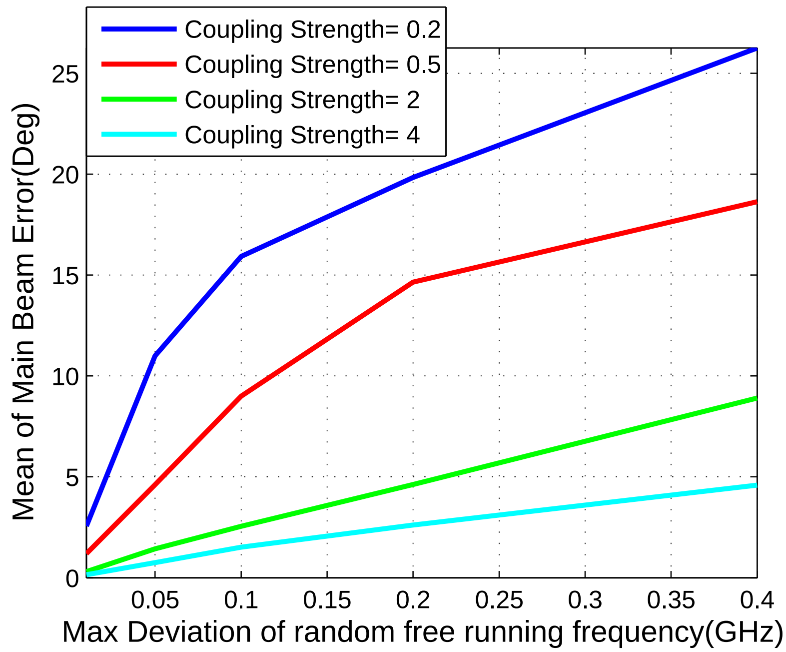

(a)

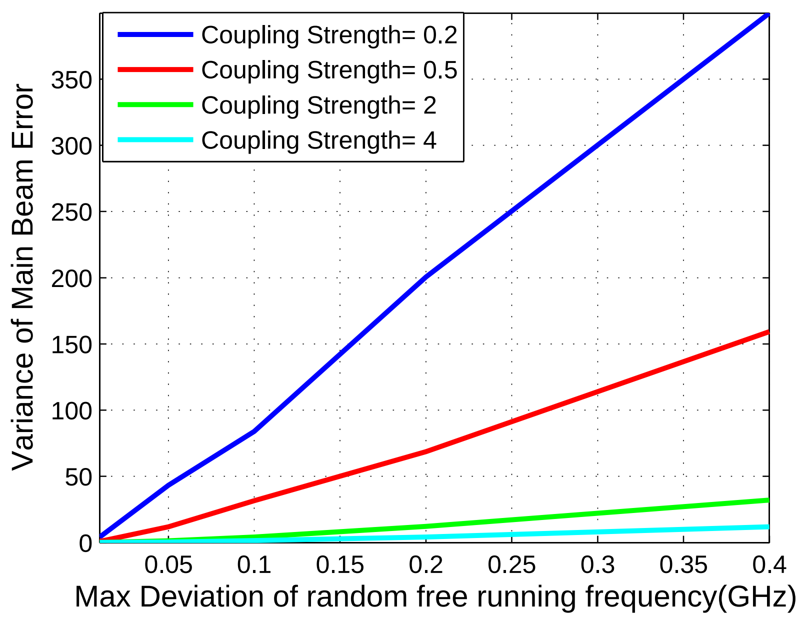

(b)

Figure 5.13: Error of main beam angle due to Gaussian free running frequency (a) Mean. (b) Variance.

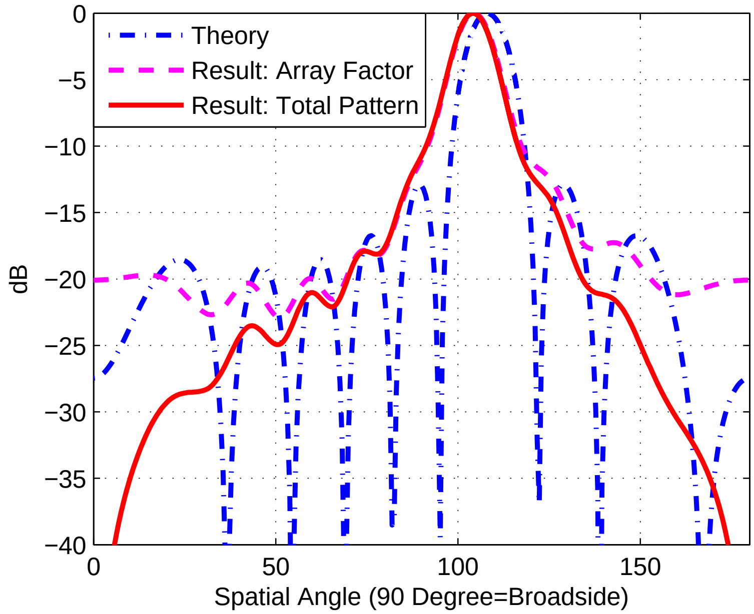

(a)

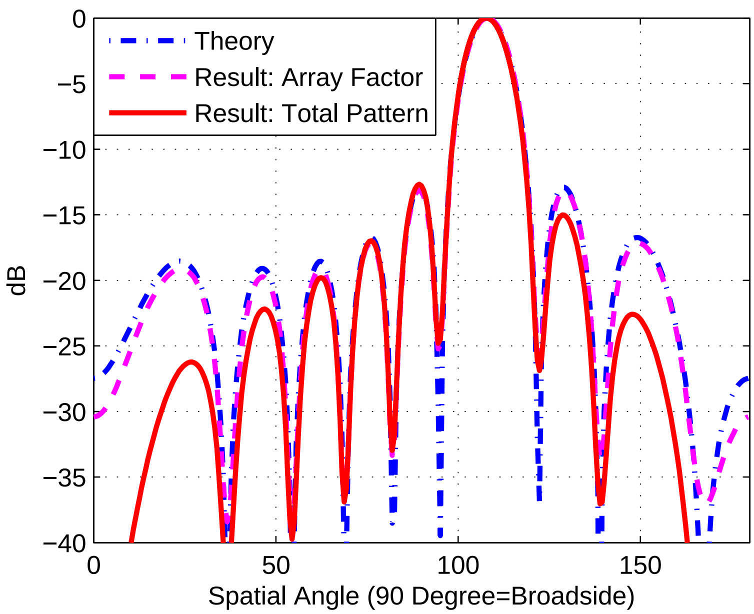

(b)

Figure 5.14: Average patterns (a) Weak coupling $|\kappa| = 0.5$. (b) Strong coupling $|\kappa| = 4$.

CHAPTER 6

CONCLUSION AND FUTURE WORK

This dissertation studies nonlinear dynamic behavior of coupled oscillator arrays (COAs), and the control of beam steering angle and shape. By modeling the microwave oscillator using a parallel or series RLC circuit, and the coupling network using a complex number, sets of nonlinear differential equations describing amplitude and phase dynamics are developed. For the parallel circuit modeling, two different approaches of time and frequency domain are used individually, and simulation results are obtained.

The phase dynamic analysis of synchronized coupled oscillators is presented and applied to one and two dimensional beam scanning array. The stability and nonlinear behaviors are studied using nonlinear control theory. The equilibrium point is solved analytically when a specific distribution of free running frequency of oscillators is chosen. It is shown that there exists a unique stable equilibrium point in a one-dimensional coupled oscillator array which is associated with desired phase shifts for achieving the beam scanning technique. However, the theory shows that COAs with the nearest neighbor coupling are only stable within a limited range of main beam scanning angle. Two-dimensional and three-dimensional phase portraits of practical design examples demonstrate that the qualitative behavior of this equilibrium point is similar to a stable node.

In the last two decades, while COAs have been extensively studied, few attentions have been given to effects of amplitude dynamics. The nonlinear behavior and stability of the COA system were mainly predicted by phase dynamics while effects of amplitude dynamics are simply ignored. The research presented in this dissertation investigated, exclusively, effects of amplitude dynamics for the nearest neighbor COA with different coupling strength for different synchronization frequencies. Results show that amplitude dynamics have significant influence on the main beam scanning angle when the oscillators are strongly coupled, and effects are strongly associated with the nonlinear parameter μ which denotes the saturation rate of the active device. For COAs using triangular amplitude distribution, free running frequencies of all oscillators, except the center one, need to be detuned to achieve the desired constant phase shifts along the array. It is also demonstrated that amplitude control of individual elements in a coupled oscillator array can be achieved, as is shown with the triangular and Chebyshev amplitude distribution. They corroborate the notion that control of the SLL and the main beam scanning angle can be achieved with a strongly coupled oscillator array. The influence of random free running frequencies is also investigated for COAs with different coupling strengths using Monte Carlo simulation. Results demonstrate that the oscillator array with strong coupling is more robust against the random deviation of the free running frequencies and also gives better beam scanning resolution.

Being an attractive technique, there are still many interesting problems, limitations and applications which needs to be understood for COAs. Future research may focus on oscillator bandwidth, coupling network design, modulation applications, and experimental verifications. It is also interesting to use more complicated and accurate model for the oscillator instead of using the Van der Pol's oscillator model, for example using the commercial software for modeling and demonstration of the beam scanning technique.

APPENDIX A

DOLPH-CHEBYSHEV ARRAY

Design Procedure

The Dolph-Chebyshev Oscillator Array(DCOA) was developed through the Chebyshev polynomials, so it is important for us to give a brief review of them. The Chebyshev (sometimes spelled "'Tchebyscheff"') polynomials are defined by

$$T_n(x) = \begin{cases} (-1)^n cosh(ncosh^{-1}|x|) & x < -1 \\ cos(ncos^{-1}x) & -1 < x < 1 \\ cosh(ncosh^{-1}x) & x > 1 \end{cases} \tag{A.1}$$

By letting $\delta = cos^{-1}x$, in the range $-1 < x < 1$, the term $cosm\delta$ can be expanded in powers of $cos\delta$. For example, $T_3(x) = cos(3cos^{-1}x) = cos3\delta = 4cos^3\delta - 3cos\delta$. Thus

$T_3(x) = 4x^3 - 3x$. Similarly, a few of the lower order polynomials are

$$\begin{aligned}
T_0(x) &= 1 \\
T_1(x) &= x \\
T_2(x) &= 2x^2 - 1 \\
T_3(x) &= 4x^3 - 3x \\
T_4(x) &= 8x^4 - 8x^2 + 1 \\
T_5(x) &= 16x^5 - 20x^3 + 5x \\
T_6(x) &= 32x^6 - 48x^4 + 18x^2 - 1 \\
T_7(x) &= 64x^7 - 112x^5 + 56x^3 - 7x \\
T_8(x) &= 128x^8 - 256x^6 + 160x^4 - 32x^2 + 1
\end{aligned} \tag{A.2}$$

The recursion formula for generating higher order polynomials can be derived as

$$T_{n+1}(x) = 2xT_n(x) - T_{n-1}(x) \tag{A.3}$$

For an equally spaced linear array with interelement spacings d, the array factor for P number is

$$\begin{aligned}
f(\theta) &= \sum_{m=-N}^{N} i_m e^{j2\pi m(d/\lambda)cos\theta} && \text{Odd} \\
&= \sum_{m=1}^{N} (i_m e^{-j\pi(2m-1)(d/\lambda)cos\theta} + i_m e^{j\pi(2m-1)(d/\lambda)cos\theta}, && \text{Even}
\end{aligned} \tag{A.4}$$

with the physical center of the array is located at the origin for simplicity. The number of elements P is equal to $2N$ for even and $2N + 1$ for odd. A real-valued array factor can be obtained using symmetrical excitation as

$$f(\varphi) = \begin{cases} i_0 + 2\sum_{m=1}^{N} i_m cosm\varphi & \text{P Odd} \\ 2\sum_{m=1}^{N} i_m cos\left[(2m-1)\frac{\varphi}{2}\right] & \text{P Even} \end{cases}$$

where $\varphi = 2\pi(d/\lambda)cos\theta$. This array factor for either odd or even number P can be written in a sum of $cos(m\varphi/2)$ terms up to $m = P - 1$, and each term of $cos(m\varphi/2)$ can be written as a sum of terms with powers of $cos(m\varphi/2)$ up to m, through the use of trigonometric identities. That is

$$\begin{aligned} cos(0) &= 1 \\ cos(\varphi/2) &= cos(\varphi/2) \\ cos(2\varphi/2) &= 2cos^2(\varphi/2) - 1 \\ cos(3\varphi/2) &= 4cos^3(\varphi/2) - 3cos(\varphi/2) \\ cos(4\varphi/2) &= 8cos^4(\varphi/2) - 8cos^2(\varphi/2) + 1 \\ cos(5\varphi/2) &= 16cos^5(\varphi/2) - 20cos^3(\varphi/2) + 5cos(\varphi/2) \\ cos(6\varphi/2) &= 32cos^6(\varphi/2) - 48cos^4(\varphi/2) + 18cos^2(\varphi/2) - 1 \\ cos(7\varphi/2) &= 64cos^7(\varphi/2) - 112cos^5(\varphi/2) + 56cos^3(\varphi/2) - 7cos(\varphi/2) \\ cos(8\varphi/2) &= 128cos^8(\varphi/2) - 256cos^6(\varphi/2) + 160cos^4(\varphi/2) - 32cos^2(\varphi/2) + 1 \end{aligned} \tag{A.5}$$

For higher order, the recursive formula

$$cos((n+1)\frac{\varphi}{2}) = 2cos(\frac{\varphi}{2})cos(\frac{n\varphi}{2}) - cos((n-1)\frac{\varphi}{2}), \tag{A.6}$$

could be used. It can be shown that using the transformation

$$x = x_0 cos\frac{\varphi}{2}, \tag{A.7}$$

the Chebyshev polynomials (A.2) are able to match the array factor expansions as

$$f(\varphi) = T_{P-1}\left(x_0 cos\frac{\varphi}{2}\right) \tag{A.8}$$

where x_0 is the point on the Chebyshev polynomial curves that corresponds to the maximum main beam point for the array factor. Let R denote the main beam-to-side lobe ratio and the side lobe ratio level magnitude to be unity, then R will be the value of the array factor at the main beam maximum. It should be noted that for Dolph-Chebyshev array it is more convenient to normalized the array factor f to a maximum value of R and the side lobe level to be unity. The side lobe level for an array factor normalized to a maximum value of unity is set to be SLL and in that case the side lobe level is 1/R. The relationship between the SLL and R can be derived as

$$SLL = -20log_{10}R \quad dB \tag{A.9}$$

From (A.8), at the maximum main beam point

$$R = T_{P-1}(x_0) = cosh\left[(P-1)cosh^{-1}x_0\right]. \tag{A.10}$$

Solving for x_0, we obtain

$$x_0 = cosh\left(\frac{1}{P-1}cosh^{-1}R\right). \tag{A.11}$$

Example

Based on the theoretical analysis above, a nine element Dolph-Chebyshev oscillator array(DCOA) with -30 side lobe level is designed. The array factor from (A.5) is

$$f(\varphi) = i_0 + 2i_1cos\varphi + 2i_2cos2\varphi + 2i_3cos3\varphi + 2i_4cos4\varphi, \tag{A.12}$$

From (A.5), the $cosm\varphi$ terms can be written as

$$
\begin{aligned}
cos(\varphi) &= cos(2\varphi/2) = 2cos^2(\varphi/2) - 1 \\
cos(2\varphi) &= cos(4\varphi/2) = 8cos^4(\varphi/2) - 8cos^2(\varphi/2) + 1 \\
cos(3\varphi) &= cos(6\varphi/2) = 32cos^6(\varphi/2) - 48cos^4(\varphi/2) + 18cos^2(\varphi/2) - 1 \\
cos(4\varphi) &= cos(8\varphi/2) = 128cos^8(\varphi/2) - 256cos^6(\varphi/2) + 160cos^4(\varphi/2) - 32cos^2(\varphi/2) + 1
\end{aligned}
\tag{A.13}
$$

Substituting (A.13) into (A.12), the array factor is found as

$$
\begin{aligned}
f(\varphi) = (i_0 - 2i_1 + 2i_2 - 2i_3 + 2i_4) + cos^2\frac{\varphi}{2}(4i_1 - 16i_2 + 36i_3 - 64i_4) \\
+ cos^4\frac{\varphi}{2}(16i_2 - 96i_3 + 320i_4) + cos^6\frac{\varphi}{2}(64i_3 - 512i_4) + 256i_4cos^8\varphi 2.
\end{aligned}
\tag{A.14}
$$

The corresponding Chebyshev polynomial is

$$
T_8\left(x_0cos\frac{\varphi}{2}\right) = 128x_0^8cos^8\frac{\varphi}{2} - 256x_0^6cos^6\frac{\varphi}{2} + 160x_0^4cos^4\frac{\varphi}{2} - 32x_0^2cos^2\frac{\varphi}{2} + 1 \tag{A.15}
$$

From (A.8), equal the coefficient of $cos^8\frac{\varphi}{2}$ term

$$
128x_0^8 = 256i_4. \tag{A.16}
$$

To solve i_4, we need to know

$$
R = 10^{-\frac{SLL}{20}} = 10^{1.5} = 31.623, \tag{A.17}
$$

so that

$$
\begin{aligned}
x_0 &= cosh\left(\frac{1}{P-1}cosh^{-1}R\right) \\
&= cosh\left(\frac{1}{8}cosh^{-1}(31.623)\right) = 1.1374.
\end{aligned}
\tag{A.18}
$$

From (A.16),

$$i_4 = \frac{x_0^8}{2} = 1.4003. \tag{A.19}$$

By taking i_4 into the equation,

$$64i_3 - 512i_4 = -256x_0^6 \Rightarrow i_3 = 2.5426. \tag{A.20}$$

Similarly,

$$16i_2 - 96i_3 + 320i_4 = 160x_0^4 \Rightarrow i_2 = 3.9854. \tag{A.21}$$

and

$$4i_1 - 16i_2 + 36i_3 - 64i_4 = -32x_0^2 \Rightarrow i_1 = 5.1131. \tag{A.22}$$

Substituting $i_1 - i_4$ into the constant term gives,

$$i_0 = 5.5401. \tag{A.23}$$

The final element currents are

$$\begin{aligned} i_{-4} = i_4 &= 1.4003, & i_{-3} &= i_3 = 2.5426 \\ i_{-2} = i_2 &= 3.9854, & i_{-1} &= i_1 = 5.1131 \\ i_0 &= 5.5401. \end{aligned} \tag{A.24}$$

BIBLIOGRAPHY

[1] R. Adler, "A study of locking phenomena in oscillators," *Proceedings of the IEEE*, vol. 61, no. 10, pp. 1380–1385, 1973.

[2] K. Kurokawa, "Injection-locking of solid-state microwave oscillator," *Proceedings of the IEEE*, vol. 61, no. 10, pp. 1386–1409, 1973.

[3] K. Kurokawa, "Some basic characteristics of broadband negative resistance oscillator circuits," *Bell System Technical Journal*, vol. 48, pp. 1937–1955, 1969.

[4] K. Stephan and W. Morgan, "Analysis of inter-injection-locked oscillators for integrated phased arrays," *IEEE Trans. Antennas Propagat.*, vol. 35, pp. 771–781, 1987.

[5] R. York, "Nonlinear analysis of phase relationships in quasi-optical oscillator arrays," *IEEE Trans. Microwave Theory Tech.*, vol. 41, no. 10, pp. 1799–1809, 1993.

[6] P. Liao and R. York, "A new phase-shifterless beam-scanning technique using arrays of coupled oscillators," *IEEE Trans. Microwave Theory Tech.*, vol. 41, no. 10, pp. 1810–1815, 1993.

[7] R. A. York and R. C. Compton, "Measurement and modelling of radiative coupling in oscillatro arrays," *IEEE Trans. Microwave Theory Tech.*, vol. 41, no. 3, pp. 438–443, 1993.

[8] R. A. York, P. Liao, and J. J. Lynch, "Oscillator array dynamics with broadband n-port coupling network," *IEEE Trans. Microwave Theory Tech.*, vol. 42, no. 11, pp. 2040–2045, 1994.

[9] A. Georgiadis, A. Collado, and A. Suárez, "New techniques for the analysis and design of coupled-oscillator systems," *IEEE Trans. Microwave Theory Tech.*, vol. 54, no. 11, pp. 3864–3877, 2006.

[10] J.-H. Hwang and N. Myung, "A new beam-scanning technique by controlling the coupling angle in a coupled oscillator array," *IEEE Microwave and Guided Wave Lett.*, vol. 8, pp. 191–193, May 1998.

[11] R. J. Pogorzelski, P. F. Maccarini, and R. York, "A continuum model of the dynamics of coupled oscillator arrays for phase-shifterless beam scanning," *IEEE Trans. Microwave Theory Tech.*, vol. 47, no. 4, pp. 463–470, 1999.

[12] T. Heath, "Simultaneous beam steering and null formation with coupled, nonlinear oscillator arrays," *IEEE Trans. Antennas Propagat.*, vol. 53, no. 6, pp. 2031–2035, 2005.

[13] R. J. Pogorzelski, "A two-dimensional coupled oscillator array," *IEEE Microwave and Guided Wave Lett.*, vol. 10, pp. 478–480, Nov. 2000.

[14] J. Shen and L. Pearson, "A design for a two-dimensional coupled oscillator beam-steering antenna array," *IEEE Antennas Wireless Propagat. Lett.*, vol. 2, no. 24, pp. 360–362, 2004.

[15] T. Heath, "Two-dimensional, nonlinear oscillator array antenna," *IEEEAC*, no. 1070, pp. 1–12, 2004.

[16] J. Shen and L. Pearson, "The phase error and beam-pointing error in coupled oscillator arrays," *IEEE Trans. Antennas Propagat.*, vol. 53, no. 1, pp. 386–393, 2005.

[17] T. Heath, "Beam shaping of coupled, nonlinear oscillator arrays," *Proc. SPIE-Radar Sensor Technology VI*, vol. 4374, pp. 114–222, 2001.

[18] H. Jiang, K. Pasala, and R. Penno, "Effects of amplitude dynamics for nonlinear coupled oscillator arrays," *Proc. IEEE AP-S Int. Symp.*, pp. 1–4, 2008.

[19] B. V. der Pol, "The nonlinear theory of electric oscillations," *Proceedings of the IRE*, vol. 22, pp. 1051–1085, 1934.

[20] Suárez and Quéré, eds., *Stability Analysis of Nonlinear Microwave Circuits.* Norwood, MA: Artech House, 2003.

[21] C. A., R. F., S. A., and P. J., "Harmonic-balance analysis and synthesis of coupled-oscillator arrays," *IEEE. Microw. Wireless Compon. Lett.*, vol. 14, no. 5, pp. 192–194, 2004.

[22] Ngoya and Larcheveque, "A new method for the transient and steady state analysis of microwave communication circuits and systems," *IEEE MTT-S Int. Microwave Symp. Dig.*, pp. 1365–1368, 1996.

[23] B. V. der Pol, "A theory of the amplitude of free and forced triode vibrations," *The Radio Review*, pp. 701–754, 1920.

[24] S. Nogi, J. Lin, and T. Itoh, "Mode analysis and stabilization of a spatial power combining array with strongly coupled oscillators," *IEEE Trans. Microwave Theory Tech.*, vol. 41, no. 10, pp. 1827–1837, 1993.

[25] Wikipedia *http://en.wikipedia.org/*.

[26] H. K. Khalil, ed., *Nonlinear Systems*. New York: Prentice Hall., 3rd ed., 2002.

[27] W. L. Stutzman and G. A. Thiele, eds., *Antenna Theory and Design*. John Wiley and Sons, 1st ed., 1981.

[28] T. Heath, "Difference pattern beam steering of coupled, nonlinear oscillator arrays," *IEEE Microwave and Wireless Components Lett.*, vol. 11, no. 8, pp. 343–345, 2001.

[29] C. L. Dolph, "A current distribution for broadside arrays which optimizes the relationship between beam width and side-lobe level," *Proc. IRE*, vol. 34, pp. 335–348, 1946.

[30] Y. Yamaguchi, K. Komentani, and H. Shimizu, "Self-synchronization of nonlinear oscillators in the presence of fluctuations," *J. Statistical. Phys.*, vol. 26, pp. 719–743, 1981.

[31] S. H. Strogatz and R. E. Mirollo, "Phase-locking and critical phenomena in lattices of coupled nonlinear oscillators with random intrinsic frequencies," *Physica D*, vol. 31, pp. 143–168, 1988.

[32] P. Liao and R. York, "A six-element beam-scanning array," *IEEE Microwave and Guided Wave Lett.*, vol. 4, no. 1, pp. 20–22, 1994.

[33] P. Liao and R. York, "A 1 watt x-band power combining array using coupled vcos," *IEEE MTT-S Int. Microwave Symp. Dig.*, pp. 1235–1238, 1994.

[34] X. Cao and R. York, "Coupled-oscillator scanning technique for receiver applications," *Proc. IEEE AP-S Int. Symp.*, pp. 1311–1313, 1995.